LA-9647-PR
Progress Report

Los Alamos National Laboratory is operated by the University of California for the United States Department of Energy under contract W-7405-ENG-36.

Nuclear Data

Measurement and Development

Los Alamos
Los Alamos National Laboratory
Los Alamos, New Mexico 87545

The four most recent reports in this series, unclassified, are LA-8874-PR, LA-9060-PR, LA-9262-PR, and LA-9468-PR.

This work was performed under the auspices of the US Department of Energy's Division of Reactor Research and Technology, Office of Basic Energy Sciences and Office of Fusion Energy; the Spent Fuel Project Office under the technical direction of the Savannah River Laboratory; the Electric Power Research Institute; and the Nuclear Regulatory Commission.

Prepared by Alice Mutschlecner, Group T-2

LA-9647-PR
Progress Report

UC-34c
Issued: April 1983

Applied Nuclear Data Research and Development

April 1, 1982—September 30, 1982

Compiled by
E. D. Arthur

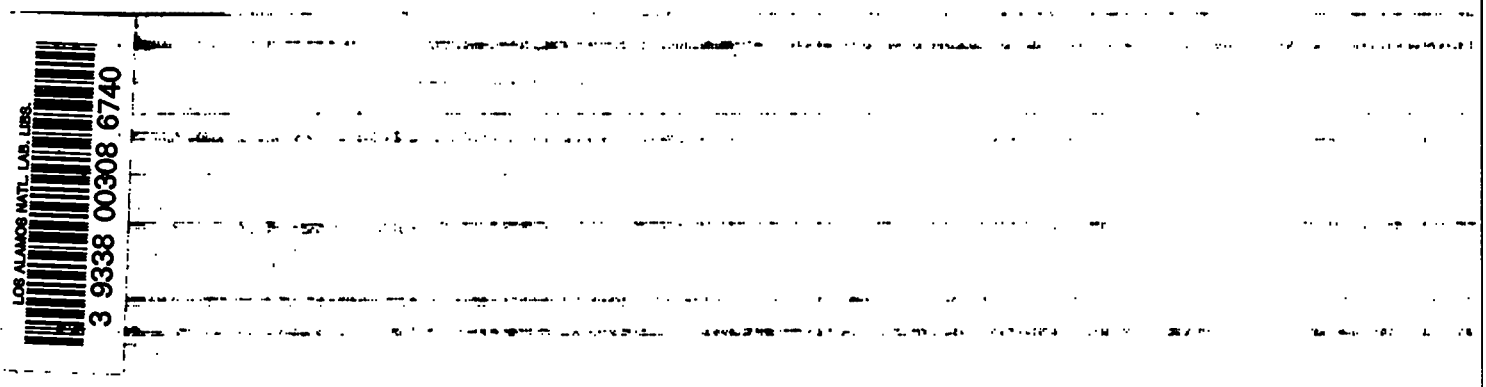

Los Alamos National Laboratory
Los Alamos, New Mexico 87545

CONTENTS

APPLIED NUCLEAR DATA RESEARCH AND DEVELOPMENT
SEMIANNUAL PROGRESS REPORT
April 1, 1982 — September 30, 1982

Compiled by

E. D. Arthur

ABSTRACT

This progress report describes the activities of the Los Alamos Nuclear Data Group for April 1, 1982, through September 30, 1982. The topical content is summarized in the Contents.

I. THEORY AND EVALUATION OF NUCLEAR CROSS SECTIONS

A. Fusion Cross Sections for Polarized Particles [G. M. Hale, D. C. Dodder, and P. W. Keaton (ADPA)]

Recently, a suggestion by M. Goldhaber led R. Kulsrud and collaborators at the Princeton Plasma Physics Laboratory to propose using polarized particles to modify fusion cross sections.[1] Polarizing the projectile and target changes both the angular distribution and integral for the cross section of a fusion reaction. Polarizing d and T so that their spins are parallel, for instance, enhances the integrated cross section for the T(d,n) reaction by a factor of as much as 1.5. In addition, Kulsrud's study shows it is plausible that polarized particles in a plasma will maintain their polarization for a relatively long time in the presence of a strong magnetic field.

We have provided the Princeton group with cross sections for polarized d-T and d-d reactions, calculated with the Los Alamos R-matrix code EDA. These calculations are based on comprehensive studies of reactions in the ^{4}He and ^{5}He systems, using EDA's capability to analyze and predict data for interacting

particles in any combination of polarization states. For the case of parallel spins in the d+T reaction, we calculate an enhancement factor for the integrated cross section at low energies very close to the theoretical maximum of 1.5. The situation for the d+d reactions, where enhancements as large as a factor of 3 are theoretically possible, is more complex.

Results of our calculations for the d+d reactions are summarized in Table I. The quantity $\sigma_{m,n}$ is the integrated cross section for the deuterons in pure spin states, having projections m and n, respectively, along the center-of-mass momentum direction of the incident deuteron. Because the deuterons are identical, $\sigma_{m,n} = \sigma_{n,m}$, and reflection invariance implies $\sigma_{-m,-n} = \sigma_{m,n}$, there are only four independent combinations, (m,n) = (1,1), (1,0), (1,-1), and (0,0). The unpolarized integrated cross section σ_0 is related to the sum of the polarized cross sections by

$$\sigma_0 = 1/9(2\sigma_{1,1} + 4\sigma_{1,0} + 2\sigma_{1,-1} + \sigma_{0,0}) \quad .$$

Table I lists the unpolarized cross sections σ_0 and the ratios $\frac{\sigma_{m,n}}{\sigma_0}$ for the four independent (m,n) combinations at deuteron energies between 100 and 500 keV for both d+d reactions.

According to these calculations, the best configuration for enhancing the cross section is (1,0) and the best one for suppressing it is (1,-1) with (1,1) a close second. The results are moderately energy dependent and somewhat reaction dependent, with the maximum enhancement ($\sim$ 1.6) well below the theoretical limit. The reason for this is that a number of transitions are important in the low energy d+d reactions, in contrast to the single $J^\pi = 3/2^+$ transition that completely dominates the d+T reaction at low energies. However, the increased complexity of the d+d reactions, coupled with the relative scarcity of reliable polarization data at low energies, makes the results of Table I much less certain than those for the T(d,n) reaction. We are attempting to improve the reliability of the d+d predictions by including more recent low-energy polarized d+d data in the four-nucleon analysis, but we point out that the most directly useful measurements, involving polarized deuterons incident on polarized deuterons, have not yet been done.

TABLE I

POLARIZED CROSS SECTIONS FOR THE d+d REACTIONS

A. D(d,p)

E_d(keV)	σ_0(mb)	$\frac{\sigma_{1,1}}{\sigma_0}$	$\frac{\sigma_{1,0}}{\sigma_0}$	$\frac{\sigma_{1,-1}}{\sigma_0}$	$\frac{\sigma_{0,0}}{\sigma_0}$
100	16.05	.949	1.146	.672	1.175
200	33.68	.776	1.334	.550	1.011
300	45.14	.672	1.468	.448	.889
400	53.18	.603	1.562	.371	.803
500	59.18	.554	1.626	.320	.749

B. D(d,n)

E_d(keV)	σ_0(mb)	$\frac{\sigma_{1,1}}{\sigma_0}$	$\frac{\sigma_{1,0}}{\sigma_0}$	$\frac{\sigma_{1,-1}}{\sigma_0}$	$\frac{\sigma_{0,0}}{\sigma_0}$
100	15.87	.745	1.289	.668	1.020
200	35.60	.573	1.491	.535	.820
300	49.70	.479	1.621	.436	.687
400	60.08	.421	1.706	.367	.600
500	67.99	.382	1.762	.321	.546

B. Coulomb Corrections in Light Nuclei: Difference of Neutron and Proton Analyzing Powers in Elastic N-d Scattering Between 5 and 14 MeV [G. M. Hale and H. Zankel (University of Graz, Austria)]

We are studying the Coulomb distortion of the "nuclear" amplitudes for light charged-particle scattering using an "on energy-shell" approximation, in which the scattering Green's function is approximated as $G^+(E',E) = i\pi\delta(E'-E)$ in the two-potential integral equation for the transition operator. In an earlier application[2] of the theory to N-d scattering, we predicted n-d observables from p-d phase shifts for E_N = 5 MeV, and saw sizeable Coulomb effects in some of the polarizations. Unfortunately, p-d phase shifts over a range of energies, as required by the calculations, were not available at energies where both p-d and n-d measurements had been made that could check the predicted differences.

Recently, we have reported[3] the same sort of correction for nucleon analyzing powers in N-d scattering that starts with n-d amplitudes calculated from the Fadeev equations. These can be calculated at any energy, and we have given

results at E_n = 5, 10, and 14 MeV. Figure 1 shows the calculations and measurements for nucleon analyzing powers at 10 MeV. The Fadeev calculation[4] (dashed curve) does not quite reproduce the magnitude of the neutron analyzing power seen in recent measurements[5] (circles), but the qualitative differences between the neutron data[5] and proton data[6] (triangles) are well reproduced by the calculated proton curve (solid line). This indicates that the differences seen in observables for the charge-symmetric branches of N-d scattering can be accounted for by this approximate Coulomb correction.

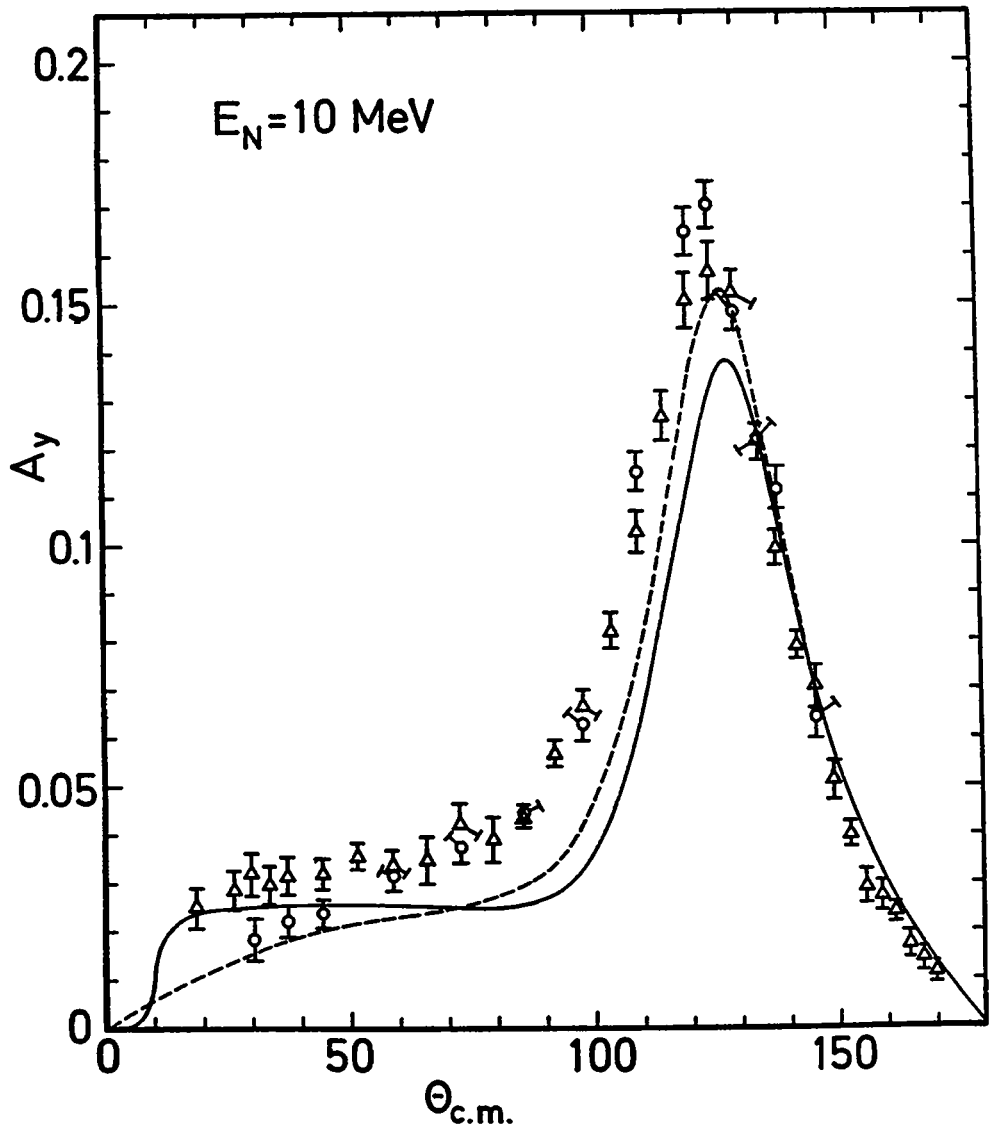

Fig. 1. Measurements and calculations of N-d analyzing powers. The dashed curve is the (neutron) Fadeev calculation of Ref. 4; the solid curve is the Coulomb-corrected proton prediction. The circles represent recent neutron data[5] and the triangles represent proton data.[6]

C. Charged-Particle Elastic Cross Sections [G. M. Hale, D. C. Dodder, J. C. DeVeaux (University of Illinois)]

Our work on charged-particle elastic cross sections, some of which has been described previously,[7] was reported at the Antwerp Conference on Nuclear Data for Science and Technology.[8] A main point of the paper was that, if the Rutherford, or "pure Coulomb," cross section is subtracted from the elastic scattering cross section, the remainder, $\sigma_{NI}(\mu)$, has an exact expansion in Legendre polynomials,

$$\sigma_{NI}(\mu) = -\frac{2\eta}{1-\mu}\,\mathrm{Re}\left[e^{i\eta\ell n\frac{1}{2}(1-\mu)}\sum_{\ell=0}^{\ell_{mx}}\frac{2\ell+1}{2}\,a_\ell P_\ell(\mu)\right] + \sum_{\ell=0}^{2\ell_{mx}}\frac{2\ell+1}{2}\,b_\ell P_\ell(\mu) \quad ,$$

in which μ is the cosine of the center-of-mass scattering angle, η is the Coulomb parameter, and ℓ_{mx} is the highest partial wave that participates in the nuclear scattering. The complex expansion coefficients a_ℓ and real coefficients b_ℓ are energy dependent and are interrelated in complicated ways that can only be imposed by a unitary parameterization of the collision matrix (such as the R-matrix or phase shifts).

Examples of these coefficients calculated from R-matrix parameters are shown in Figs. 2 and 3 for d-T scattering at energies below 5 MeV. The prominent d-T S-wave resonance is clearly evident as structure in the a_0 and b_0 coefficients at energies between 150 and 250 keV. The large values of a_0 and b_0 at low energies produce significant deviations from pure Rutherford scattering at energies below the lowest energy cross-section measurements.

We are exploring ways of incorporating the exact polynomial expansion for σ_{NI} into the treatment of the slowing-down of ions in a plasma through elastic collisions at small-to-moderate angles. These treatments currently take into account only the effects of Rutherford scattering.

D. Cross-Section Calculations for n+^{169}Tm [P. G. Young, E. D. Arthur, and C. Philis (Bruyéres-le-Châtel)]

We have carried out a final adjustment of our deformed optical-model analysis[9] of n+^{169}Tm reactions using recent measurements of elastic and inelastic neutron scattering from ^{169}Tm by Haouat and Patin.* Before these measurements, the only ^{169}Tm data available for our analysis were s- and p-wave

*G. Haouat and Y. Patin, Bruyères-le-Châtel, Montrouge, France, provided this information in June 1982.

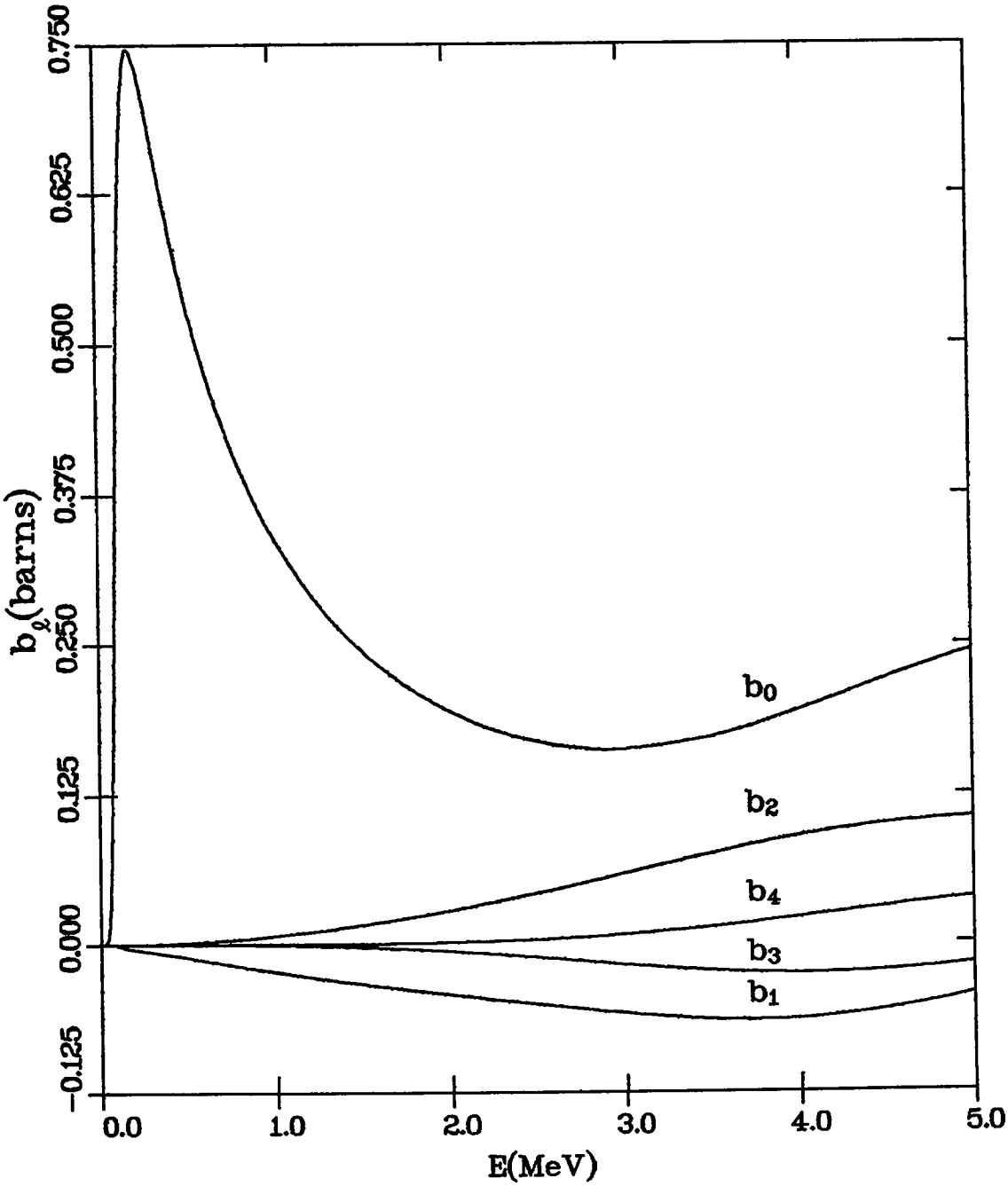

Fig. 2. Significant b_ℓ coefficients for d-T scattering at energies below 5 MeV.

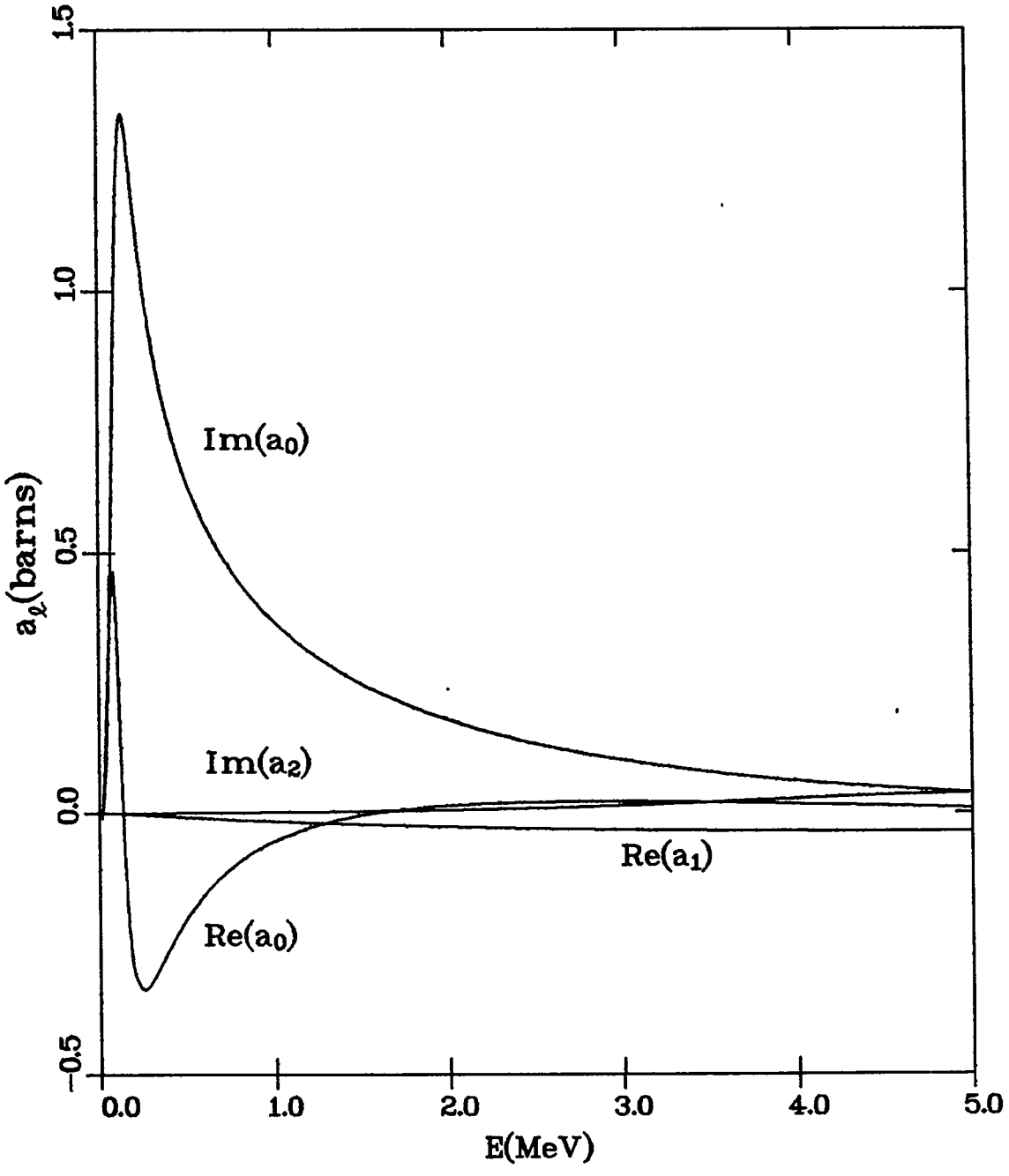

Fig. 3. Significant a_ℓ coefficients for d-T scattering at energies below 5 MeV.

neutron strengths (S_0,S_1), potential scattering radii (R'), and neutron total (n,γ) and (n,xn) cross sections. We therefore relied on the neighboring nucleus ^{165}Ho for angular distribution data[10] in our previous analysis.

As before, the coupled-channel code ECIS[11] was used for the deformed optical-model calculations. The first five states of ^{169}Tm were coupled in the calculations, but it was possible over most of the neutron energy range to approximate this case using fictitious 0^+, 2^+, 4^+ states according to the scheme of Lagrange, Bersillon, and Madland[12] (see Table II). We empirically verified that the approximate calculations reproduced the more precise five-state ones to better than ~ 1%, except near thresholds for the (n,n') cross sections.

Beginning with parameters from our previous iteration,[9] the real and surface-derivative imaginary well depths, diffusivities, and radii were varied in a nonautomated scan of the parameter space. The β_2 and β_4 deformation parameters were held fixed at their values from our previous analysis. Values of χ^2 were computed relative to Haouat and Patin's neutron elastic angular distribution measurements at 0.57, 1.1, and 2.0 MeV. The measured distributions were corrected for compound nucleus contributions and the unresolved 8.4 keV first excited state of ^{169}Tm using parameters from our previous analysis. At the same time that a minimum χ^2 relative to the elastic angular distributions was sought, we attempted to improve agreement with measurements of S_0, S_1, and R' for low neutron energies and to maintain good agreement with measurements of the neutron total cross section. (Values of S_0 and S_1 were inferred from the neutron transmission coefficients calculated with ECIS at 10 keV.)

The parameters that resulted from this analysis are listed in Table III. Comparisons between Haouat and Patin's experiment and angular distributions calculated with parameters from both the previous and present analyses are given in Figs. 4-6. Compound nucleus contributions for the various theoretical curves were calculated from the two parameter sets using the COMNUC reaction theory code.[13]

Although not apparent from Figs. 4-6, the new analysis resulted in a small reduction for χ^2 from the elastic angular distribution measurements. Perhaps more significantly, the new parameters improved overall agreement in calculated values of S_0, S_1, and R' with experiment, particularly S_1, as is indicated in Table IV. Additionally, the new parameters led to improved calculations of (n,2n) and (n,3n) cross sections near the thresholds for these reactions, which are shown in Figs. 7 and 8. [The (n,xn) calculations were performed with the

GNASH statistical-preequilibrium theory code,[14] as described in Ref. 9]. Finally, the new parameters result in calculated total and (n,γ) cross sections that agree with experiment roughly as well as the previous analysis, and these comparisons are shown in Figs. 9 and 10.

The statistical, preequilibrium, and deformed optical-model parameters from this analysis will be used to calculate a variety of reaction cross sections for thulium isotopes having A = 167-170.

TABLE II

STATES INCLUDED IN THE COUPLED-CHANNEL CALCULATIONS

^{169}Tm		^{169}Tm (Fictitious States)	
E_x (keV)	J^π	E_x (keV)	J^π
0	$1/2^+$	0	0^+
8.4	$3/2^+$		
118.2	$5/2^+$	72	2^+
138.9	$7/2^+$		
331.9	$9/2^+$	240	4^+

TABLE III

DEFORMED OPTICAL-MODEL PARAMETERS FOR n+^{169}Tm[a]

			r	a
V	= 47.0 - 0.26 E		1.29	0.60
W_{VOL}	= -1.8 + 0.2 E	E > 9 MeV	1.29	0.60
V_{SO}	= 6.0		1.29	0.60
W_{SD}	= 2.5 + 0.6 E	E < 7.5 MeV	1.29	0.48
	= 7.0 - 0.03(E-7.5)	E ≥ 7.5 MeV	1.29	0.48
β_2	= 0.31	β_4 = -0.01		

[a]All well depths are in MeV and geometrical parameters in fm.

TABLE IV

SUMMARY OF n+^{169}Tm S_0, S_1, AND R' RESULTS

	Exp	Previous	Present
S_0 ($\times 10^4$)	1.5 ± 0.2	1.65	1.50
S_1 ($\times 10^4$)	0.5 - 1.5[a]	3.60	2.15
R' (fm)	7.7 ± 0.5	7.55	6.97

[a]From systematics.

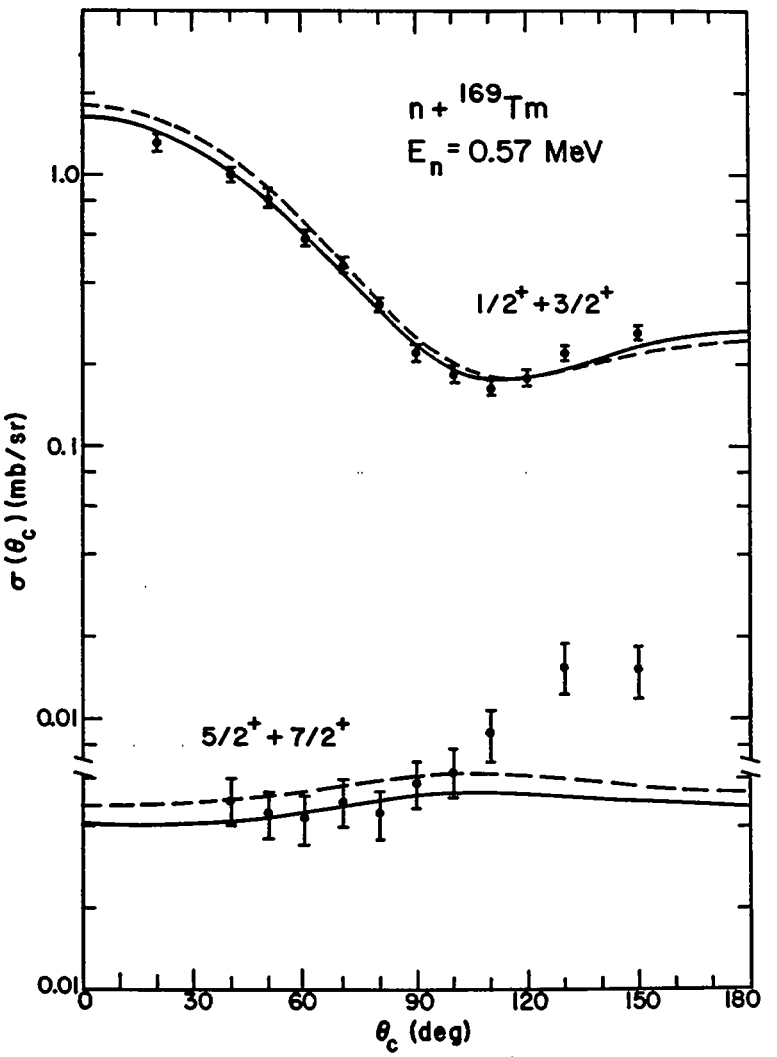

Fig. 4. Comparison of calculated and measured[a] neutron angular distributions with several states in ^{169}Tm at an incident neutron energy of 0.57 MeV. The solid curve represents results from the present analysis; the dashed curve indicates the analysis of Ref. 9.

[a]G. Haouat and Y. Patin, Bruyères-le-Châtel, Montrouge, France, provided this information in June 1982.

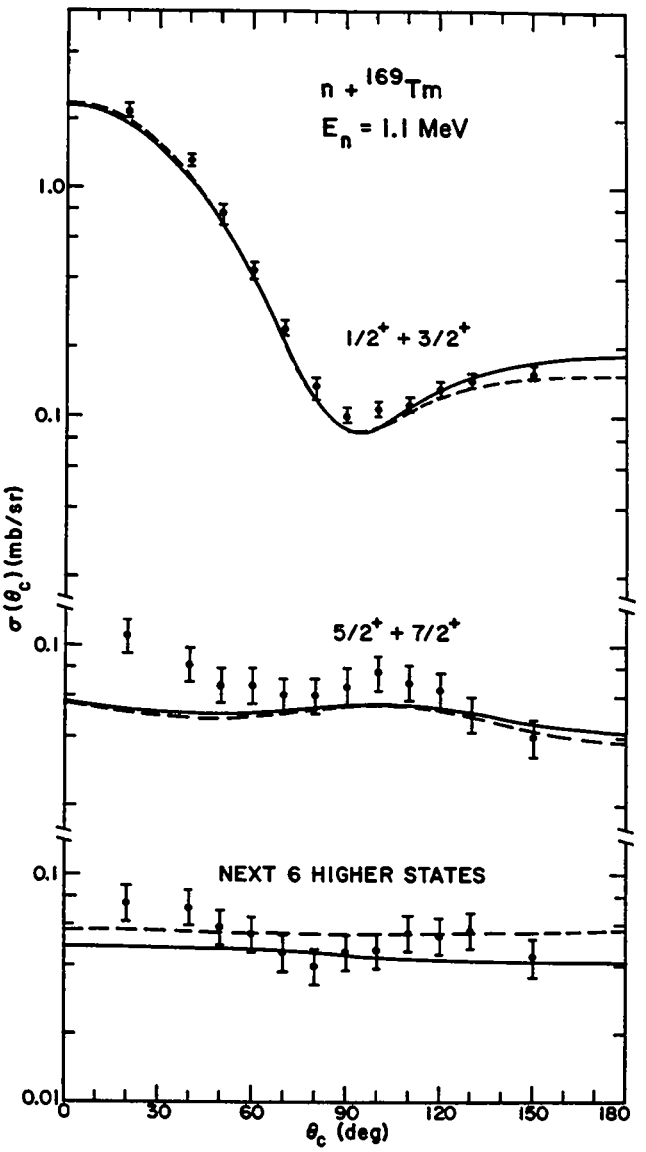

Fig. 5. Comparison of calculated and measured[a] neutron angular distributions with several states in ^{169}Tm at an incident neutron energy of 1.10 MeV. The solid curve represents results from the present analysis; the dashed curve indicates the analysis of Ref. 9.

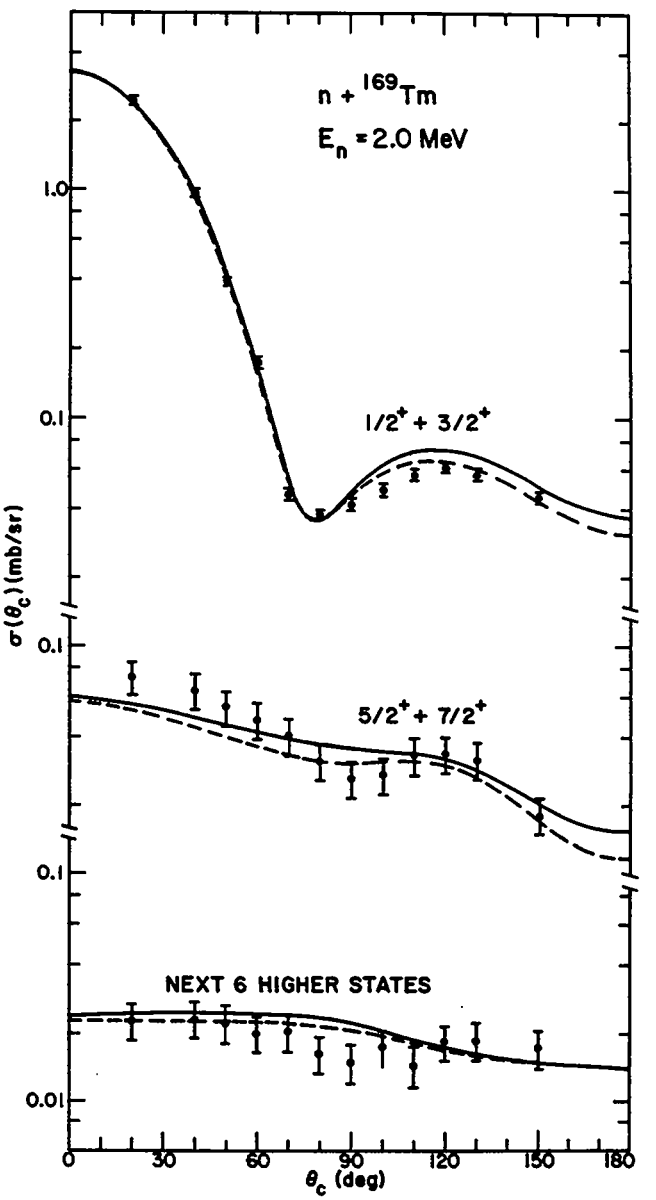

Fig. 6. Comparison of calculated and measured[a] neutron angular distributions with several states in ^{169}Tm at an incident neutron energy of 2.00 MeV. The solid curve represents results from the present analysis; the dashed curve indicates the analysis of Ref. 9.

[a]G. Haouat and Y. Patin, Bruyères-le-Châtel, Montrouge, France, provided this information in June 1982.

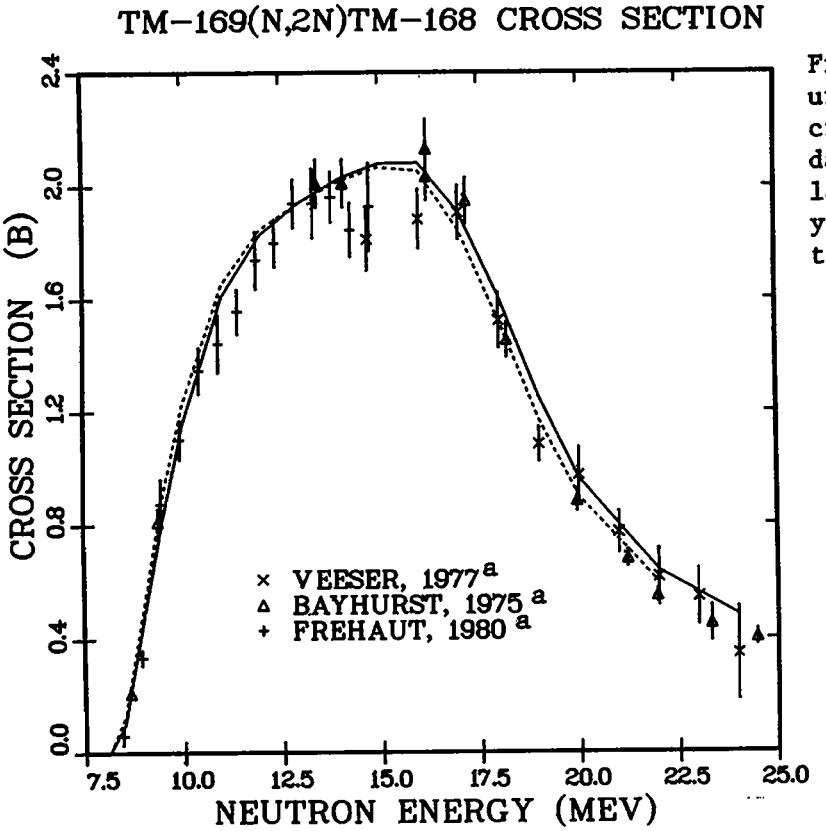

Fig. 7. Calculated and measured values of the ^{169}Tm(n,2n) cross section. The solid and dashed curves represent calculations from the present analysis and from Ref. 9, respectively.

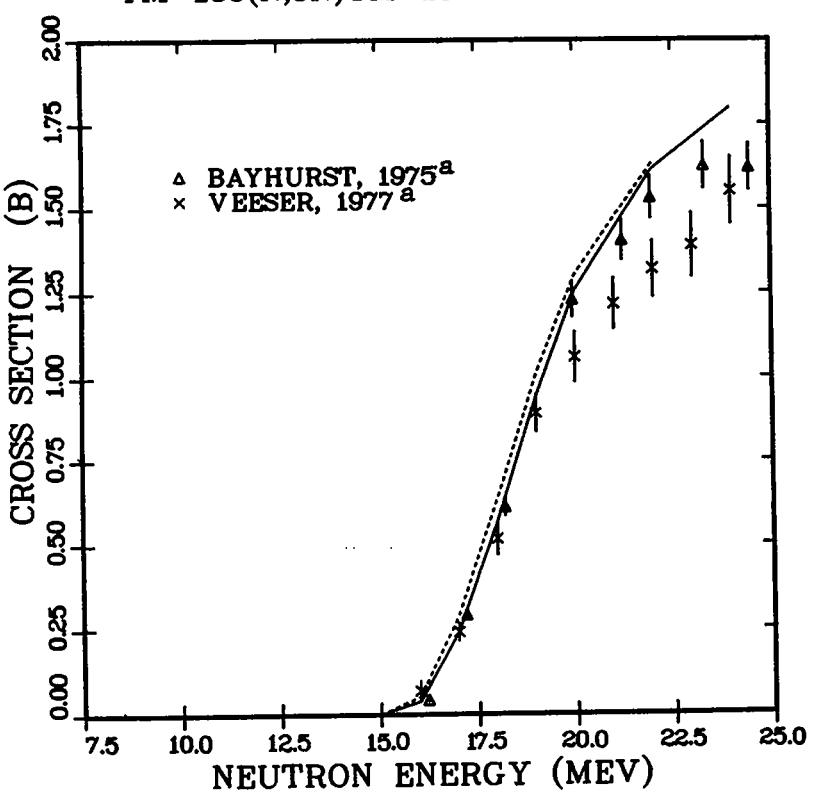

Fig. 8. Calculated and measured values of the ^{169}Tm(n,3n) cross section. The solid and dashed curves represent calculations from the present analysis and from Ref. 9, respectively.

[a] This information was provided on tape from the National Nuclear Data Center, Brookhaven National Laboratory, Upton, New York, in July 1981.

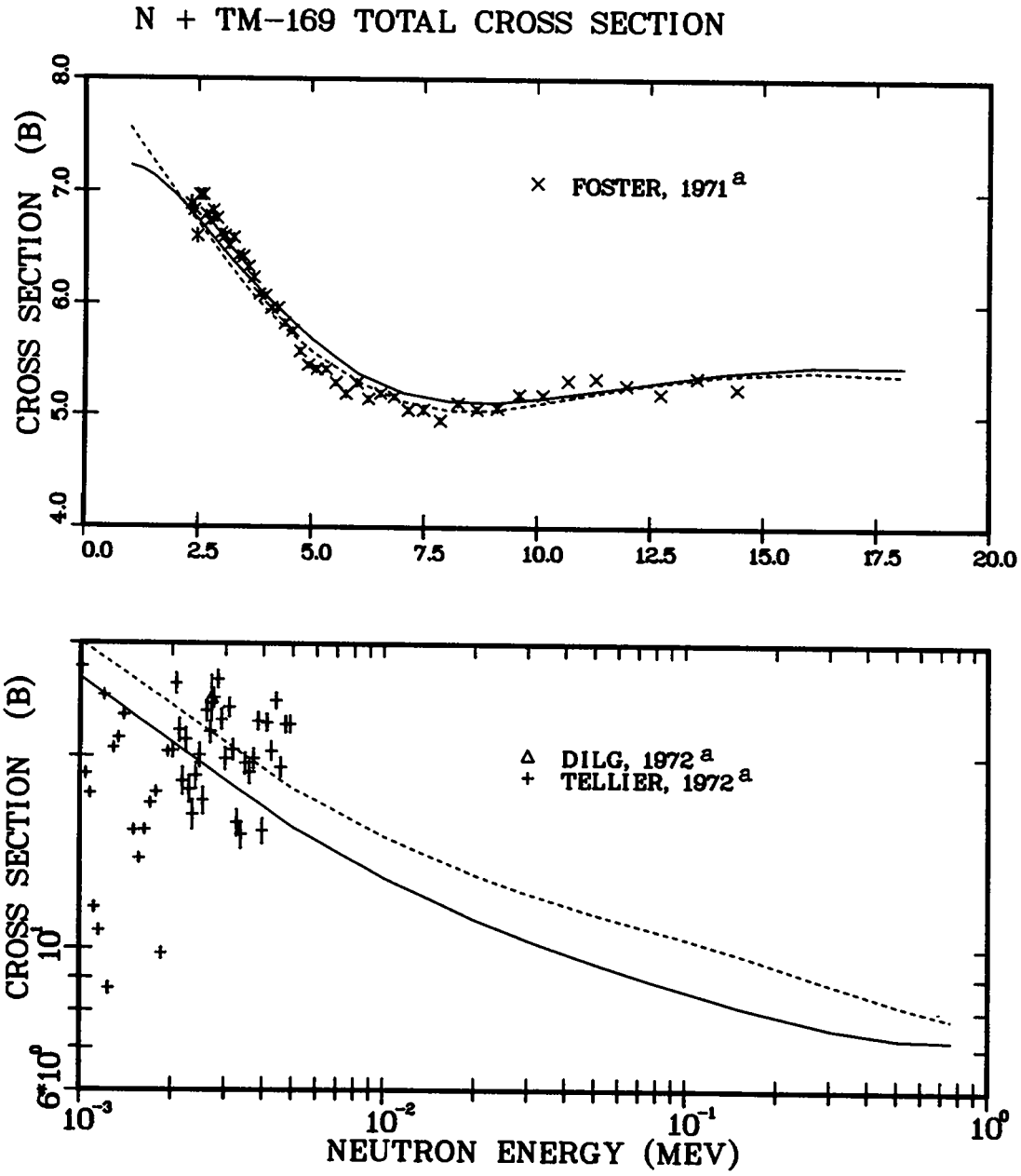

Fig. 9. Calculated and measured values of the neutron total cross section for ^{169}Tm. The solid and dashed curves represent calculations from the present analysis and from Ref. 9, respectively.

[a]This information was provided on tape from the National Nuclear Data Center, Brookhaven National Laboratory, Upton, New York, in 1981.

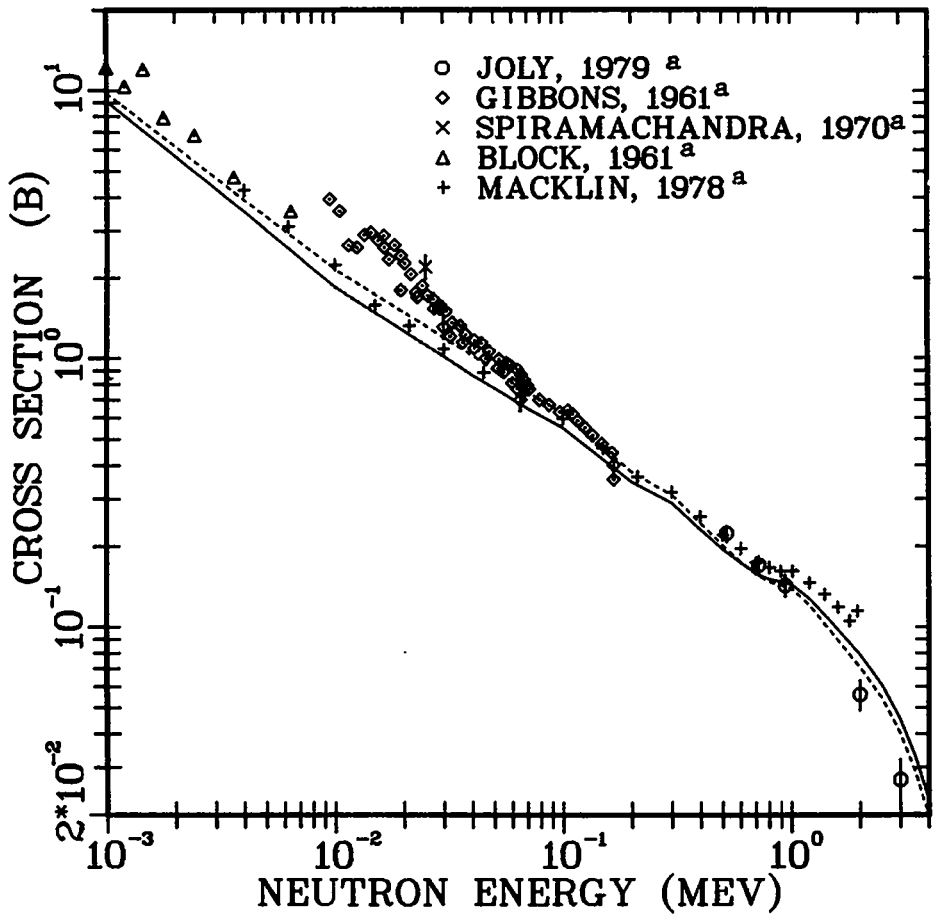

Fig. 10. Calculated and measured values of the ^{169}Tm(n,γ) cross section. The solid and dashed curves represent calculations from the present analysis and from Ref. 9, respectively.

[a]This information was provided on tape from the National Nuclear Data Center, Brookhaven National Laboratory, Upton, New York, in July 1981.

E. New Calculations of ^{88}Y(n,2n) Cross Sections from Threshold to 20 MeV (E. D. Arthur)

In the period since our original 1978 yttrium and zirconium cross-section calculations,[15] pertinent discrete level information in the mass 90 has improved substantially, particularly for ^{87}Y. In this case, the amount of information has almost doubled, a situation that affects not only the explicit discrete level parameters (E_x, J, π) appearing in nuclear model calculations but also the level densities used. This occurs since constant temperature parameters in the level density expression are adjusted to reproduce the cumulative number of levels at a given excitation energy. Figure 11 illustrates the

difference between the level density used in the present recalculation (dashed line) and that originally used in 1978 (dotted curve). The histogram represents the cumulative number of levels versus excitation energy resulting from the new level information.

With these new ^{87}Y levels, Hauser-Feshbach preequilibrium calculations were repeated keeping the other parameter types (optical-model, gamma-ray strengths, preequilibrium constants, and discrete level data for other nuclei) fixed at their original 1978 values. To be consistent with these improvements, however, these other parameter classes should be reviewed and updated, and a complete recalculation of the entire $^{86-92}Y$ set should be made. This first attempt, as described here, is probably reasonable, except for possible weaknesses that depend on other discrete level information. But, because the ^{87}Y level information underwent substantial improvements and because of the importance of this nucleus in these types of calculations, this effort should improve significantly the original cross-section set.

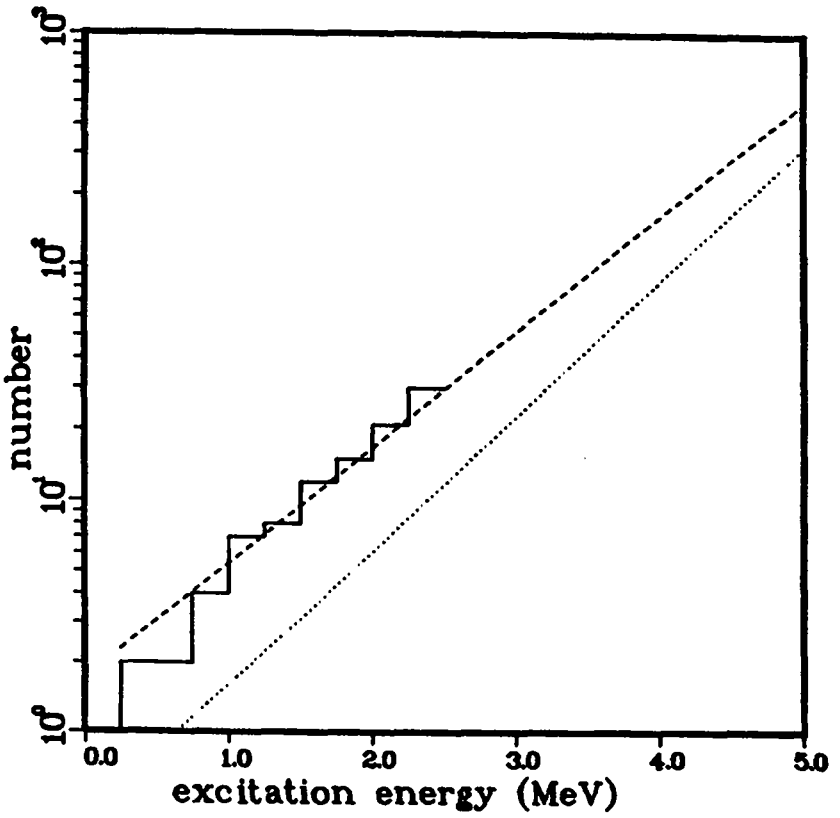

Fig. 11. The cumulative number of discrete levels for ^{87}Y used in these recalculations is shown by the histogram. The dashed curve indicates the fit obtained through use of a constant temperature level density expression, whereas the dotted curve indicates similar results from our earlier work.

Figure 12 compares our recalculated values (solid curve) of the $^{88}Y(n,2n)^{87}Y$ cross section with data* measured at Lawrence Livermore Laboratory for neutron energies of 14.2 and 14.8 MeV. The agreement is much improved with respect to this data, as is seen from comparison with our earlier calculations (dashed curve).

Since ^{88}Y can also be produced through the $^{89}Y(n,2n)$ reaction in one of its two isomeric states, similar recalculations have been made for them. Around 14 MeV, these recalculated cross sections for ^{88m1}Y and $^{88m2}Y(n,2n)$ reactions are 4 and 25% higher, respectively. From $^{89}Y(n,2n)$ cross-section information at 14 MeV,** approximately 73% of ^{88}Y is produced in its ground state, 12% in its first metastable state, and 15% in its second isomeric state. If these productions are folded with changes in the calculated $^{88}Y(n,2n)$ cross sections described here, then the average overall increase in ^{87}Y production would be about 11% higher than would be obtained with our previous cross sections.

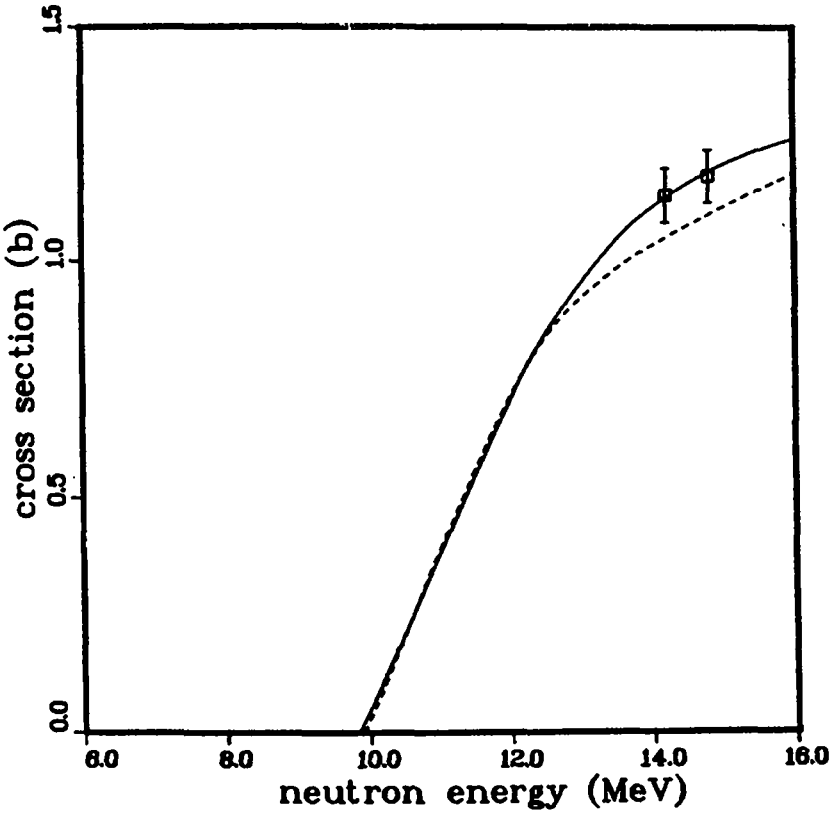

Fig. 12. The recalculated $^{88}Y(n,2n)$ cross section (solid curve) is compared with experimental data. The dashed curve represents the 1978 values.

*D. Nethaway, Lawrence Livermore National Laboratory, provided this information in 1981.

**D. Barr, Los Alamos National Laboratory, provided this information in 1978.

F. Determination of "Equivalent" Spherical Optical-Model Parameters for Neutron Reactions on Thulium Isotopes [M. Collin (Bruyères-le-Châtel) and E. D. Arthur]

As part of the calculation of neutron cross sections for thulium isotopes, we have developed a set of spherical optical-model parameters that reproduce results available from coupled-channel calculations using realistic optical-model parameters. The coupled-channel calculations performed using the ECIS code[16] are described in this progress report and reproduce well measured total cross sections, s- and p-wave strengths, plus new elastic and inelastic angular distributions recently measured at Bruyères-le-Châtel.* The deformed nature of the thulium isotopes makes determination of spherical parameters difficult, but we have attempted to minimize such difficulties through use of the shape-elastic and compound nucleus formation cross sections, along with $\ell = 0$ and $\ell = 1$ transmission coefficients obtained from the coupled-channel calculations. These data were then used in the spherical optical-model search code, SCATOPT,** to produce a set of spherical optical parameters through a chi-square minimization process.

Although it was possible to fit the provided shape-elastic and compound nucleus formation cross-section values relatively easily, the introduction of the coupled-channel transmission coefficients into the search procedure complicated the search somewhat. There was a tendency for trial sets of spherical optical-model parameters to overpredict the $\ell = 0$ and $\ell = 1$ transmission coefficients, while reproducing reasonably well the total compound nucleus formation cross section. This implies a general underprediction of higher order ℓ transmission coefficients relative to the coupled-channel case. To circumvent this, the weighting on the lower order ℓ transmission coefficients was reduced, resulting in the determination of the spherical optical parameters mainly through the influence of the compound nucleus formation cross sections. The resulting parameter set appears in Table V. To check the overall effect of transmission coefficients generated using these spherical optical parameters, we repeated two ^{169}Tm(n,2n) calculations, one at 9 MeV and the other at 14 MeV. The compound nucleus formation cross section calculated with these parameters agreed to within +1.8% and -0.3% of the coupled-channel results at these two energies.

---

*G. Haouat and Y. Patin Bruyères-le-Châtel, Montrouge, France, provided this information in June 1982.

**O. Bersillon, Bruyères-le-Châtel, Montrouge, France, provided this information in 1979.

For the (n,2n) cross section, the equivalent agreement was +6% at 9 MeV and -0.1% at 14 MeV. This information, along with the quality of fits obtained in the spherical optical-model calculations, indicates that these parameters should reproduce the input coupled-channel results to within 5-10% over the energy range between 5 keV and 20 MeV.

TABLE V

"EQUIVALENT" SPHERICAL OPTICAL PARAMETERS FOR $n+^{169}Tm$[a]

	r	a
$V = 44.95 - 0.1125E$	1.189	0.441
$W_{SD} = 9.513 - 0.0518E$	1.235	0.635
$W_{vol} = -1. + 0.176E$	1.189	0.441
$V_{SO} = 7.$	1.26	0.66

[a]All well depths are in MeV; geometrical parameters are in fermis.

G. Addition of a Fission Model to the GNASH Code (E. D. Arthur)

A multihumped fission model has been added to the GNASH preequilibrium Hauser-Feshbach statistical model code. This model uses uncoupled oscillators to represent the barriers in a manner similar to that described recently[17] for our improved COMNUC program. For GNASH, however, one has the choice of a double-humped representation or, if desired, a three-barrier representation, consisting of two standard barriers plus one in parallel with the outer barrier. In this case the total fission transmission coefficient is determined according to

$$T_F = \frac{T_A \cdot (T_B + T_{B'})}{T_A + T_B + T_{B'}} \quad , \tag{1}$$

where T_A, T_B, and $T_{B'}$ are fission transmission coefficients for barriers A, B, and the parallel outer one, B'. These are described in further detail in Ref. 17.

Several features have also been added. The first of these is a subroutine to automatically calculate a spectrum of fission transition states from given

bandhead information. Secondly, the level density parameters at each barrier are automatically adjusted to reproduce the cumulative number of such transition states computed, as just described. A third feature is the ability to input directly an initial compound nucleus spin distribution. This allows one to compute fission probabilities to compare with direct-reaction measurements.

In order to check certain elements of the code, particularly the integration required in the determination of fission transmission coefficients, we compared the GNASH calculations with results from the COMNUC code for n+^{235}U reactions below 10 MeV. This problem utilized a single-humped fission barrier description, a simplified spectrum of transition states, no level-density enhancements, and no preequilibrium corrections. This comparison uncovered several inadequacies in both codes, the principal one of which was a breakdown of the gamma-ray cascade approximation in COMNUC for this particular sample problem. Initially, a large value of $2\pi\langle\Gamma\gamma\rangle/\langle D\rangle$ was used to normalize gamma-ray transmission coefficients for the ^{235}U compound nucleus. In COMNUC this led to an erroneously large correction for (γ,x) processes that represent gamma decay followed by particle emission or fission. For the final comparison problem, this was remedied through use of a much smaller $2\pi\langle\Gamma\gamma\rangle/\langle D\rangle$ value, which led to negligible contribution from (γ,x) processes. This comparison also led to an expansion in GNASH of the number of energy integration bins that can be subdivided to improve calculational accuracies around threshold. This option can now be applied to the upper five continuum energy bins rather than the first two as existed previously.

Results from the n+^{235}U comparison problem indicated differences in calculated (n,n'), (n,2n), (n,f) and (n,n'f) cross sections to be less than 3% between the two codes. Since this is approximately the accuracy obtainable using various integration parameterizations, the GNASH fission additions appear to be operating properly. The code is now ready to be applied to the calculation of actinide cross sections at higher energies where multiparticle emissions occur and preequilibrium effects are important.

H. An Improved Method for Use of Measured Fission Probabilities in Neutron Fission Cross-Section Determination (E. D. Arthur)

Fission probabilities (P_f), measured through direct-reaction excitation of compound nuclei that then fission, have provided valuable information concerning fission barrier parameters for a variety of actinide nuclei. Additionally,

fission probability measurements offer the potential to determine fission cross sections for neutron reactions on unstable nuclei that cannot generally be measured because of their short half-lives. Some efforts have been made[18,19] to deduce equivalent (n,f) cross sections from such data, but these have neglected differences in compound nucleus spin distributions populated in direct reactions and those from neutron absorption, particularly involving low-energy neutrons. Such equivalent (n,f) cross sections were obtained generally through multiplication of a measured fission probability by a compound nucleus formation cross section, usually assumed to be constant.

We are interested in this problem for several reasons. First, we would like to use available P_f data to deduce reasonably accurate fission cross sections for neutron reactions on unstable nuclei. Doing this through use of barrier parameters deduced from systematic trends that are then used in nuclear model calculations can lead to large uncertainties. This occurs because of the extreme sensitivity of calculated (n,f) cross sections to small changes in barrier parameters. However, to use such P_f data to predict unstable nuclei (n,f) cross sections with confidence, one must account for the compound nucleus spin distribution differences that occur between these two reaction types.

With regard to barrier parameters extracted previously[20,21] from such P_f measurements, we have found some difficulty in using them directly, either in a predictive sense or for an accurate reproduction of measured (n,f) data. This results from the fact that extraction of such barrier parameters is dependent upon the details of the models used, particularly with regard to the interplay between barrier parameters and transition state spectra and density enhancements. Again, analysis of P_f data using the fission models embodied in the COMNUC and GNASH codes could lead to barrier parameters readily applicable to cross-section prediction or calculation. As a further extension of such analyses, one could hope that the extraction of barrier parameters in this manner would provide a basis to confidently apply them to fit higher energy neutron-induced fission cross sections, which involve multichance fission [(n,n'f), (n,2nf), etc.], where again the relevant target system is often unstable. Although such parameters might require further adjustment to "fine tune" them to reproduce the neutron data more accurately, having them as a starting basis would reduce the number of free parameters available for adjustment in such calculations.

As a means of investigating possible spin differences occurring in compound nuclei populated in direct reactions and neutron absorption, we have compared fission probabilities measured explicitly in direct-reaction measurements with those inferred from neutron cross-section data. Results for four compound nuclei appear in Fig. 13, where the points are experimentally measured P_f values.[20,21] The solid curves are the equivalent fission probabilities determined from neutron data by taking the ratio of measured (n,f) cross sections to reaction cross sections determined from coupled-channel calculations[22] that employ realistic deformed optical parameters. This comparison shows a general agreement for compound systems (^{239}U, ^{243}Pu) in which the fission probabilities are small at low equivalent neutron energies. For so-called fissile nuclei (^{236}U, ^{240}Pu), which have large low-energy fission probabilities, there is significant disagreement occurring at low energies. The accuracy of the direct-reaction P_f measurements is estimated to be about 10%. Because (n,f) cross section data are as well or better known, and because we have confidence in the reaction cross sections predicted from the coupled-channel calculations, we attribute the differences to a sensitivity of P_f to the compound nucleus spin distributions populated through these two reaction mechanisms.

The spin distribution difference appears explicitly in Fig. 14, where the compound nucleus spins populated in the interaction of 0.1 MeV neutrons on ^{239}Pu are compared with those deduced from DWBA calculations* for the 15-MeV $^{238}Pu(t,pf)^{240}Pu$ direct reaction. Such low-energy neutrons, which are principally s- and p-wave, incident on the low target spin (1/2) ^{239}Pu nucleus, produce mainly low J-valued compound nucleus spin states. The equivalent distribution from the DWBA calculations has no such restrictions. It does, however, have the restriction that only natural parity states are excited, because the calculations were performed under the assumption that two neutrons are transferred in a relative s-motion.

Our next step was to employ such calculated DWBA spin distributions in a calculation of the fission probability for the ^{240}Pu compound system resulting from the $^{238}Pu(t,pf)^{240}Pu$ direct reaction. The barrier parameters we used were those we had extracted previously from the analysis of $^{239}Pu(n,f)$ data between 0.001 and 5 MeV. These parameters produce fission probabilities that essentially agree with the solid curve shown for the ^{240}Pu compound system. (Note

*H. C. Britt, Los Alamos National Laboratory, provided this information in 1982.

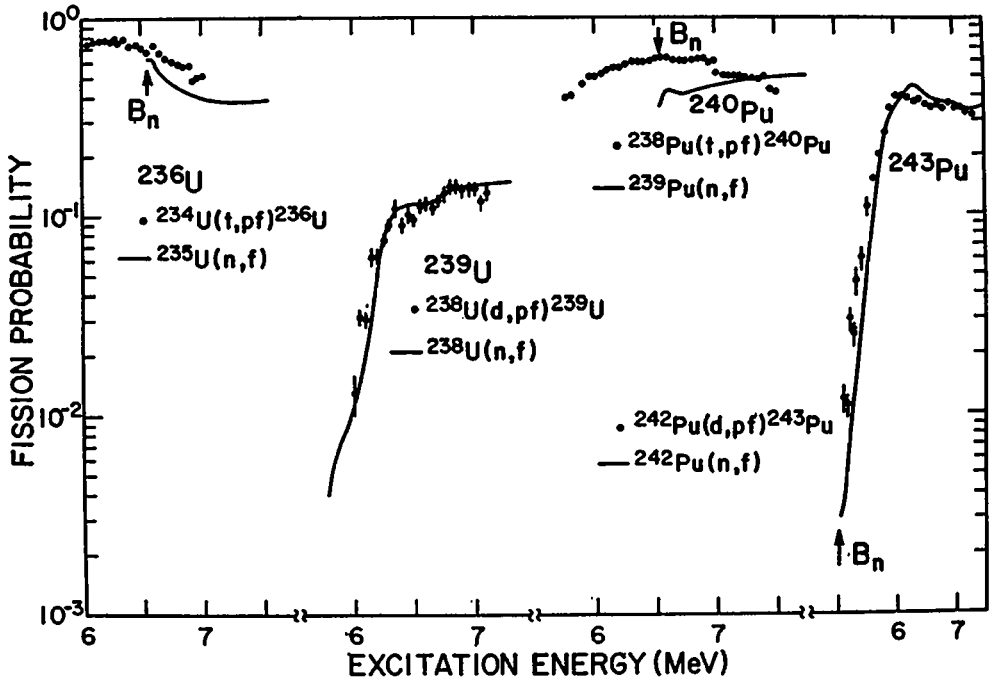

Fig. 13. Fission probabilities resulting from direct-reaction measurements (points) and as deduced from neutron cross-section data (solid curves).

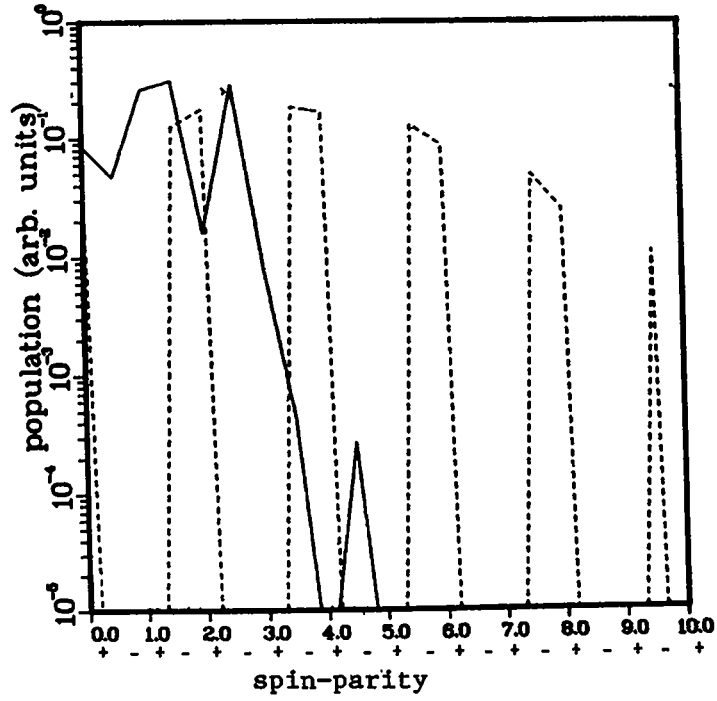

Fig. 14. The difference in compound nucleus spin distributions populated in the ^{240}Pu compound nucleus. The solid curve results from optical-model calculations of 0.1-MeV $n+^{239}Pu$ absorption, whereas the dashed curve results from DWBA calculations of the $^{238}Pu(t,pf)^{240}Pu$ reaction.

that this approach is essentially backwards from the one that we would normally assume in the use of such P_f data. We chose it because of the availability of barrier parameters that reproduce (n,f) cross sections in our calculations.)

Figure 15 shows the results when the DWBA (t,pf) spin distribution was used with these parameters. Again, the solid curve represents the fission probability deduced from neutron data. The fission probability (dashed curve) obtained from the neutron data under this spin "transformation" now agrees with the measured[20] direct-reaction P_f values (squares). Similar success was obtained for the case of the ^{236}U compound system.

Since this approach was essentially backward to the one we wished to use, we have deduced barrier parameters from direct-reaction P_f information for the ^{242}Pu compound system, employing the appropriate direct-reaction-induced compound nucleus spin distribution. When "translated" to the equivalent neutron reaction case through use of spin distributions obtained from neutron optical model calculations, the predicted (n,f) cross sections agreed well (~ 5-10%) with available experimental data for $^{241}Pu(n,f)$.

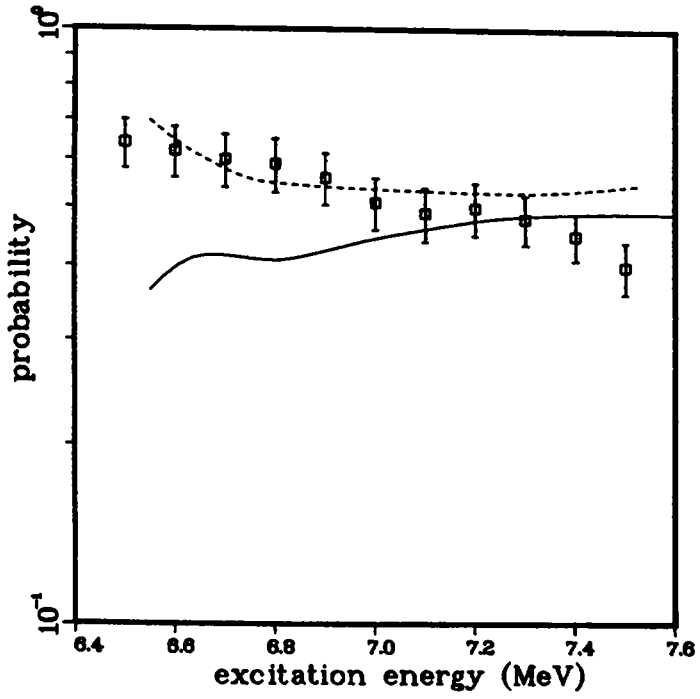

Fig. 15. Fission probabilities for the ^{240}Pu compound nucleus. When barrier parameters deduced from COMNUC calculations that reproduce $n+^{239}Pu$ fission cross sections (and hence the P_f given by the solid curve) are used with spin distributions calculated for (t,pf) direct reactions, the dashed calculated curve results. These calculated results are in essential agreement with the P_f data (squares) measured using direct reactions.

We therefore believe that if reliable P_f data exist from direct-reaction measurements, this technique provides a method to accurately exploit them in the analysis and determination of neutron-induced fission cross sections.

I. Use of Fission Probability Data in the Calculation of n+^{237}U Fission Cross Sections (E. D. Arthur)

The technique, as described in the previous section, of using measured direct-reaction fission probability (P_f) data to deduce (n,f) cross sections has been applied to the case of neutron reactions on the unstable ^{237}U target nucleus. In this technique, fission barrier parameters are deduced from fits to P_f data using the COMNUC code in which direct-reaction spin populations were utilized for the initial compound system. Neutron fission cross sections are then determined through a "translation" to the incident neutron system through use of the compound nucleus spin distributions obtained from neutron optical-model calculations.

Application of these techniques to the ^{238}U compound system is attractive for several reasons. First, the ground-state spin of ^{237}U is low (1/2) so that low-energy neutron absorption populates only a few compound nucleus spin states in contrast to the situation with direct reactions. Secondly, there are numerous ^{236}U(t,pf)^{238}U data[19,20] available that span low excitation energies in the ^{238}U compound system; whereas, at higher excitations, there are P_f data available from the ^{238}U(γ,f) reaction.[23] Finally, this compound system has been the subject of some study[24] because of evidence for the existence of a second parallel outer fission barrier.

We have performed fits to ^{236}U(t,pf)^{238}U fission probability data using the calculated (t,pf) spin distribution (described earlier) in conjunction with the COMNUC Hauser-Feshbach statistical model code. The code was further upgraded to include a three-barrier representation analogous to that necessary to fit similar data, as described in Ref. 24. Figure 16 shows the calculated probability for direct-reaction fission (solid curve) compared with the P_f data cited earlier. Table VI summarizes the ^{238}U barrier parameters deduced from this fit. The dashed curve is the equivalent neutron fission probability obtained when the barrier parameters used to generate the solid curve are used with compound nucleus spin distributions obtained from neutron optical-model calculations. The difference between the solid and dashed curve again illustrates the impact of the compound nucleus spin distribution assumed in such calculations.

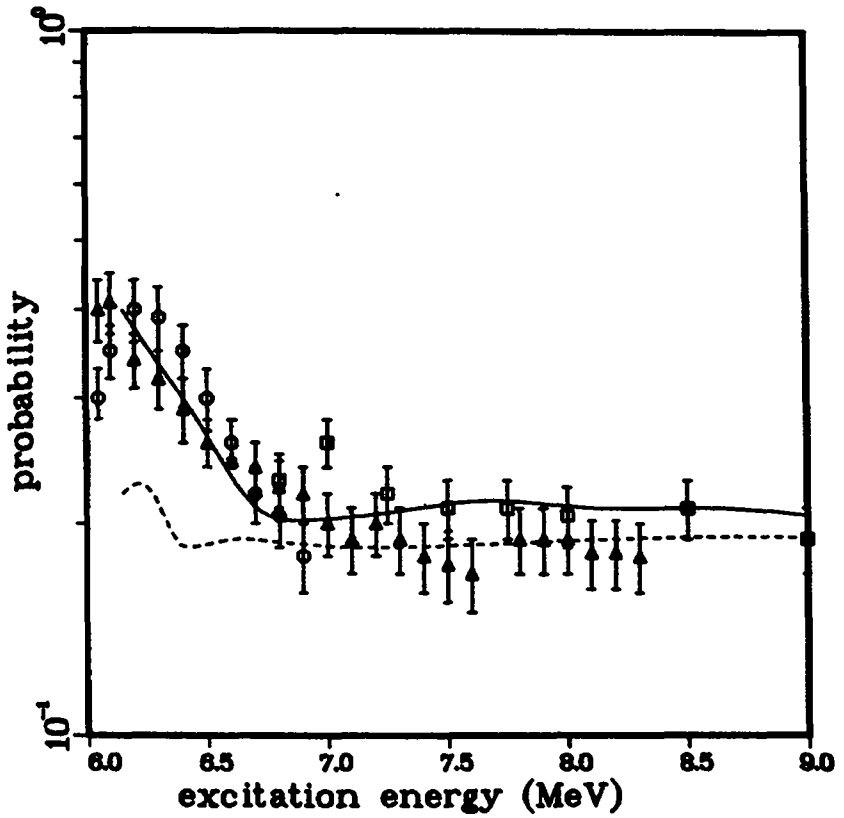

Fig. 16. Calculated (solid curve) and measured (circles, triangles, and squares) fission probabilities for the ^{238}U compound system from (t,pf) and (γ,n) reactions. The dashed curve illustrates the analogous P_f deduced for incident neutrons, as described in the text.

TABLE VI

BARRIER PARAMETERS DEDUCED FOR THE ^{238}U COMPOUND SYSTEM FROM THE PRESENT ANALYSIS

	Height (MeV)	Curvature (MeV)	Density Enhancement[a] Factor
Barrier A	5.60	1.15	2.5
Barrier B	5.50	0.85	2.0
Barrier B'[b]	5.6	0.85	2.5

[a] To compute an overall level density enhancement, this factor is multiplied by $U^{\frac{1}{4}}$ for excitation energies (U) $\geq$ 1.

[b] B' is the third barrier, assumed to be parallel to the outer one, B.

Figure 17 compares our calculation with experimental data that exists for the $^{237}U(n,f)$ reaction[25] (open squares) as well as cross sections (solid circles) inferred from systematics.* Also shown by the dashed curve is an earlier calculation by Gardner,[26] which, in the region from 0.5-2 MeV, reproduces the inferred $^{237}U(n,f)$ cross sections given by Cramer[19] without allowance for compound nucleus spin distribution effects.

*J. Behrens, National Bureau of Standards, Washington, D.C., provided this information in 1982.

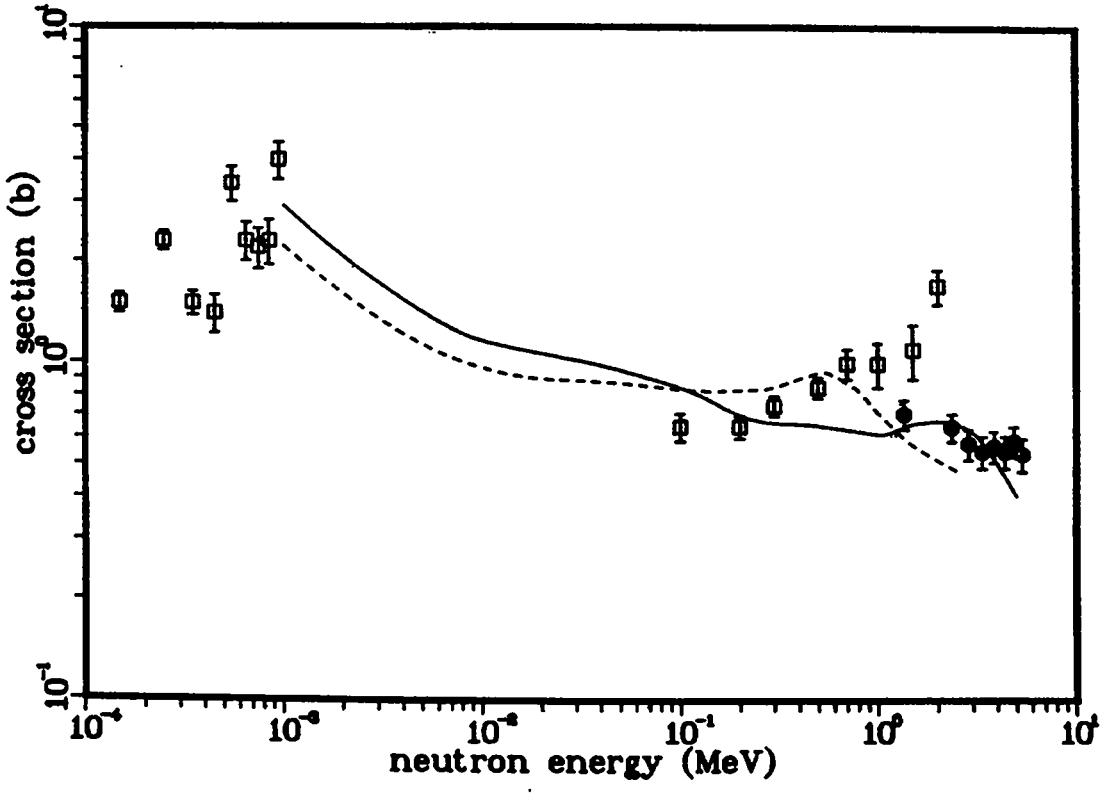

Fig. 17. Our present calculations (solid curve) for the $^{237}U(n,f)$ cross sections are compared with experimental data (squares) and cross sections deduced from data systematics (circles). The dashed curve results from an earlier calculation by Gardner.[26]

If the unstable ^{237}U nucleus is produced by $^{238}U(n,2n)$ ions, then it can exist in two isomeric states in addition to the ground state. These are the $5/2^+$ and $7/2^-$ states at 0.16 and 0.274 MeV. Figure 18 compares the calculated $^{237}U(n,f)$ cross sections for these two target states (dashed and dotted curves, respectively) with that calculated for the ground-state target case. For both excited target-state calculations, the higher spins of these isomeric levels (5/2 and 7/2) shift the compound nucleus spin distribution to higher J^π values at lower incident neutron energies. The partial fission widths have their maximum values occurring for such higher spins because of the transition-state spectra employed, so that this situation increases the relative fission probability for such excited-state targets. At higher incident energies, this advantage begins to disappear because of increased inelastic-scattering competition.

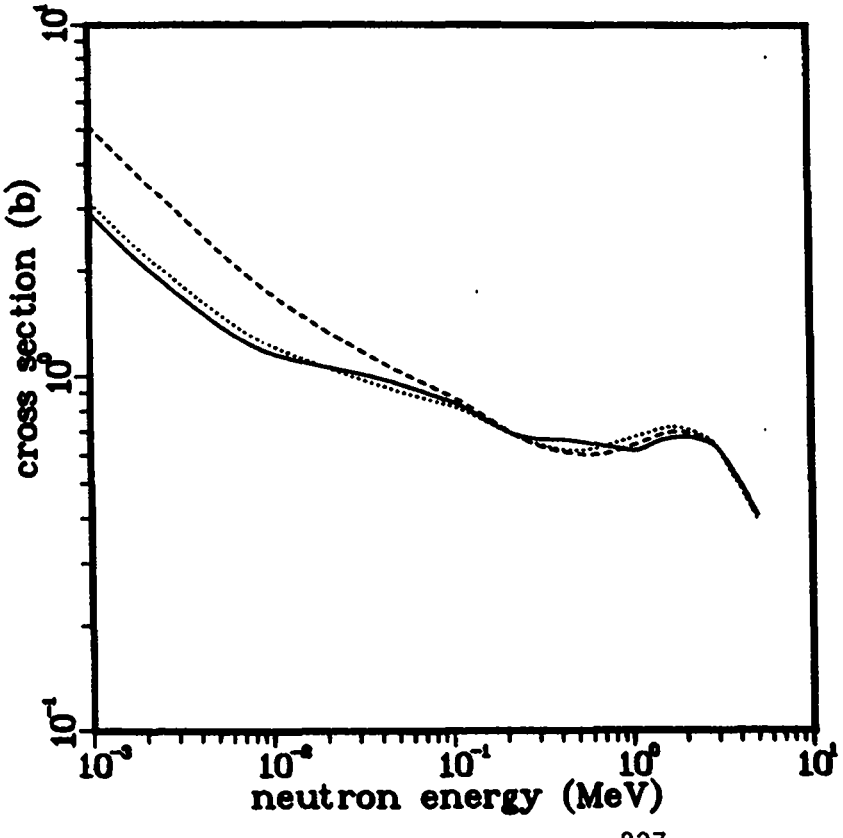

Fig. 18. Calculated fission cross sections for ^{237}U in three target states. The solid curve is for the ground-state case, whereas the dashed and dotted curves apply to ^{237}U in its 0.16- and 0.274-MeV excited isomeric states, respectively.

J. Coupled-Channel Optical-Model Calculations for Evaluating Neutron Cross Sections of Odd-Mass Actinides [D. G. Madland, Ch. Lagrange and O. Bersillon (Bruyères-le-Châtel)]

As coupled-channel calculations are very time consuming when applied to odd-mass target nuclei using the actual level schemes, the adequacy of the following approximation has been studied.

Coupled-channel calculations are performed for a fictitious even-even nucleus with the same mass number as the odd-mass target of interest. The ground-band excitation energies of the fictitious nucleus are determined using the moment of inertia and single particle energy extracted from the ground-band level structure of the actual nucleus. Quadrupole and hexadecapole deformation parameters are obtained from a theoretically based systematic available in the actinide mass region, and the coupled-channel optical-model parameters used are extrapolated from those determined for the neighboring even-even nuclei. Direct elastic- and inelastic-scattering cross sections resulting from the calculations are distributed among the true ground-band levels by use of the appropriate Wigner coefficients. Calculations have been performed with a fixed set of optical-model parameters, but using either the actual or the fictitious level scheme, for ground-state bands of $K = 1/2(^{239}Pu)$ and $K = 5/2(^{241}Pu)$. A comparison of our results shows that the approximation can be applied with great confidence over the energy region 10 keV-20 MeV in the case of $K = 1/2$. In the case of $K = 5/2$, the approximation gives satisfactory results over the limited energy range 4-20 MeV.

This work is described in detail in a manuscript that has been accepted for publication in Nuclear Science and Engineering.[27]

K. Calculation of Excited-State Cross Sections for Actinide Nuclei (D. G. Madland)

The code JUPXST for performing coupled-channel calculations on target nuclei existing in excited states is essentially complete. The total, shape-elastic, direct inelastic, reaction, and compound nucleus formation cross sections are calculated for projectiles of spin 0 or 1/2 incident on targets of even or odd A that exhibit collective rotational behavior. The target can exist either in its ground state or in a low-lying member of the ground-state rotational band.

Particular emphasis has been placed on the calculation of coupled-channel transmission coefficients for use in Hauser-Feshbach calculations of compound

nucleus reactions. The generalized coupled-channel transmission coefficient depends upon eight quantum numbers and is written $T(J,\Pi;n,\ell,j;n',\ell',j')$, where J and Π are the total angular momentum and parity, respectively, and (n,ℓ,j), (n',ℓ',j') label the coupled state, the projectile orbital angular momentum, and the projectile total angular momentum, in entrance (unprimed) and exit (primed) channels, respectively. The code JUPXST calculates and outputs the following transmission coefficient sets derived from the most general set:

1. $T(J,\Pi,n,\ell,j)$, by summing over exit channels.
2. $T(J,\Pi,1,\ell,j) \equiv T(J,\Pi,\ell,j)$, corresponding to the physical state of the target nucleus, be it the ground state or an excited state.
3. $T(J,+,1,\ell,j) \equiv T(J,+,\ell,j)$, the positive parity subset of (2).
4. $T(J,-,1,\ell,j) \equiv T(J,-,\ell,j)$, the negative parity subset of (2).
5. $T(\Pi,\ell,j)$, by compacting the set (2) according to the prescription

$$T(\Pi,\ell,j) = \frac{\sum_J (2J + 1)T(J,\Pi,\ell,j)}{\sum_J (2J + 1)} .$$

6. $T(+,\ell,j)$, the positive parity subset of (5).
7. $T(-,\ell,j)$, the negative parity subset of (5).
8. $T(\Pi,\ell)$, by averaging the set (5) over the projectile total angular momentum j

$$T(\Pi,\ell) = \frac{\sum_j (2j + 1)T(\Pi,\ell,j)}{\sum_j (2j + 1)} .$$

Note that in all of the transmission coefficient sets, the parity $\Pi = \Pi_n(-1)^\ell$, where Π_n is the parity of the nth target state. Thus, for even parity target states, one need not carry the index Π.

In order to convey the dimensions of the various transmission coefficient sets and the effects of compacting and averaging, we summarize an example in Table VII for the scattering of 15-MeV neutrons by ^{239}Pu in the ground state and in the first excited state. In this example the first five members of the ground band ($1/2^+$,$3/2^+$, $5/2^+$, $7/2^+$,$9/2^+$) are coupled and the value of ℓ_{max} for the incident neutron is 17.

The transmission coefficient sets (1)-(8) are presently being calculated on incident neutron energy meshes of interest for ^{235}U, ^{238}U, and ^{239}Pu.

TABLE VII

EXAMPLE OF DIMENSIONS OF TRANSMISSION COEFFICIENT SETS FROM JUPXST FOR THE SCATTERING OF 15-MEV NEUTRONS BY ^{239}PU IN THE GROUND STATE AND IN THE FIRST EXCITED STATE[a]

Set	T	Number (Ground-State Scattering)	Number (1st Excited-State Scattering)
1	$T(J,\Pi,n,\ell,j)$	930	950
2	$T(J,\Pi,\ell,j)$	70	136
3	$T(J,+,\ell,j)$	34	66
4	$T(J,-,\ell,j)$	36	70
5	$T(\Pi,\ell,j)$	35	35
6	$T(+,\ell,j)$	17	17
7	$T(-,\ell,j)$	18	18
8	$T(\Pi,\ell)$	18	18

[a]Five coupled states, $\ell_{max} = 17$; see text.

L. Calculation of the Prompt Neutron Spectrum and Average Prompt Neutron Multiplicity for the Spontaneous Fission of ^{252}Cf [D. G. Madland and J. R. Nix (T-9)]

On the basis of new developments[28] in the theory of the prompt fission neutron spectrum N(E) and average prompt neutron multiplicity $\bar{\nu}_p$, we calculate these quantities for the spontaneous fission of ^{252}Cf. We study this particular reaction because it is used as a standard in many measurements and applications of neutron physics. The new developments are based upon conventional nuclear-evaporation theory and account for the effects of (1) the motion of the fission fragments, (2) the distribution of fission-fragment residual nuclear temperature, and (3) the energy dependence of the cross section for the inverse process of compound-nucleus formation.

As an approximation to the result of Terrell,[29] we take the residual nuclear-temperature distribution to be triangular in shape, extending linearly from zero to a maximum value T_m. For some of our purposes, we calculate the compound-nucleus cross section from the optical model, whereas in other cases

we use a constant cross section and readjust the value of the nuclear level-density parameter to simulate the energy dependence. The value of T_m is determined from the average energy release, the total average fission-fragment kinetic energy, and the level-density parameter of the Fermi-gas model.

Whereas for ^{252}Cf spontaneous fission, the total average fission-fragment kinetic energy is a measured quantity and the Fermi-gas level-density parameter is inferred from measurements, the average energy release must be calculated. Previously, we have calculated this quantity by use of a seven-point approximation[28] to the integral of the energy release over the fission-fragment mass and charge distributions, using measured or systematic masses of the 1977 Wapstra-Bos evaluation[30] when they exist and otherwise the droplet-model mass formula of Myers.[31] Here we replace these with the new 1981 Wapstra-Bos evaluation[32] and the new macroscopic/microscopic mass formula of Möller and Nix.[33] We then perform the integration for the average energy release without approximation. An identical set of changes is made in the integration for the average fission-fragment neutron separation energy, which is required in the calculation of the average prompt neutron multiplicity. With these improvements, we calculate the prompt fission spectrum N(E), the average prompt neutron multiplicity $\bar{\nu}_p$, and its decomposition into $\bar{\nu}_p(A_H)$, where A_H is the mass number of the heavy fragment. Some of the results presented here have already appeared in Refs. 28 and 34.

Calculated spectra depend primarily upon the values of three constants, namely, the average kinetic energies per nucleon E_f^L and E_f^H of the average light and heavy fragments, respectively, and the maximum temperature T_m of the distribution of fission-fragment residual nuclear temperature.

The values of E_f^L and E_f^H are obtained by use of momentum conservation from the total average fission-fragment kinetic energy $\langle E_f^{tot} \rangle$, the mass number A of the compound nucleus undergoing fission, and the average mass numbers A_L and A_H of the light and heavy fragments, respectively. In this work, as in Ref. 2, we use the values $\langle E_f^{tot} \rangle$ = 185.9 MeV, A_L = 108, and A_H = 144 that are obtained from the measurements of Unik et al.[35]

The value of T_m is obtained from the observation of Terrell[29] that in the triangular approximation, T_m is related to the initial total average fission-fragment excitation energy $\langle E^* \rangle$ approximately by

$$T_m = (\langle E^* \rangle / a)^{1/2} , \qquad (2)$$

where a is the nuclear level-density parameter. For spontaneous fission, $\langle E^* \rangle$ is given by

$$\langle E^* \rangle = \langle E_r \rangle - \langle E_f^{tot} \rangle \ , \tag{3}$$

where $\langle E_r \rangle$ is the average energy release in fission.

In Ref. 28 we evaluated the integral for $\langle E_r \rangle$ by a seven-point approximation to this integral that is centered about the average values of the distributions, as illustrated in Fig. 1 of Ref. 28. In applying this approximation, the average or central fragments are obtained from the measurements of Unik et al.,[35] which yield $^{108}_{42}$Mo and $^{144}_{56}$Ba for the ^{252}Cf(sf) reaction. The required energy differences are then obtained using experimental or derived systematic masses when they exist and, otherwise, a mass formula. The resulting value of $\langle E_r \rangle$ is used in Eq. (3) to obtain the initial total average fission-fragment excitation energy $\langle E^* \rangle$.

The remaining quantity required to evaluate Eq. (2) for T_m is the nuclear level-density parameter a. In Ref. 28 we used the value

$$a = A/(11 \text{ MeV}) \tag{4}$$

for energy-dependent cross-section calculations and

$$a_{eff} = A/(10 \text{ MeV}) \tag{5}$$

for constant cross-section calculations that simulate the energy dependence.

We now discuss four calculations of the prompt fission neutron spectrum that have been performed using the seven-point approximation. We do not show comparisons of these calculations with experimental data, but instead present the essential results in the first four lines of Table VIII.

The first line of Table VIII gives the results for the energy-dependent cross-section calculation obtained using a value of $\langle E_r \rangle$ determined from the 1977 Wapstra-Bos[30] evaluation for eight of the required masses and the mass formula of Myers[31] for the remaining seven. The optical-model potential of Becchetti and Greenlees[36] is used to calculate $\sigma_c(\varepsilon)$ and the level-density parameter is given by Eq. (4). This spectrum is identical to that calculated and compared in Refs. 28 and 34 with experiments #1 and #7 of Boldeman et al.[37]

TABLE VIII

SUMMARY FOR ^{252}Cf(sf) OF THE CALCULATED PROMPT FISSION NEUTRON SPECTRUM AND AVERAGE PROMPT NEUTRON MULTIPLICITY*

Integration	Mass Source	$\langle E_r \rangle$ (MeV)	$\sigma_c(\varepsilon)$	Level-Density Parameter (1/MeV)	$\langle E \rangle$ (MeV)	$\langle S_n \rangle$ (MeV)	$\bar{\nu}_p$
seven-point	W-B 77[a] Myers[b]	219.408	B-G[e]	A/11	2.279	5.473	3.803
seven-point	W-B 77 Myers	219.408	const	A/10	2.306	5.473	3.788
seven-point	W-B 81[c] M-N[d]	216.581	B-G	A/11	2.213	5.233	3.554
seven-point	W-B 81 M-N	216.581	const	A/10	2.240	5.233	3.540
full	W-B 81 M-N	218.886	B-G	A/11	2.267	5.439	3.737
full	W-B 81 M-N	218.886	const	A/10	2.294	5.439	3.723[f] 3.714[f]
full	W-B 81 M-N	218.886	B-G	A/9.6	2.168	5.439	3.791
full	W-B 81 M-N	218.886	const	A/8.4	2.167	5.439	3.792[f] 3.783[f]

*In obtaining a mass value, we use the indicated experimental mass evaluation if possible, and the indicated mass formula otherwise; the level-density parameter is either a for energy-dependent cross-section calculations or a_{eff} for constant cross-section calculations; unless otherwise noted, $\bar{\nu}_p$ is calculated using Eq. (10).

[a]The 1977 Wapstra-Bos mass evaluation (Ref. 30).
[b]The droplet-model mass formula of Myers (Ref. 31).
[c]The 1981 Wapstra-Bos mass evaluation (Ref. 32).
[d]The macroscopic-microscopic mass formula of Möller and Nix (Ref. 33).
[e]Calculated using the optical-model potential of Becchetti and Greenlees (Ref. 36).
[f]Calculated using Eq. (12).

The second line of Table VIII gives the results for the constant cross-section calculation. This spectrum, illustrated in Ref. 34, is very similar to the first spectrum, having an average energy $\langle E \rangle$ = 2.306 MeV that is only 27 keV larger than that of the first spectrum.

The third and fourth lines of Table VIII correspond, respectively, to the first and second lines, except that new sources of masses are used in the calculation of $\langle E_r \rangle$. These are the 1981 Wapstra-Bos evaluation,[32] from which ten of the required masses are obtained, and the new mass formula of Möller and Nix,[33] from which the remaining five masses are obtained. As Table VIII shows, the new value of $\langle E_r \rangle$ is reduced by 2.827 MeV, or 1.3%. This produces corresponding reductions of 8.4% in the excitation energy $\langle E^* \rangle$ and 4.2% in the maximum temperature T_m, which reduces the average energies of the third and fourth spectra by 66 keV relative to those of the first and second. However, although it is true that the third spectrum agrees with experiment[37] better than do the other three calculations discussed, the value of the average prompt neutron multiplicity $\bar{\nu}_p$ that we simultaneously calculate is in this case significantly smaller than experimental values. In an attempt to resolve this discrepancy, we improve upon the seven-point approximation to the integral for the average energy release $\langle E_r \rangle$ by performing the full integration without approximation.

The average energy release in fission $\langle E_r \rangle$ is given exactly by

$$\langle E_r \rangle = \frac{\sum_{A_H} Y(A_H)\, E_r(A_H)}{\sum_{A_H} Y(A_H)} \quad , \qquad (6)$$

where $Y(A_H)$ is the fission-fragment mass-yield distribution, A_H is the heavy-fragment mass number, and $E_r(A_H)$ is the average energy release for a given mass division. It is, in turn, obtained by summing the contributions from all participating charge divisions, namely

$$E_r(A_H) = \frac{\sum_{Z_H} \rho(Z_H, A_H)\, E_r(Z_H, A_H)}{\sum_{Z_H} \rho(Z_H, A_H)} \quad , \qquad (7)$$

where $\rho(Z_H,A_H)$ is the heavy fission-fragment charge distribution, Z_H is the heavy-fragment atomic number, and $E_r(Z_H,A_H)$ is the energy release for a given mass and charge division.

We use the fission-fragment mass-yield distribution $Y(A_H)$ measured by Weber et al.[38] and assume the fission-fragment charge distribution $\rho(Z_H,A_H)$ to be of Gaussian form,

$$\rho(Z_H,A_H) = \frac{1}{(2\pi\sigma_z^2)^{1/2}}\exp[-(Z_H-ZP_H)^2/(2\sigma_z^2)], \tag{8}$$

with the most probable heavy-fragment charge ZP_H given by

$$\frac{ZP_H + c}{A_H} = \frac{Z}{A} = \frac{ZP_L - c}{A_L} \tag{9}$$

In this equation, we use the value of 0.5 charge units determined by Unik et al.[35] for the charge division parameter c, except for symmetric fission, where c = 0. We also use a value of 0.5 charge units for the width σ_z, which is approximately midrange in the set of values determined by Wahl[39] in studies of fission-product charge distributions.

With these parameters, we perform the full integration and obtain a value for $\langle E_r \rangle$ of 218.886 MeV. Our calculations of the spectrum corresponding to those obtained with the seven-point approximation, but using the full integration instead, are summarized in the fifth and sixth lines of Table VIII and are compared with experiment in Figs. 19 and 20. These figures show that, although both calculations agree fairly well with experiment #7 of Boldeman et al.,[37] the energy-dependent cross-section calculation is preferred. However, this spectrum is itself somewhat hard in the tail region and somewhat soft in the peak region. It thus appears that some further adjustment is necessary in our calculations of the spectrum. The clue to this adjustment is found by studying also the average prompt neutron multiplicity $\bar{\nu}_p$, which we calculate simultaneously with N(E).

The average prompt neutron multiplicity is given in Ref. 28 by

$$\bar{\nu}_p = \frac{\langle E^* \rangle - \langle E_\gamma^{tot} \rangle}{\langle S_n \rangle + \langle \varepsilon \rangle} , \tag{10}$$

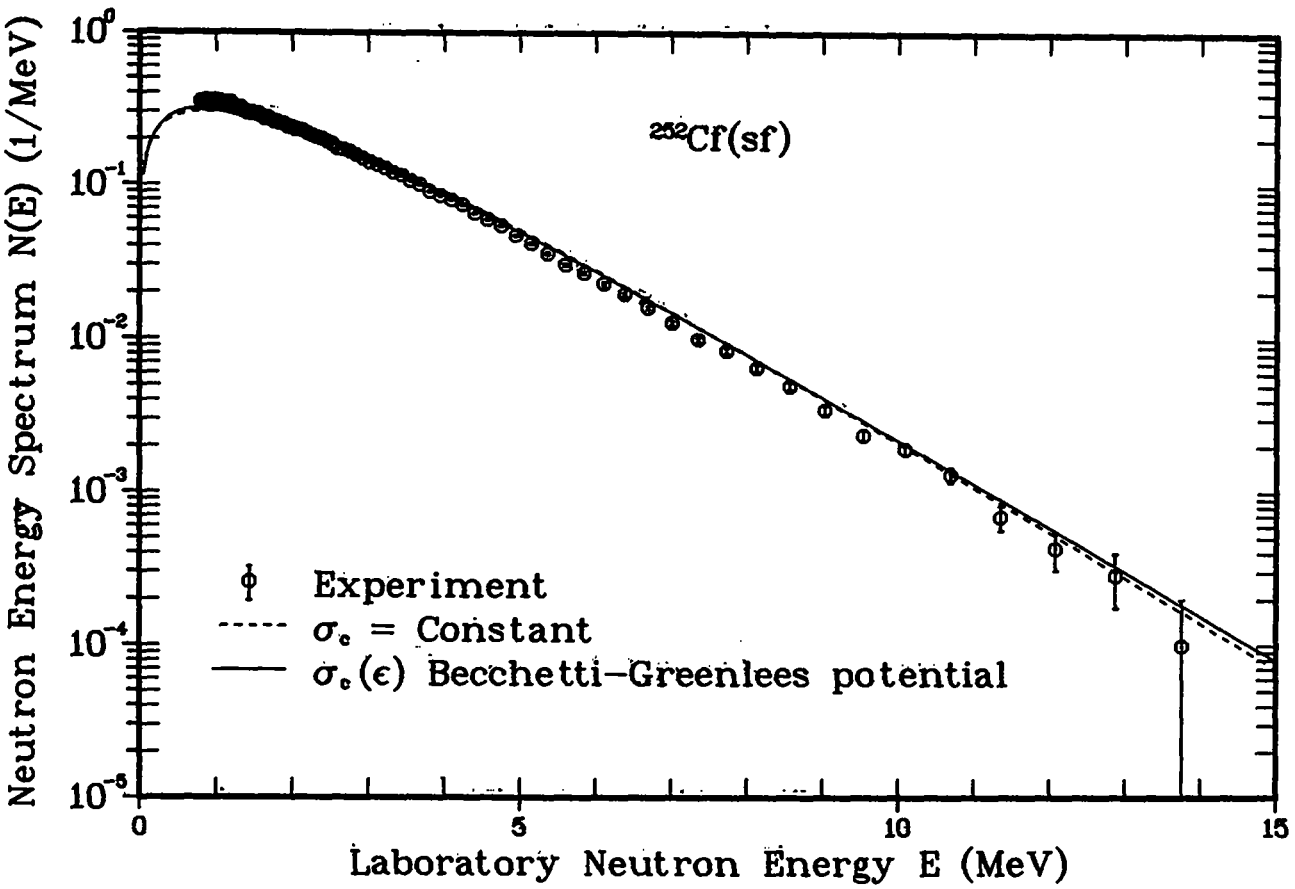

Fig. 19. Prompt fission neutron spectrum for the spontaneous fission of ^{252}Cf. The dashed curve gives the spectrum calculated for a constant cross section, using T_m = 1.444 MeV resulting from Eq. (5), whereas the solid curve gives the spectrum calculated with energy-dependent cross sections, using T_m = 1.200 MeV resulting from Eq. (4). For both calculated spectra, the values of E_f^L and E_f^H are 0.984 and 0.553 MeV, respectively. The experimental data are from experiment #7 of Boldeman et al. (Ref. 37). The potential is that of Becchetti and Greenlees (Ref. 36).

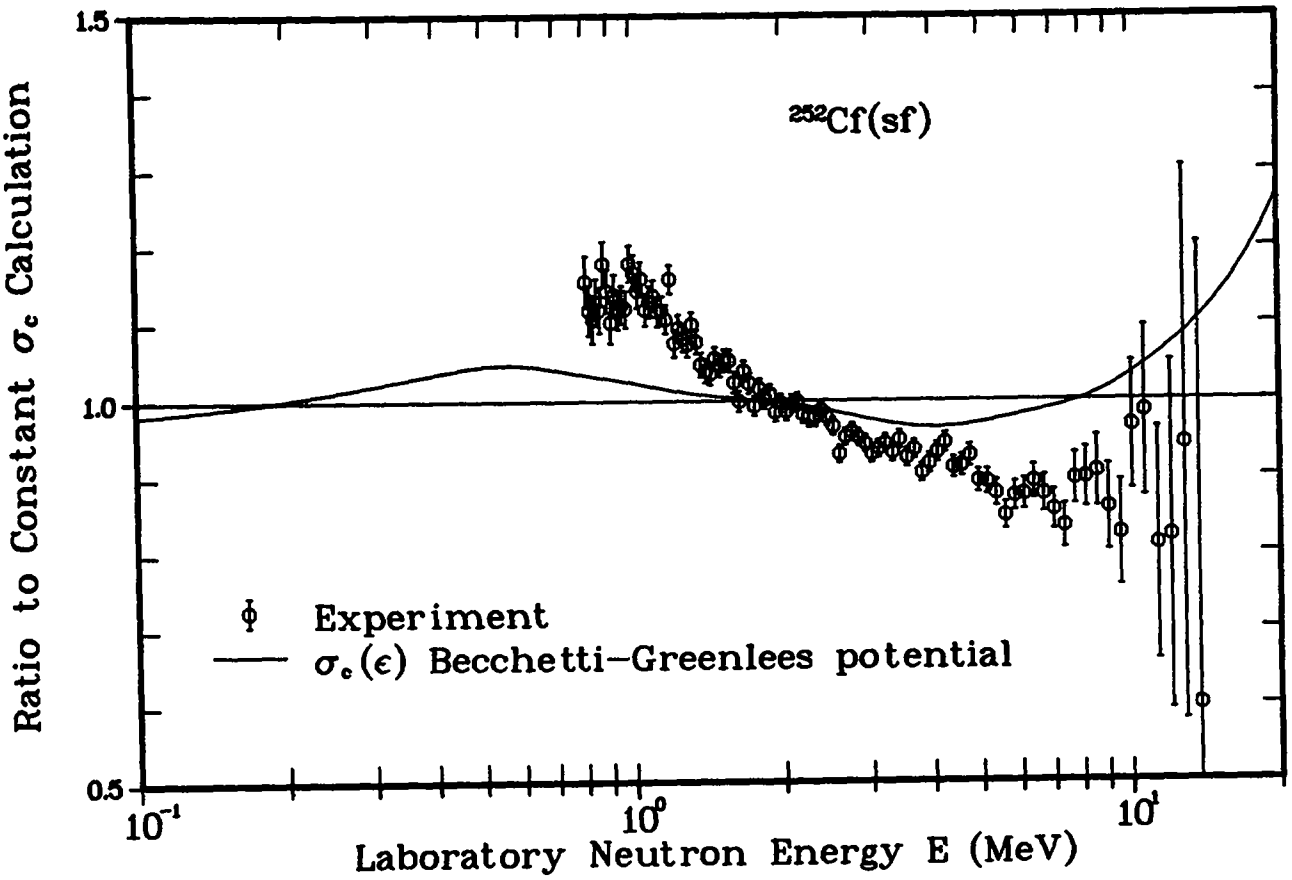

Fig. 20. Ratio of the spectrum calculated using energy-dependent cross sections and the experimental spectrum to the spectrum calculated using a constant cross section, corresponding to the curves shown in Fig. 19. The potential is that of Becchetti and Greenlees (Ref. 36).

where $\langle E_\gamma^{tot} \rangle$ is the measured total average prompt gamma energy, $\langle S_n \rangle$ is the average fission-fragment neutron separation energy, and $\langle \varepsilon \rangle$ is the average center-of-mass energy of the emitted neutrons. For the energy-dependent cross-section calculation, $\langle \varepsilon \rangle$ is calculated numerically using the center-of-mass spectrum, whereas for the constant cross-section calculation, $\langle \varepsilon \rangle$ is given by $(4/3)T_m$.

For spontaneous fission, the total average fission-fragment excitation energy $\langle E^* \rangle$ is given by Eq. (3). Thus, for a fixed value of $\langle E_f^{tot} \rangle$, $\bar{\nu}_p$ is very sensitive to the average energy release $\langle E_r \rangle$. It is also sensitive to the value of $\langle S_n \rangle$ because the average center-of-mass neutron energy $\langle \varepsilon \rangle$ is only about $0.2\langle S_n \rangle$. Moreover, because only $\langle \varepsilon \rangle$ in Eq. (10) depends on the level-density parameter, $\bar{\nu}_p$ is largely insensitive to the value of a. This is in contrast to Eq. (2) for T_m, which is sensitive to both $\langle E_r \rangle$ and a for a fixed value of $\langle E_f^{tot} \rangle$.

Thus, unsatisfactory agreement between calculated and measured N(E) means that $\langle E_r \rangle$ and/or a are in error, whereas unsatisfactory agreement between calculated and measured $\bar{\nu}_p$ means that $\langle E_r \rangle$ and/or $\langle S_n \rangle$ are in error. Therefore, a good calculation of $\bar{\nu}_p$ imposes a constraint on the corresponding N(E) calculation in that only the level-density parameter a is free to be adjusted.

Our calculations of $\bar{\nu}_p$ corresponding to the use of the seven-point approximation to calculate $\langle E_r \rangle$ are summarized in the first four lines of Table VIII. In these calculations, $\langle S_n \rangle$ is also calculated using the seven-point approximation. We use the value $\langle E_\gamma^{tot} \rangle = 6.95$ MeV given by Hoffman and Hoffman.[40] The calculated values of $\bar{\nu}_p$ are to be compared with the experimental value of 3.757 ± 0.009 obtained from the measurements of Amiel[41] and Smith,[42] or the value of 3.773 ± 0.007 measured by Spencer et al.[43]

The first two calculations of $\bar{\nu}_p$ agree with experiment to within approximately 1%, whereas the second two are more than 5% low. On the other hand, the second two calculations of N(E) are closer to experiment than are the first two. From the four $\bar{\nu}_p$ calculations, their corresponding values of $\langle E_r \rangle$ and $\langle S_n \rangle$, and experiment, we conclude that the calculated values of $\langle E_r \rangle$ are probably not excessively high. From the four N(E) calculations, their corresponding values of $\langle E_r \rangle$ and a, and experiment, we conclude that $\langle E_r \rangle$ is somewhat high and/or a is somewhat low. Taking these conclusions together, we infer that the level-density parameter a is somewhat low.

However, before acting on this inference, we test it by repeating the third and fourth calculations of $\bar{\nu}_p$ contained in Table VIII, except that we

again perform the full integration for $\langle E_r \rangle$, given by Eqs. (6) and (7), instead of using the seven-point approximation. Similarly, we perform the full integration to obtain $\langle S_n \rangle$. Indeed, with the full integration technique we are able to calculate the average prompt neutron multiplicity as a function of mass division, $\bar{\nu}_p(A_H)$, and integrate this quantity over the fragment mass-yield distribution to obtain $\bar{\nu}_p$ with greater accuracy. Thus,

$$\bar{\nu}_p(A_H) = \frac{\langle E_r(A_H) \rangle - \langle E_f^{tot}(A_H) \rangle - \langle E_\gamma^{tot}(A_H) \rangle}{\langle S_n(A_H) \rangle - \langle \varepsilon(A_H) \rangle} \quad (11)$$

and

$$\bar{\nu}_p = \frac{\sum_{A_H} Y(A_H)\, \bar{\nu}_p(A_H)}{\sum_{A_H} Y(A_H)} \quad . \quad (12)$$

In these equations, we use the experimental results of Weber et al.[38] for $\langle E_f^{tot}(A_H) \rangle$ and $Y(A_H)$, except that the $\langle E_f^{tot}(A_H) \rangle$ are renormalized to the value $\langle E_f^{tot} \rangle = 185.9$ MeV. We use the experimental results of Pleasonton et al.* for $\langle E_\gamma^{tot}(A_H) \rangle$ and we calculate $\langle \varepsilon(A_H) \rangle$ in the constant cross-section approximation, namely $(4/3)T_m(A_H)$.

Our calculations using the full integration for $\langle E_r \rangle$, $\langle S_n \rangle$, and $\bar{\nu}_p$ are summarized in the fifth and sixth lines of Table VIII. As in the case of $\langle E_r \rangle$, discussed earlier, the new value of $\langle S_n \rangle$ lies between those obtained in the two previous sets of calculations. The two values of $\bar{\nu}_p$ calculated using Eq. (10) are approximately 1% smaller than experiment. The more accurate calculation of $\bar{\nu}_p$, given by Eq. (12), is 1.1% less than the experimental value of 3.757. As discussed earlier, the corresponding spectra are somewhat hard in the tail region and somewhat soft in the peak region compared with experiment #7 of Boldeman et al.[37] We conclude that with full integrations to obtain the average energy release $\langle E_r \rangle$ and the average fragment neutron separation energy $\langle S_n \rangle$, the nuclear level-density parameter a is still somewhat low. We therefore perform a least squares adjustment to the spectrum of experiment #7 of

*F. Pleasonton, R. L. Ferguson, and H. W. Schmitt, Oak Ridge National Laboratory, provided this information in April 1982.

Boldeman et al.,[37] with respect to the value of the nuclear level-density parameter, and recalculate N(E) and $\bar{\nu}_p$. Using these results, we also calculate $\bar{\nu}_p(A_H)$.

We perform two least squares adjustments to the experimental spectrum. The first is performed using the energy-dependent cross-section calculation, with the level-density parameter given initially by Eq. (4), and the second is performed using the constant cross-section calculation, with the level-density parameter given initially by Eq. (5). To obtain an absolute value of χ^2, the normalization of the experiment is recalculated for each iteration in the value of the level-density parameter. In these calculations an iteration is taken as an increment of 0.1 MeV in the denominator of Eq. (4) or Eq. (5).

For the energy-dependent cross-section case, χ^2_{min} (per degree of freedom) occurs for a = A/(9.6 MeV) and has a value of 4.37. For the constant cross-section case, χ^2_{min} occurs for a_{eff} = A/(8.4 MeV) and has a value of 7.49. In both least squares adjustments, the level-density parameter corresponding to χ^2_{min} has increased somewhat, relative to its initial value given by Eq. (3) or Eq. (5).

Our calculations of N(E) and $\bar{\nu}_p$ using the least squares adjusted level-density parameters are summarized in the seventh and eighth lines of Table VIII and are illustrated in Figs. 21 and 22. The energy-dependent cross-section calculation clearly agrees better with experiment than does the constant cross-section calculation, as expected from the ratio 1.7 in the values of χ^2_{min} for the two cases. Despite the clear preference of the energy-dependent cross-section calculation, the average energies for the two cases are almost identical, as are the corresponding values of $\bar{\nu}_p$ calculated using Eq. (10). The average energies are, however, approximately 30 keV larger than the average value 2.136 MeV obtained by Boldeman et al.[37] in a Maxwellian fit to several experiments, whereas the values of $\bar{\nu}_p$ are well within 1% of the experimental value 3.757 ± 0.009 due to Amiel[41] and Smith[42] and the experimental value 3.773 ± 0.007 obtained by Spencer et al.[43]

Our most accurate calculation of $\bar{\nu}_p$, using Eq. (12), yields a value of 3.783 that differs from the former experimental result by 0.7% and differs from the latter experimental result by 0.3%. The decomposition of this calculated value into $\bar{\nu}_p(A_H)$, by use of Eq. (11), is shown in Fig. 23, where the calculated values are compared with the experimental data of Walsh and Boldeman,[44] which have been renormalized to the value 3.757 for $\bar{\nu}_p$. The calculation and

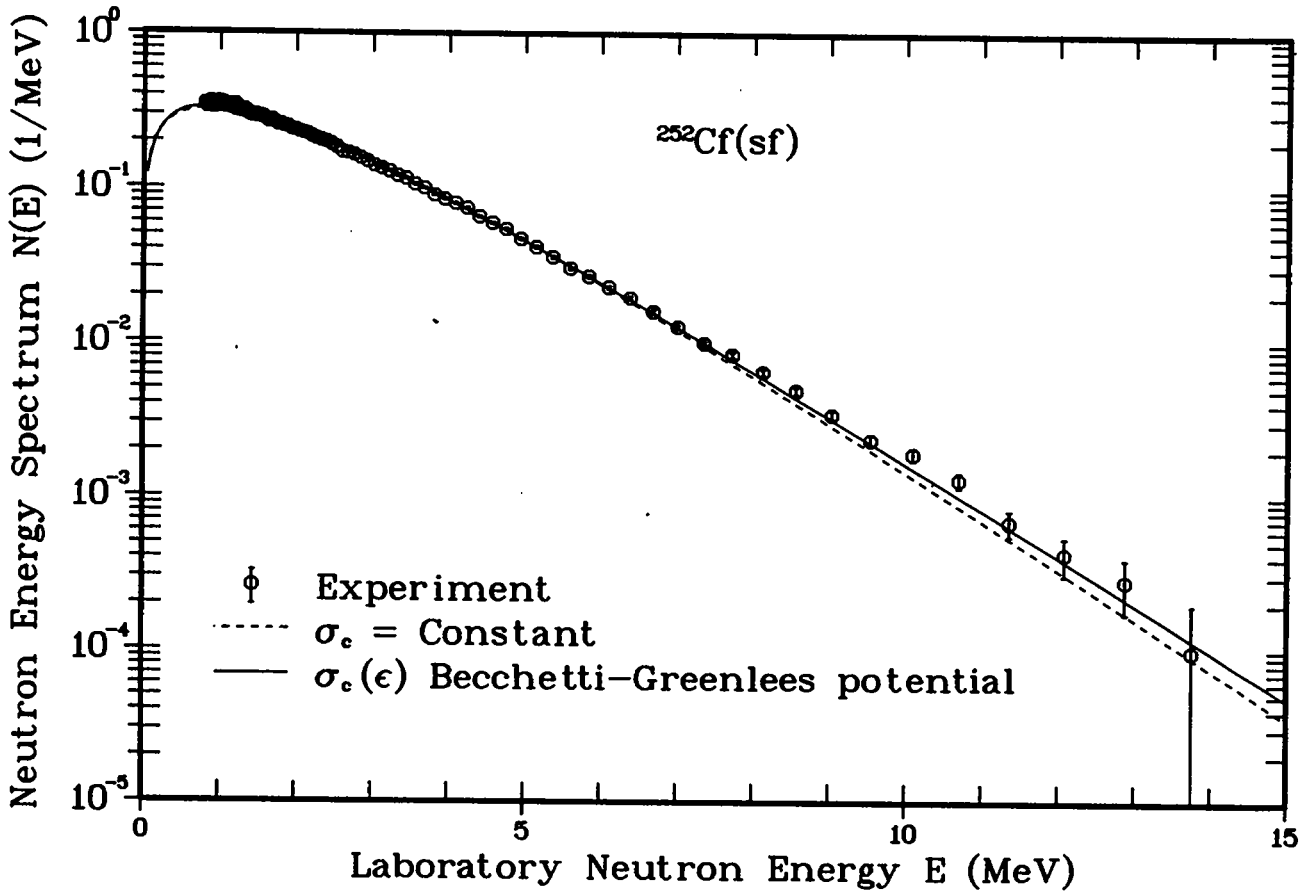

Fig. 21. Prompt fission neutron spectrum for the spontaneous fission of ^{252}Cf. The dashed curve gives the spectrum calculated for a constant cross section, using T_m = 1.049 MeV resulting from the least squares adjustment with a $_{eff}$ = A/(8.4 MeV), whereas the solid curve gives the spectrum calculated for an energy-dependent cross section, using T_m = 1.121 MeV resulting from the least squares adjustment with a = A/(9.6 MeV). For both calculated spectra, the values of E_f^L and E_f^H are 0.984 MeV and 0.553 MeV, respectively. The experimental data are from experiment #7 of Boldeman et al. (Ref. 37). The potential is that of Becchetti and Greenlees (Ref. 36).

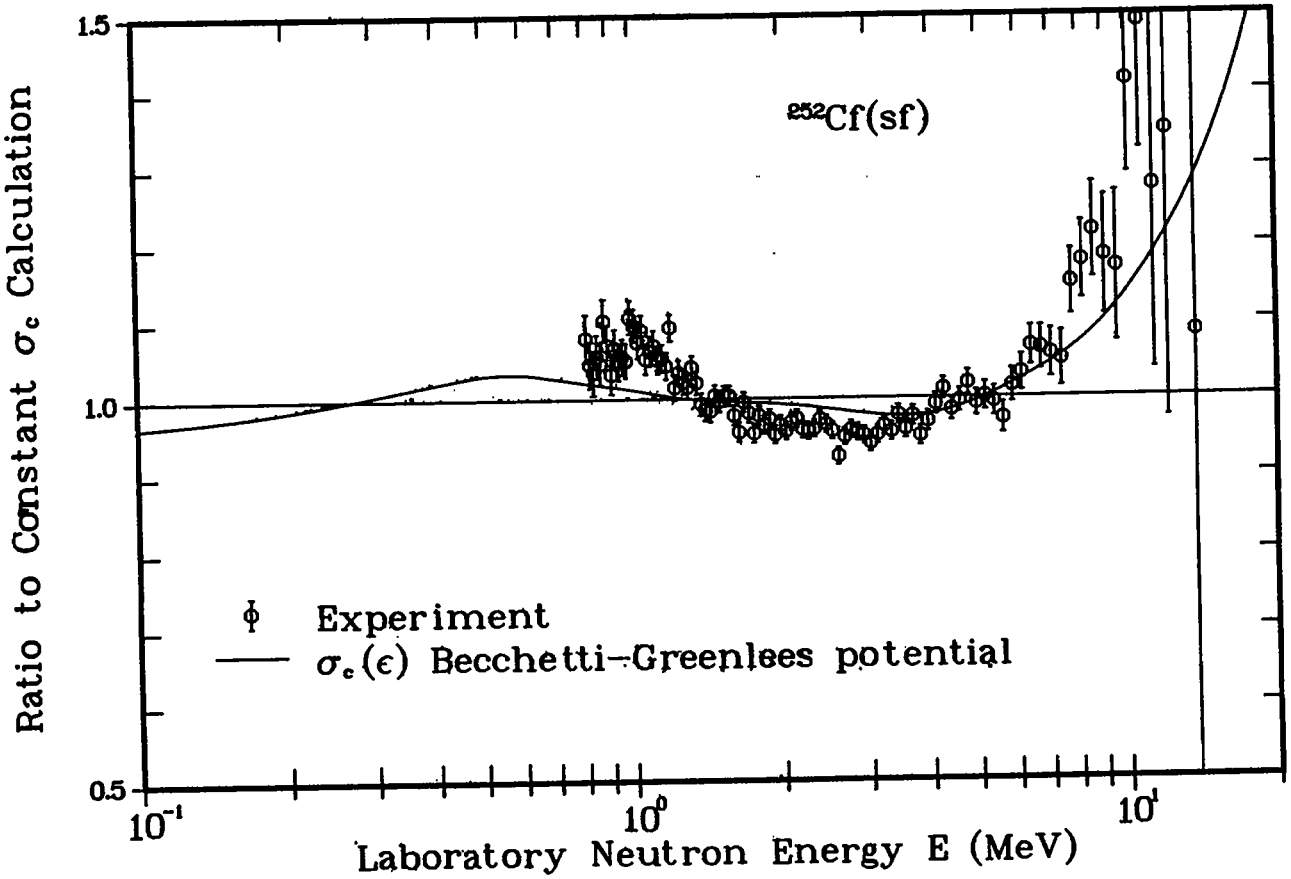

Fig. 22. Ratio of the spectrum calculated using energy-dependent cross sections and the experimental spectrum to the spectrum calculated using a constant cross section, corresponding to the curves shown in Fig. 21. The potential is that of Becchetti and Greenlees (Ref. 36).

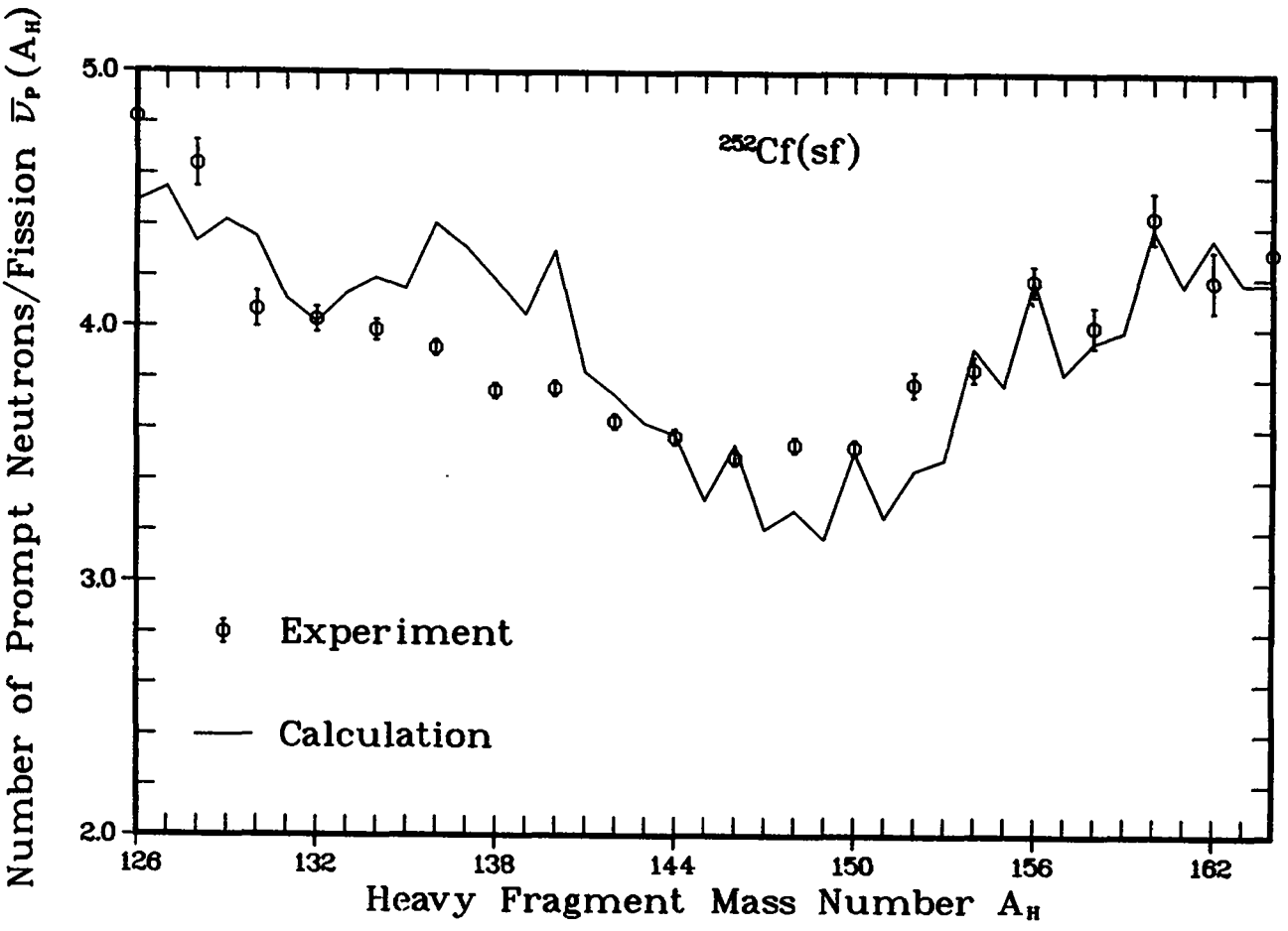

Fig. 23. Average prompt neutron multiplicity as a function of the heavy-fragment mass for the spontaneous fission of ^{252}Cf. The calculation is performed with Eq.(11), using a_{eff} = A/(8.4 MeV) resulting from the least squares adjustment to the spectrum calculated for a constant cross section. The experimental data are those of Walsh and Boldeman (Ref. 44). Note the suppressed zero of the vertical scale.

experiment agree very well in the peaks and wings of the fragment mass distribution, but discrepancies as large as 15% occur near A_H = 138, where the descent into the valley is well under way. It is clear from the figure that even better agreement of the integral of $\bar{\nu}_p(A_H)$ with experiment can be achieved if refinements to the calculation of $\bar{\nu}_p(A_H)$ are made. A more detailed discussion of our results is given in Ref. 45.

M. New Fission Neutron Spectrum Representation for ENDF (D. G. Madland)

The new representation[28] of the prompt fission neutron spectrum proposed[46] for use in the Evaluated Nuclear Data File (ENDF) has been accepted* by the Cross Section Evaluation Working Group (CSEWG) for such use commencing in June 1983.

The new representation consists of the closed-form theoretical expression for the spectrum given in Ref. 28. This expression results from the constant cross-section approximation for the process inverse to neutron emission, namely compound-nucleus formation. Three constants are required in the evaluation of the spectrum. Detailed discussions and recommendations on the evaluation of the constants are given in Refs. 28 and 46. An example of the ENDF format for the new spectrum representation is given in Ref. 46.

II. NUCLEAR CROSS-SECTION PROCESSING AND TESTING

A. NJOY Code Development (R. E. MacFarlane, D. W. Muir, and R. M. Boicourt)

In late 1981, NJOY(10/81) was released, and since then there has been a steady growth in the size of the NJOY user community. NJOY is now in use in at least 20 different research installations, including several in foreign countries. Feedback from the users has been very helpful in locating minor errors in the released (10/81) version of the code. Corrections have been communicated back to the users through a series of "NJOY Notes." The third note in this series was issued in September 1982. (Persons interested in being placed on the mailing list to receive existing and future Notes should contact the code authors.)

Many of the recent code changes are needed only to suppress IBM compiler diagnostics. Another change was necessary to prevent a possible infinite loop in GAMINR. A large block of comment cards was added to the DTFR plotting routines in order to better explain the function of certain local Los Alamos subroutines called by DTFR.

The remaining changes fix actual errors or improve numerical precision on IBM machines. Two different errors were found in the routines that process ENDF/B photon transition probability arrays. In ENDF/B-V, this format is used only for Cl, K, Eu-151, and Eu-153. A problem with SCANA led to occasional

*Minutes to the Cross Section Evaluation Working Group (CSEWG), Formats Subcommittee Meeting, May 20, 1982, Brookhaven National Laboratory, available through Raphael J. LaBauve, Los Alamos National Laboratory.

errors with threshold reactions in GROUPR. In CCCCR, the IFOPT = 2 option, which prints out scattering matrices by Legendre order, now works. The small P_3 scattering cross sections for heavy isotopes have been improved somewhat by using double precision for the angular integration in GETFF. The IBM results still do not exactly satisfy the sum rule that says that the total laboratory P_3 scattering should be zero for reactions specified as isotropic in the center-of-mass frame. The calculation of the LAW=7 representation of the fission spectrum has also been improved for IBM machines. The previous version would give small random numbers (sometimes even negative) at low emission energies. Finally, in order to make sure that energies are within the integration panel (see PANEL in GROUPR and GPANEL in GAMINR), it is necessary that RNDOFF*DELTA be slightly less than 1. The choice of DELTA=.999 999 5 and RNDOFF=1.000 000 4 satisfies this criterion for REAL*4 variables on IBM machines.

A new IBM version (10/81-3I) of the entire code system, which contains all of the corrections discussed above, has been sent to the code centers. The corresponding code changes have also been supplied in the form of CDC UPDATE directives for users with CDC computer systems.

B. Covariance Processing (D. W. Muir, R. E. MacFarlane, and R. M. Boicourt)

The ERRORR covariance processing module (Ref. 47, pp. 39-46) of NJOY has been modified extensively in recent months and now treats all approved ENDF/B-V formats. Recent work has centered on the full implementation of the capability to process "ratio-to-standard" covariance data. Such data have had an approved format for several years, and ratio covariances appear in six ENDF/B-V evaluations (^{10}B, ^{235}U, ^{238}U, ^{239}Pu, ^{241}Am, and ^{242}Pu). Also now fully implemented are two recent format modifications, namely, "lumped-partial" covariances and a new covariance "law," LB=6. The extended ERRORR module is compatible with the distributed (10/81) version of NJOY. Because of the large number of code changes, users who are interested in these new capabilities should request a replacement source deck for the entire ERRORR module.

In order to describe the new ratio-data capability, it is useful to first review the general problem. Let $x(E_x)$ be the value of the cross section for reaction "x" at energy E_x, and $y(E_y)$ the cross section for reaction "y." (Reactions x and y may or may not be distinct.) In some energy region (L_x, H_x), suppose that the best knowledge of $x(E_x)$ is obtained through the application of a measured ratio, $f(E_x)$;

$$x(E_x) = f(E_x)\, z(E_x), \text{ if } L_x \leq E_x \leq H_x, \tag{13}$$

where $z(E_x)$ is an official ENDF/B standard cross section throughout the energy region (L_x, H_x). Similarly, suppose y is derived from the same standard, over a possibly different energy range,

$$y(E_y) = g(E_y)\, z(E_y), \text{ if } L_y \leq E_y \leq H_y. \tag{14}$$

By applying the propagation-of-errors formula, one can obtain an expression for the contribution to the relative covariance $\text{relcov}[x(E_x), y(E_y)]$ that is attributable to the ratio measurements. In the usual case, where the ratios f and g are only weakly correlated with the standard cross section z, the result is quite simple:

$$\text{relcov}[x(E_x), y(E_y)]_{\text{ratio}} = \text{relcov}[f(E_x), g(E_y)] + \text{relcov}[z(E_x), z(E_y)] \tag{15}$$

if $L_x \leq E_x \leq H_x$ and $L_y \leq E_y \leq H_y$, and

$$\text{relcov}[x(E_x), y(E_y)]_{\text{ratio}} = 0 \tag{16}$$

otherwise.

Thus, in this fairly common evaluation situation, the covariance separates naturally into a part involving only the ratio data itself and a part involving only the standard. Because the second contribution, cov(z,z), can be read directly from the evaluation for the standard, it is not included explicitly in the ENDF/B covariance subsections for the derived quantities, cov(x,x) or cov(x,y). Instead, the existence of this contribution to the covariance is signalled by the presence of a very short block of data, an "NC-type" sub-subsection, containing only the material number and reaction identifier of z and a few other items.

The strategy adopted for processing this information in the ERRORR module is to load the explicit covariance information from the evaluation of the

standard into the same storage array that is used to store explicit covariances from the evaluation for reaction x. From that point on, the data from the standard is handled just as if it had come from the evaluation for x, but with one exception. As indicated by Eq. (16), the covariance contribution cov[$z(E_x)$, $z(E_y)$] is <u>not</u> added into the total covariance matrix for the current reaction pair if either E_x or E_y lies outside the corresponding energy "window" (L_x, H_x) or (L_y, H_y).

In addition to identifying the standard reaction, the "NC-type" sub-subsection contains a control parameter LTY and two energies EL and EH whose significance depends on LTY. LTY is used to identify particular evaluation scenarios, such as when reaction x is the same as reaction y (or, at least, they are derived from z over the same energy range) (LTY=1), y is identical to the standard (LTY=2), or x is identical to the standard (LTY=3). A fourth possibility, namely, that x, y, and z are entirely distinct, cannot presently be treated with a single NC-type sub-subsection; that is, there is no LTY-value defined for this case. However, as discussed later, it is still possible to process covariances for this situation by combining information from sub-subsections in two different evaluations. For convenience, we shall refer to this fourth case as LTY=4.

The interrelationship of LTY, EL, EH, and the windows (L_x, H_x) and (L_y, H_y) used in ERRORR for the "zeroing-out" operation, Eq. (16), is summarized below.

LTY = 1

$(L_x, H_x) = (L_y, H_y) = (EL, EH)$

LTY = 2

$(L_x, H_x) = (EL, EH)$

$(L_y, H_y) = (10^{-5}$ eV, 20 MeV)

LTY = 3

$(L_x, H_x) = (10^{-5}$ eV, 20 MeV)

$(L_y, H_y) = (EL, EH)$

LTY = 4

$(L_x, H_x) = (EL, EH)$

$(L_y, H_y) = (EL', EH')$

If the user requests covariance data cov(x,y), where x and y are different and both are distinct from the standard (LTY=4), the ERRORR module obtains (EL,

EH) from the LTY=2 subsection in the evaluation for x that "points" to z. Then the covariance file for z is read to obtain both (a) the explicit covariances cov(z,z) and (b) the second energy window (EL', EH'), the latter being found in the LTY=3 sub-subsection that "points" back to y.

Table IX lists all ENDF/B-V reactions that contain ratio-to-standard covariance data. The symbols entered in the reaction-by-reaction matrix indicate which reactions are referenced as standards (*) and which reaction pairs have implicit nonzero covariances (LTY). The new version of ERRORR will produce multigroup covariances for any of the reaction pairs in Table IX that are marked with (*) or (LTY). The cross-material covariances (LTY=2, 3, or 4) must be requested individually using the IREAD=2 option (see Ref. 48). An attempt to process covariances for any of the cases LTY=1 through 4 without supplying a separate ENDF/B tape containing the needed standard will result in an error stop. The user input needed to specify the unit number of the standard tape, as well as that required to process the LTY=4 case, is described in the comment cards located at the beginning of the new version of the module.

TABLE IX

COVARIANCE MATRICES AFFECTED BY RATIO MEASUREMENTS IN ENDF/B-V

	$^{10}B(n,\alpha)$	$^{238}U(n,\gamma)$	$^{235}U(n,f)$	$^{239}Pu(n,f)$	$^{239}Pu(n,\gamma)$	$^{241}Am(n,f)$	$^{242}Pu(n,f)$
$^{10}B(n,\alpha)$	*	3					
$^{238}U(n,\gamma)$	2	1					
$^{235}U(n,f)$			*	3	3	3	3
$^{239}Pu(n,f)$			2	1	1	4	4
$^{239}Pu(n,\gamma)$			2	1	1	4	4
$^{241}Am(n,f)$			2	4	4	1	4
$^{242}Pu(n,f)$			2	4	4	4	1

* = standard

Integer = LTY value (see text)

As an example of the new capabilities of ERRORR, in Fig. 24 are shown the covariances between the fission cross sections of ^{239}Pu (x) and the important actinide ^{241}Am (y). This is an LTY=4 case where (L_x, H_x) = (0.2 MeV, 15 MeV) and (L_y, H_y) = (0.2 MeV, 20 MeV). The effect of the use of two different windows is apparent in the lower right corner of the correlation matrix.

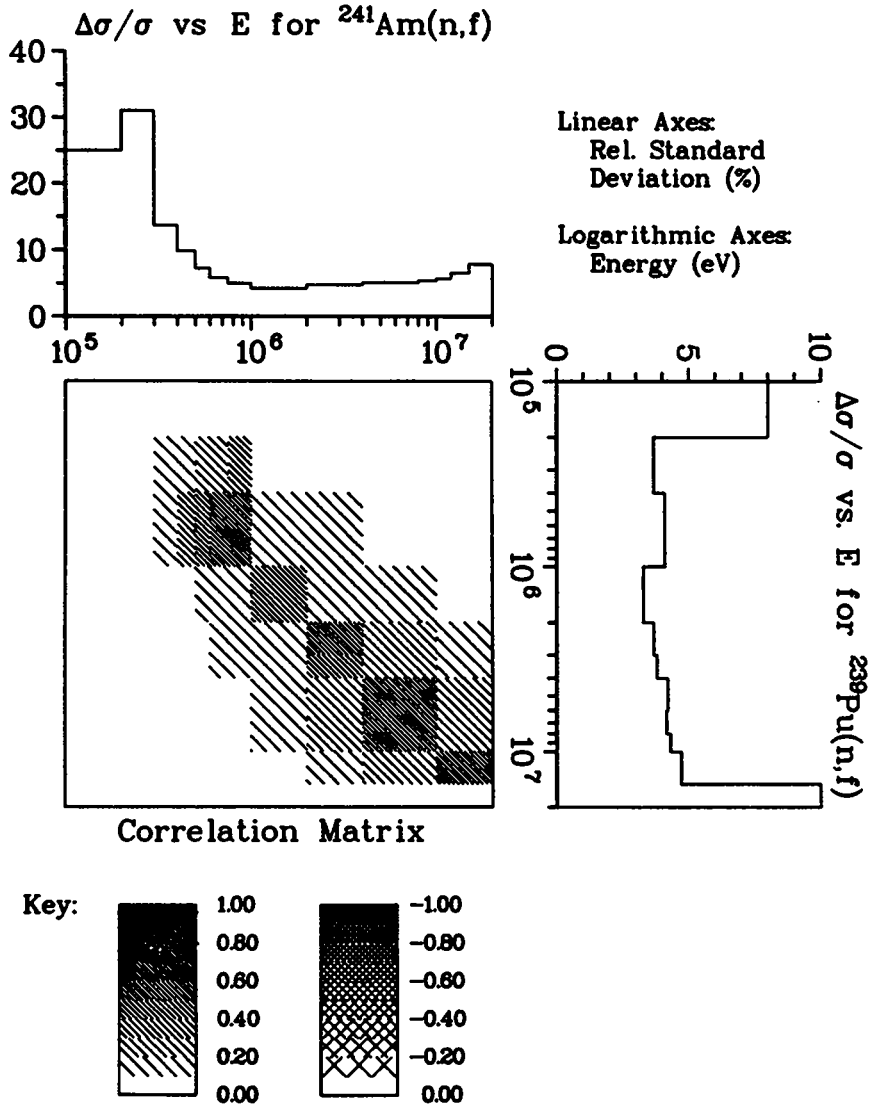

Fig. 24. Covariance data for $^{239}Pu(n,f)$ with $^{241}Am(n,f)$.

C. Fast Reactor Code Development (R. E. MacFarlane)

The MAX system for generating space-and-energy self-shielded macroscopic cross sections for fast reactor analysis is based on a cross-section module (TRANSX), a one-dimensional transport module (ONEDA), and several smaller codes used for manipulating libraries and cross sections. In order to check for transportability, we converted these modules to run on the VAX minicomputer at Los Alamos. This shares a 32-bit word size with the IBM machines and has a FORTRAN-77 compiler. It was possible to generate a single program for each module, which can be changed from CDC to VAX (or IBM) using comment cards (CCDC, CIBM) to control a preprocessing program. Some basic functions had to be segregated into machine-dependent subroutine libraries. However, some of the new features of FORTRAN-77 were avoided for compatibility (for example, CHARACTER, block-IF).

The MATXS cross-section format used with MAX currently stores fission matrices as square arrays. This is inefficient for most fine-group structures because the shape of the fission spectrum does not change with incident energy at low energies. The problem is especially severe for libraries with many thermal groups. One partial solution to this problem has been incorporated into the latest 80-group MATXS library and into TRANSX. The fission matrix is used at high energies as though there were a threshold. The remaining "slow fission" is represented as a "$\nu\sigma_f$" vector with zeros for the groups given in the matrix, and a "χ" vector that contains the normalized spectrum for slow fission. The boundary between the two regions is selected automatically by comparing the shapes of the fission spectra for each incident-energy group.

This representation does not require a change in the MATXS format, and it is easy to process. However, it does not account for similar inefficiencies in storing capture and fission photon production matrices. A more general solution will be incorporated into a future version of the MATXS format.

D. Thermal Reactor Codes and Libraries (R. E. MacFarlane and R. M. Boicourt)

Two new versions of EPRI-CELL have been received. One is the new standard CDC version, assembled by R. Mosteller at S. Levy, Inc., from the accumulated contributions of many laboratories. The other is an IBM version prepared by R. Q. Wright at Oak Ridge National Laboratory. These two versions have been combined into a single program using CIBM and CCDC cards to allow automatic

preparation of versions for both systems. Some tidying and simplification were done during this process. The resulting codes have been tested at Los Alamos on both CDC-7600 and VAX 11/80 machines to prove transportability.

The EPRI-CELL code uses four-group cross sections to calculate the absorption due to the many fission products that appear in a reactor as the fuel is burned. The coarse representation is most accurate if the four-group numbers are prepared using a spectrum similar to that in the reactor of interest. However, this spectrum varies with reactor composition and geometry, and the spectrum also varies with time. In EPRI-CELL, an attempt is made to change the cross sections to simulate the effects of the spectral changes by assuming that all cross sections behave in the same way the 1/v cross sections behave.

In order to check this assumption, we made EPRI-CELL runs for a conventional pressurized water reator (PWR) and for the same composition with an increased lattice pitch (that is, with a higher water-to-fuel ratio). Cross sections were collapsed for two different time steps of each run using TOAFEW.[49] Figure 25 shows the flux for the normal PWR case compared with the LWR weight function used in NJOY. Tables X and XI show how the Group 3 (0.625 eV-5.5 keV) and Group 4 (0-0.625 eV) cross sections vary with time and pitch for the important absorbers. The data have already been corrected for 1/v effects using ONEV (thermal) or SPECRF (fast); therefore, the percentage differences represent errors in the correction schemes.

These results imply that the coarse-group scheme used in EPRI-CELL is accurate to about ± 1% in aggregate absorption, for situations close to the base case. It is of interest to determine the source of the biggest differences. Most of the problems above 0.625 eV are caused by ^{103}Rh, which has one large peak near 1 eV that interacts with ^{240}Pu absorption. Other epithermal problems can also be traced to prominent resonances that prevent the cross section from behaving as 1/v. In the thermal group, ^{151}Sm, ^{148m}Pm, and ^{237}Np are all non-1/v because of resonances at low energies.

The best way to improve the accuracy of the calculation of fission-product absorption would be to go to more than four groups. This approach would also provide a more realistic energy shape for the fission-product lump, thereby improving the flux calculation.

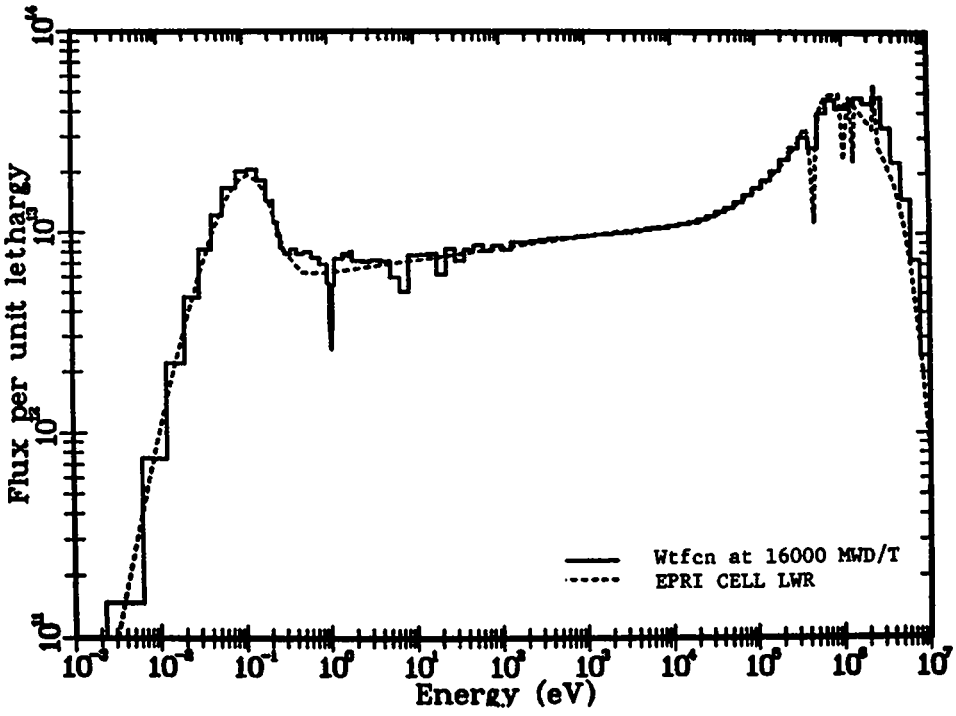

Fig. 25. Comparison of computer flux and NJOY LWR weight function for a typical PWR at midlife.

TABLE X

CHANGES IN EFFECTIVE GROUP 3 (0.625 eV-5.5 keV) ABSORPTION WITH TIME AND LATTICE PITCH

Nuclide	% of lump[a]	Base xsec[b]	Time[c]	Pitch[d]
Rh103	13.6	92.61	-4.2%	2.4%
Xe131	12.1	104.10	0.5	-0.5
Pm147	10.6	202.85	0.3	0.7
Cs133	10.2	33.86	0.3	0.4
Tc99	8.1	29.94	0.3	0.8
Sm152	7.6	230.77	0.9	0.3
Nd145	3.8	23.46	0.2	-0.4
Ag109	3.3	132.46	0.2	0.8
Eu109	3.3	142.08	-0.2	-0.3
SPECRF	---	0.8961	0.1	1.5

[a] Xe135 and Sm149 are treated separately.

[b] Normal PWR at 16 000 MWD/T.

[c] Same PWR at 32 000 MWD/T

[d] PWR with 5% higher pitch at 16 000 MWD/T.

TABLE XI

CHANGES IN EFFECTIVE GROUP 4 (BELOW 0.625 eV) ABSORPTION WITH TIME AND LATTICE PITCH USING SAME NOMENCLATURE AS TABLE X

Nuclide	% of lump	Base xsec	Time	Pitch
Nd143	21.8	318.43	0.1%	0.1%
Sm151	9.8	8113.70	4.4	1.3
Rh103	8.7	174.75	-0.7	-0.1
Pm148m	5.8	350542.00	-3.9	-0.3
Np237	3.6	233.13	2.5	-5.1
Xe131	3.6	91.43	-0.1	-0.0
Pm147	3.2	178.16	0.1	0.1

E. Multigroup Weighting Function Effects (R. B. Kidman)

This half-year we have initiated a program to quantify weighting function effects on multigroup constants and subsequent calculated results, and to investigate possible methods of automatically incorporating appropriate weighting function changes into the cross-section preparation process.

Multigroup constants are normally generated with some weighting function that we hope is only benignly different from the "actual" flux spectrum encountered in any particular problem. Some designers feel this may not be true, and they use different weighting functions to generate various sets of multigroup constants. For example, they may generate a "core" iron with their estimate of a corelike weighting function and a "reflector" iron with their estimate of a reflectorlike weighting function. Even though this solution requires a great deal more data (straining computer code capacities) and complicates code setup and execution, still it is possible to be unsure about the appropriateness of the weighting function for the cross sections in any particular region.

We wish to discover the minimal amount of additional data that would be required to allow adequate, real time interpolation of effective multigroup constants. A brief, preliminary model may aid in understanding and guiding this effort. Let Q_i represent some group-averaged quantity obtained with weighting function W_i, for example,

$$Q_i = \frac{\int W_i(E)Q(E)dE}{\int W_i(E)dE} \quad .$$

Let us further choose the W_i so that their differences are easily parameterized and with shapes that can easily simulate the resonance smoothed flux in the group. For example, assume the W_i are straight lines with slopes of S_i. Then a plot of Q_i vs S_i may (if nature is not perverse) be a smooth, gentle curve similar to the following:

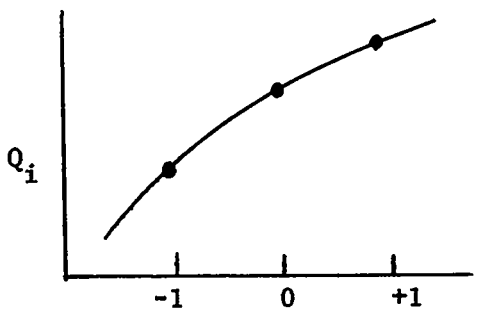

From the current flux iteration in a problem, it is simple to generate a reasonable estimate for the resonance smoothed flux slope, S, in any group. Then a proper estimate for Q for the next iteration can be obtained from the figure in the following manner:

$$Q = \sum_{i=1}^{3} Q_i \prod_{\substack{j=1 \\ j\neq 1}}^{3} \frac{S - S_j}{S_i - S_j} \quad , \text{ Lagrange interpolation,}$$

or, if uncertainties and sensitivities permit,

$$Q = Q_1 + \frac{Q_3 - Q_1}{S_3 - S_1}(S - S_1) \quad , \text{ straight-line interpolation.}$$

Our goal is to discover the simplest possible, but adequate, relation between Q and as few (Q_i, S_i) points as possible. (The two previous expressions are elucidative examples.) If all types of multigroup constants display complicated weighting function behavior throughout their energy ranges, then we are

not much ahead of the crude method mentioned earlier. However, even in this event, our method would perform the weighting function adjustments automatically and accurately.

We are optimistic that gentle behavior will be encountered because we are dealing with 80 groups and we know, ultimately, changes must cease as the number of groups increases.

Two-dimensional cross-section preparation codes are trying to rigorously accommodate regional spectra effects on cross sections. Unless multigroup constants are prepared specifically for each region (the crude method), such effects will be masked by weighting function errors. It seems a logical step to try to develop some automatic method for accommodating weighting function effects before we develop two-dimensional cross-section preparation codes. For the same accuracy in results, an automatic method could probably be judged useful if it costs less than an increased number-of-groups method.

Thus far, we have generated four sets of multigroup constants for ^{239}Pu: (a) based on a linear weighting function with slope = -1, (b) based on a constant weighting function, (c) based on a linear weighting function with slope = +1, (d) based on a 1/E weighting function. The results are being compared to determine if there is any basis for the automatic weighting function adjustment concept.

F. Integral Calculations of 21 Threshold and 6 Nonthreshold Reactions Calculated in 5 Representations of the ^{252}Cf Spontaneous Fission Spectrum Compared with Experimental Measurements (R. J. LaBauve, D. G. Madland, R. M. Boicourt, and D. W. Muir)

Five representations of the ^{252}Cf spontaneous fission spectrum were used as weighting functions in calculating integral cross sections for 6 nonthreshold and 21 threshold reactions for which good measurements are available. The ^{252}Cf spontaneous fission spectrum representations used include the NBS spectrum;[50] two Maxwellian fits to experimental spectra,[51,52] with Maxwellian temperatures of 1.439 and 1.424 MeV, respectively; and two Los Alamos theoretical models,[45] namely, an "exact theory" and an approximate model in closed form, which has been approved for use in ENDF.[46]

The NBS representation of the spectrum, $\chi(E)$, consists of five segments given by a reference Maxwellian $M_{Cf}(E)$ times a correction term $\mu(E)$ defined for each of five energy ranges as follows:

$\chi(E) = \mu(E)\, M_{Cf}(E)$, where

$M_{Cf}(E) = 0.6672\ \sqrt{E}\ \exp(-1.5E/2.13)$, E in MeV, and

from 0.0 to 0.25 MeV	$\mu(E) = 1 + 1.20E - 0.237$
from 0.25 to 0.8 MeV	$\mu(E) = 1 - 0.14E + 0.098$
from 0.8 to 1.5 MeV	$\mu(E) = 1 + 0.024E - 0.0332$
from 1.5 to 6.0 MeV	$\mu(E) = 1 - 0.0006E + 0.0037$
above 6.0 MeV	$\mu(E) = 1.0\ \exp[-0.03(E - 6.0)/1.0]$.

In Fig. 26 the NBS spectrum and the two Maxwellian spectrum representations are compared as ratios to the "exact" Los Alamos representation.

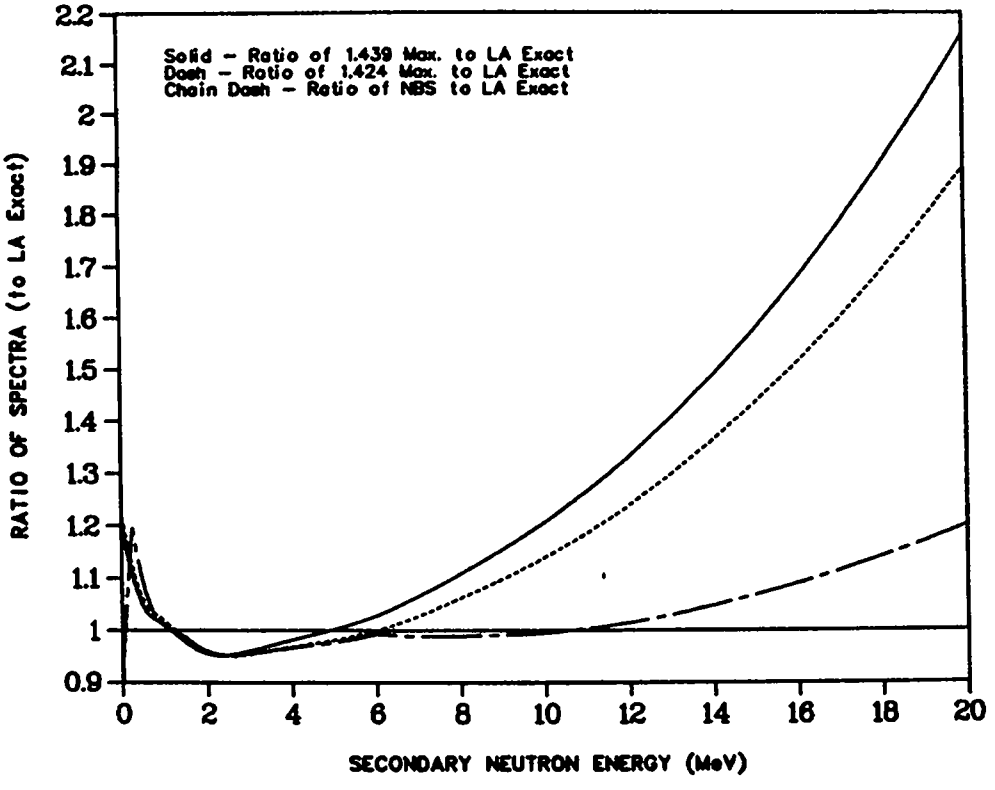

Fig. 26. Comparisons of the Cf-252 s.f. spectra.

Except for the $^{63}Cu(n,\gamma)$ reactions, referenced below, several accurate measurements of spectral indices of nonthreshold reactions in the ^{252}Cf spontaneous fission spectrum are discussed in Ref. 53. That is, the ratios of the integral cross sections in the ^{252}Cf spectrum for several reactions are given as ratios to the integral $^{238}U(n,f)$ cross section. These spectral indices can

be transformed into integral cross sections by using a value for the integral $^{238}U(n,f)$ cross section in the ^{252}Cf spectrum as measured by Gilliam.[54] The integral cross section values so derived can be directly compared with calculations using the two Maxwellian representations, the Los Alamos models, and the NBS representation of the spectrum. All microscopic cross sections used in the calculations are taken from the ENDF/B-V dosimetry file[55] and the processing of these data to get the integral cross sections is performed using the NJOY code.[56]

Results comparing these experimental values with those calculated in the NBS, the two Maxwellian, and the Los Alamos exact spectra are given in Table XII. Note from this table that, for these nonthreshold reactions, all spectra used as weighting functions in the integral calculations give reasonable agreement with experiment. For the two cases for which the calculations lie outside the 2-σ experimental error, namely, $^{62}Cu(n,\gamma)$ and $^{197}Au(n,\gamma)$, one suspects that either the evaluations for these reactions are defective or that the assigned experimental uncertainties are overly optimistic.

TABLE XII

INTEGRAL CROSS SECTIONS (MB) IN REPRESENTATIONS OF THE CF-252 SF SPECTRUM

REACTION	EFF THRESH E IN MEV	MEASURED VALUE (PCT ERROR)	(A) NBS FIT CALC	(A) NBS FIT C/E	(B) 1.439-MAX CALC	(B) 1.439-MAX C/E	(C) 1.424-MAX CALC	(C) 1.424-MAX C/E	(D) LA-ANT-EXACT CALC	(D) LA-ANT-EXACT C/E
63CU(N,G)	0.00	10.9500 (4.7)	9.6480	.88*	9.6680	.88*	9.7440	.89*	9.4490	.86*
238U(N,F)	0.00	319.0000 (2.5)	313.6000	.98	318.2000	1.00	315.2000	.99	324.1000	1.02
197AU(N,G)	0.00	81.0000 (2.3)	76.3100	.94*	76.2600	.94*	76.8800	.95*	73.7100	.91*
235U(N,F)	0.00	1205.0000 (2.2)	1236.0000	1.03	1239.0000	1.03	1239.0000	1.03	1236.0000	1.03
239PU(N,F)	0.00	1802.0000 (2.2)	1792.0000	.99	1794.0000	1.00	1793.0000	1.00	1798.0000	1.00
237NP(N,F)	0.00	1332.0000 (2.8)	1352.0000	1.02	1359.0000	1.02	1355.0000	1.02	1378.0000	1.03
		AVERAGE C/E -		.97		.98		.98		.97
		<E> IN MEV -	2.12		2.16		2.14		2.17	

* - CALCULATION OUTSIDE 2-SIGMA EXPERIMENTAL ERROR

Comparative results for the threshold reactions are shown in Table XIII. In this table, note that the Los Alamos approximate spectrum was also included in the calculations. As above for Table XII, microscopic cross-section data are taken from the ENDF/B-V dosimetry file, and processing is done with the NJOY code.

TABLE XIII

INTEGRAL CROSS SECTIONS (MB) IN REPRESENTATIONS OF THE CF-252 SF SPECTRUM

REACTION	EFF THRESH E IN MEV	MEASURED VALUE (PCT ERROR)	(A) NBS FIT CALC	C/E	(B) 1.439-MAX CALC	C/E	(C) 1.424-MAX CALC	C/E	(D) LA-ANT-EXACT CALC	C/E	(E) LA-ANT-APPRX CALC	C/E
27AL(N,P)	3.35	4.8000 (1.9)	5.1400	1.07*	5.4800	1.14*	5.3200	1.11*	5.2300	1.09*	5.0800	1.06*
27AL(N,A)	6.25	1.0060 (2.2)	1.0590	1.05*	1.2350	1.23*	1.1740	1.17*	1.0650	1.06*	.9670	.96
55MN(N,2N)	10.67	.4080 (2.2)	.4460	1.09*	.6140	1.50*	.5660	1.39*	.4310	1.06*	.3400	.83*
59CO(N,2N)	10.85	.4060 (2.5)	.4100	1.01	.5680	1.40*	.5230	1.29*	.3950	.97	.3100	.76*
59CO(N,A)	5.68	.2220 (1.8)	.2160	.97	.2500	1.13*	.2380	1.07*	.2170	.98	.2000	.90*
46TI(N,P)	3.43	14.1200 (2.6)	13.4700	.95	14.3600	1.02	13.9300	.99	13.7000	.97	13.3000	.94*
47TI(N,P)	1.56	19.2700 (2.5)	24.0600	1.25*	24.7200	1.28*	24.3200	1.26*	24.8100	1.29*	24.8000	1.29*
48TI(N,P)	5.79	.4244 (2.8)	.4093	.96	.4748	1.12*	.4517	1.06*	.4112	.97	.3700	.87*
54FE(N,P)	1.89	86.5800 (2.5)	88.2700	1.02	91.0100	1.05*	89.3400	1.03	90.8500	1.05	90.9000	1.05
56FE(N,P)	5.20	1.4680 (2.8)	1.4150	.96	1.5900	1.08*	1.5220	1.04	1.4260	.97	1.3300	.91*
58NI(N,2N)	12.57	.0089 (3.1)	.0076	.85*	.0112	1.26*	.0102	1.15*	.0071	.80*	.0053	.60*
58NI(N,P)	1.39	115.4000 (1.9)	113.8000	.99	117.2000	1.02	115.2000	1.00	117.2000	1.02	117.2000	1.02
63CU(N,A)	4.40	.6170 (2.9)	.7590	1.23*	.8530	1.38*	.8170	1.32*	.7660	1.24*	.7150	1.16*
115IN(N,N')	.76	198.3000 (2.6)	181.9000	.92*	183.6000	.93*	182.3000	.92*	187.8000	.95*	189.0000	.95
24MG(N,P)	6.08	2.0100 (3.0)	2.1590	1.07*	2.4820	1.23*	2.3650	1.18*	2.1730	1.08*	1.9930	.99
59CO(N,P)	2.89	1.6800 (2.4)	1.8280	1.09*	1.9460	1.16*	1.8900	1.13*	1.8620	1.11*	1.8160	1.08*
60NI(N,P)	4.33	2.3900 (5.4)	3.4400	1.44*	3.8130	1.60*	3.6600	1.53*	3.4800	1.46*	3.2830	1.37*
90ZR(N,2N)	12.31	.2210 (2.7)	.2222	1.01	.3226	1.46*	.2944	1.33*	.2097	.95	.1590	.72*
197AU(N,2N)	8.31	5.5000 (2.5)	5.6460	1.03	7.1150	1.29*	6.6670	1.21*	5.6120	1.02	4.7990	.87*
19 F(N,2N)	11.24	.0108 (14.8)	.0220	2.04*	.0314	2.91*	.0288	2.67*	.0209	1.94*	.0161	1.49*
63CU(N,2N)	11.12	.3000 (10.0)	.2223	.74*	.3152	1.05	.2889	.96	.2121	.71*	.1642	.55*
		AVERAGE C/E -		1.08		1.30		1.23		1.08		.97
		<E> IN MEV -	2.12		2.16		2.14		2.17		2.17	

* - CALCULATION OUTSIDE 2-SIGMA EXPERIMENTAL ERROR

An attempt has been made to get the latest experimental data for the threshold reactions, and these were taken from two sources. Measurements for the $^{27}Al(n,p)$, $^{27}Al(n,\alpha)$, $^{55}Mn(n,2n)$, $^{59}Co(n,2n)$, $^{59}Co(n,\alpha)$, $^{63}Cu(n,\alpha)$, $^{59}Co(n,p)$, $^{60}Ni(n,p)$, $^{90}Zr(n,2n)$, $^{197}Au(n,2n)$, $^{19}(n,2n)$, $^{63}Cu(n,\gamma)$, and $^{63}Cu(n,2n)$ reactions are taken from Ref. 57; the measurements for all other reactions are taken from Ref. 58.

Because many of the calculated values in Table XIII lie outside the 2-σ experimental uncertainty, it is useful to display these results graphically by plotting the ratios of the calculated integral cross sections in each spectrum representation to the corresponding measured values (C/E ratios) against "effective threshold energies" for the reactions. These "effective threshold energies" are only used for illustrative purposes and are estimated in a somewhat arbitrary manner. First, the cross-section integral for a particular reaction (i.e., with a constant weighting function = 1) is obtained by simple trapezoidal integration on the cross-section energy mesh given in the ENDF/B-V dosimetry file. We then estimate an "effective threshold energy" for the reaction by linearly interpolating to find the energy that divides the total integral at 0.1% and 99.9%. Although the 0.1% point is completely arbitrary, such a choice gives a consistent method for estimating the "effective threshold energies" for the various threshold reactions used. Incidentally, the use of the actual threshold energy for a particular reaction in a graphical comparison is generally not practical because of the long, slow-rising "tail" encountered in many cross sections. Figures 27 and 28 show how the "effective threshold energies" for the first five reactions in Table XIII relate to their corresponding cross sections and cross-section integrals, respectively.

The plots of the C/E ratios for the several ^{252}Cf spontaneous fission spectrum representations against the "effective threshold energies" are shown in Figs. 29-30. Also shown in these figures are linear least square (L.L.S) fits to the various sets of points. These fits are obtained with the ALVIN code[59] in which an inverse variance weighting is used. The variances are obtained only from the standard deviations for the experimental data shown in Table XIII, so no account is taken of any covariance data that might be available from the cross section evaluations in ENDF/B-V. A more exhaustive statistical treatment, which would include these covariance data, does not seem justified in view of the fact that the L.L.S. fits are used in the figures as "eye guides" only.

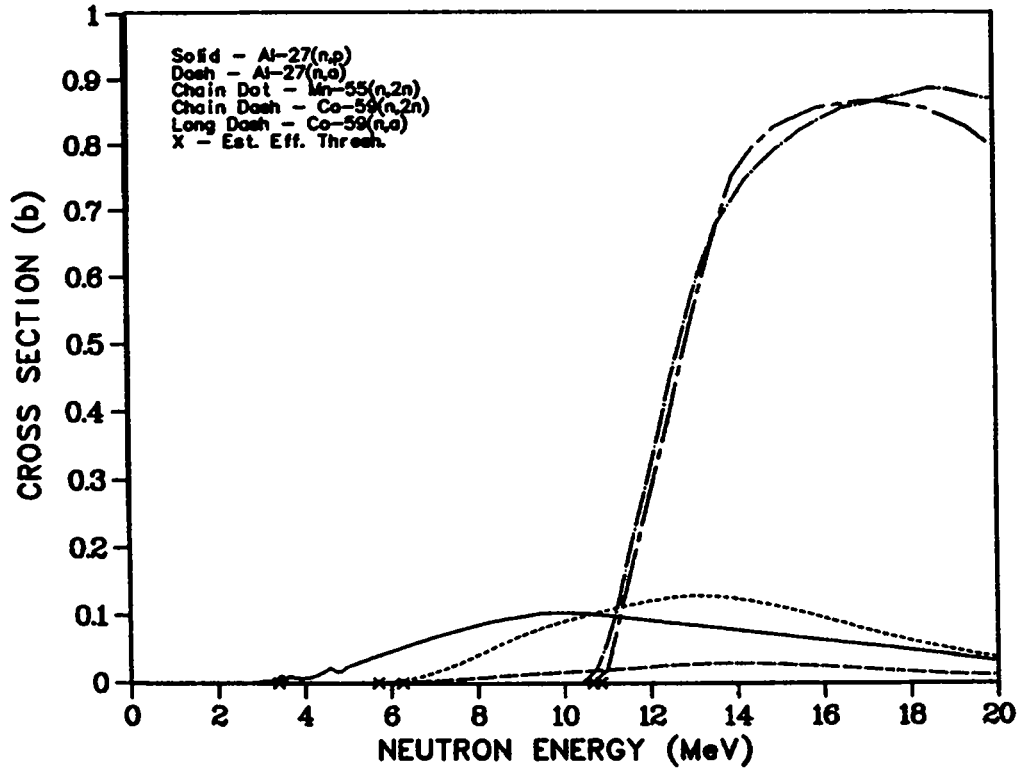

Fig. 27. Cross sections of 5 threshold reactions.

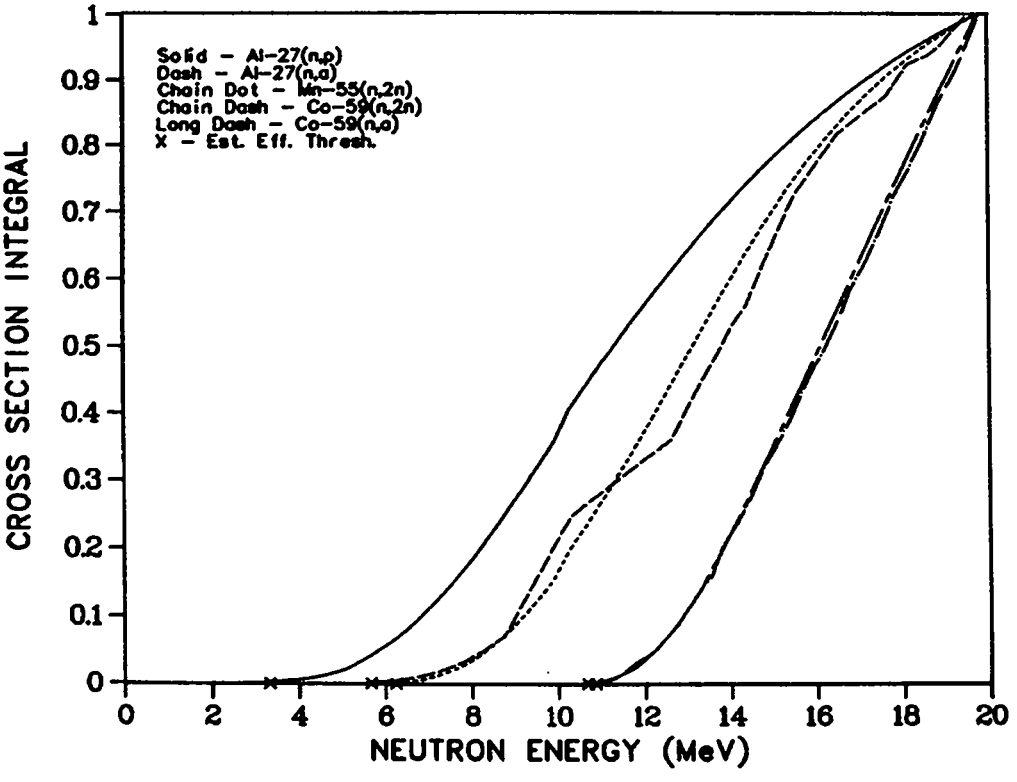

Fig. 28. Cross-section integrals of 5 reactions.

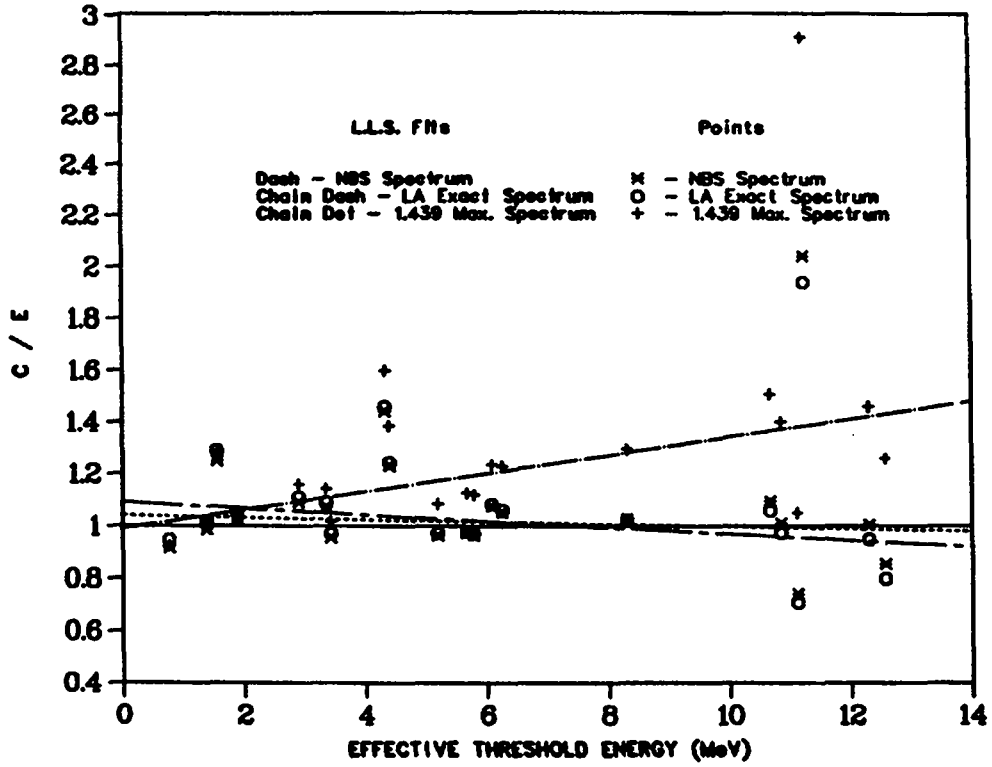

Fig. 29. C/E ratios of calculated to measured integral cross sections in Cf-252 s.f. spectrum.

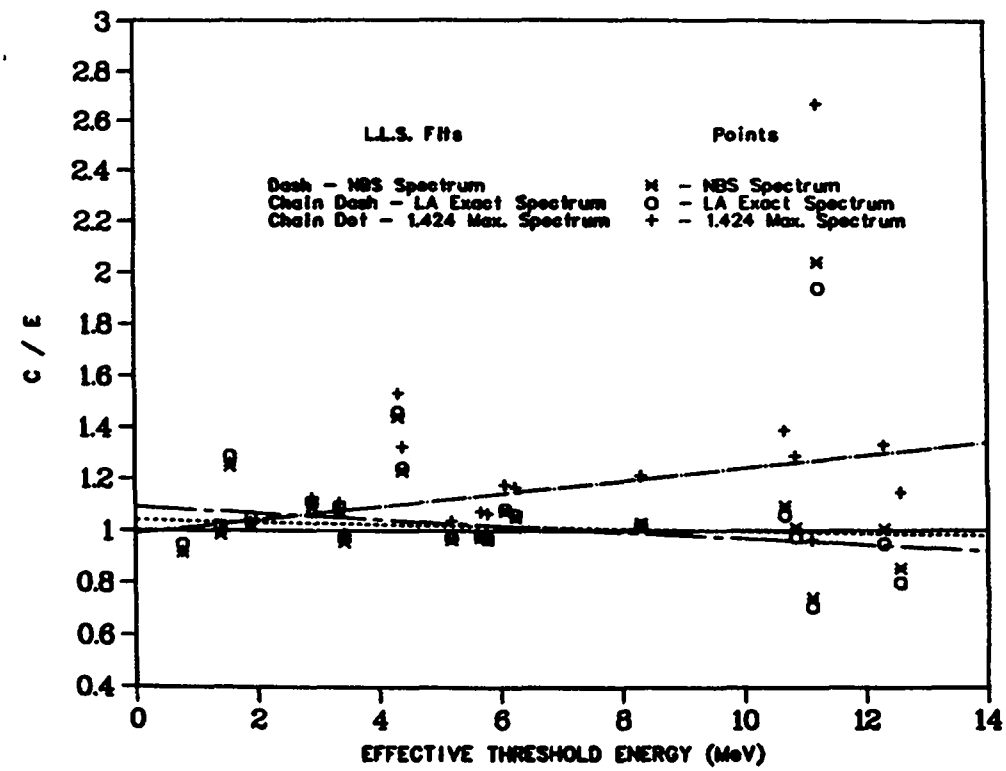

Fig. 30. C/E ratios of calculated to measured integral cross sections in Cf-252 s.f. spectrum.

From these figures and from Table XIII, one can draw the following conclusions:

a. For about half the threshold reactions in Table XII, either the cross-section evaluations are defective or the uncertainties assigned to the measurements are overly optimistic.

b. Both the NBS and the Los Alamos exact representations give equally satisfactory results.

c. The Los Alamos approximate representation needs further adjustment; however, as spontaneous fission implies no incident neutron energy dependence, a functional representation of the spectrum is not needed for a data set, as a tabulation would not be excessive.

d. Neither Maxwellian representation is adequate for use as a weighting function in the calculation of high-threshold-energy integral reactions. In fact, one can state that, on the basis of these results, a Maxwellian is a poor functional representation for the ^{252}Cf spontaneous fission spectrum.

III. FISSION PRODUCTS AND ACTINIDES: YIELDS, DECAY DATA, DEPLETION, AND BUILDUP

A. Delayed Neutron Spectra [T. R. England, W. B. Wilson, (R. E. Schenter, and F. M. Mann, Hanford Engineering Development Laboratory)]

Calculations of delayed neutron spectra for 11 fissionable nuclides at one or more neutron fission energies have been made for the total aggregate (105 precursors) and for each of the conventional 6 time groupings. The number of delayed neutrons for each group has also been calculated. Comparisons with evaluated experimental data have been made for all possible cases. The calculations use precursor emission probabilities (Pn) prepared for ENDF/B-V, spectra for each precursor, and ENDF/B-V fission-product yields. Experimental Pn values exist for ~ 68 of the 105 precursors. Some measured Pn's are discrepant, and evaluated values are used in the calculations, along with model estimates of the remaining 37 precursors. Spectral data have been measured for the 29 most important precursors. Model estimates using the BETA code[60] were used for the remaining precursors.

All results have been reported (see Ref. 61), and a Nuclear Science and Engineering article based on this reference has been reviewed and accepted for publication.

This work greatly extends the energy range of reported experimental spectra, applies to all important fissioning nuclides, and provides spectra for the unmeasured time groups 5 and 6. Spectra are computed on a 10-keV histogram basis out to ~ 3.5 MeV.

This work is continuing. A new evaluation of Pn values has been completed and reported in Ref. 62, along with improved model parameters for the unmeasured precursors. Fission product yields, noted in another section, are probably the major source of uncertainty, and these are being reevaluated.

B. Fission-Product Yields Status [T. R. England, B. F. Rider (G.E., retired), D. George, and R. J. LaBauve]

In the previous progress report (Ref. 47, p. 58), we identified 50 yield sets having a preliminary evaluation. These extensive data represent a culmination of the compilation/evaluation efforts of B. F. Rider (G.E.) over the past approximately 20 years before his retirement in December 1981. The only remotely comparable effort has been that of E. A. C. Crouch (United Kingdom), who is also retiring. Neither effort was planned to be continued by their respective laboratories.

In an effort to maintain, and possibly continue, the evaluation codes and particularly to avoid the loss of the extensive data base, Rider's files were sent to Los Alamos, with permission from G.E.'s management, during November 1981 and January 1982. These original files have been multiply stored; recently we began work on the files and conversion of the codes for the Los Alamos computers. The codes have no documentation and are largely without comment cards. Rider spent the week of September 13, 1982, working with us to get the codes operational, and he has continued to assist us in their interpretation.

Several codes have now been prepared to reconstruct the master data files (found to be missing some data), to add new data (correcting and extending the preliminary data), and ultimately to prepare the data for the ENDF/B format. The primary evaluation code and data base for the original 50-yield sets are now operational but not completely validated. Most, and probably all, differences in computer-dependent features have been resolved. We are continuing work to validate the initial data base before adding new data, correcting known errors in the experimental data, and removing duplicated data resulting from multiple publications of the same experiments. In some cases, duplicate data

result from initial publication in laboratory reports followed by journal publication; in others, they result from publication in more than one journal (often having corrections in the later publication). Most, but not all, duplications in the existing base data were removed before Rider's retirement.

Much of this work is tedious, but Rider's efforts have been a foundation for all yield evaluations in ENDF/B; either Rider's compilation or ENDF/B yields are now almost universally used internationally. His codes use distribution models developed at this Laboratory (and recommended by the CSEWG Yields Evaluation Committee for unmeasured yields), and this model work continues here. Thus, his accomplishments have been integrally connected with work at Los Alamos and to the ENDF/B data base. This would have been sufficient reason for getting his codes and base-line data operational here; however, it is more important to insure that the results of so many years of effort are not lost. Many quantities related to fission can now be accurately calculated using the increasingly accurate measurements and evaluations of direct fission yields (delayed and prompt neutrons, delayed beta and gamma energies and their spectra, etc.). It is important that the evaluation of yields should continue.

A report on the status of yield evaluations was presented at the March 1982 American Society for Testing Materials (ASTM) Meeting, and the first meeting of the American Nuclear Society 5.2 Yields Standard Committe was chaired by T. R. England in June 1982.

C. TMI-2 Fission-Product Elemental Isotopic Inventories (T. R. England and W. B. Wilson)

All TMI-2 fission-product inventories (total core atoms and kilograms), curies, and beta, gamma, and total decay energies are listed for each nuclide and grouped element in a report now completed in draft form. All results are based on the summation calculations described in Ref. 63 and are applicable at 24 cooling times out to 5.7 years. For comparison, results are also given for the same core, had it operated at its constant-rated power for 26 000 hours. This supplements the data in Ref. 63 by inclusion of long-lived and stable fission products and by elemental groups.

D. LWR Core Radionuclide Inventories for Extended Burnup Fuels (W. B. Wilson, T. R. England, and R. J. LaBauve)

The Nuclear Regulatory Commission (NRC) anticipates receiving license amendment applications for fuel cycle modifications to higher reload enrichments and discharge exposures. Analyses of hypothetical reactor accidents for these cores require the evaluation of radionuclide sources produced in extended burnup fuels. To this end, we have completed a study[64] of radionuclide inventories of equilibrium-cycle cores with reload fuel enrichments in the range 3.8-4.8% and discharge exposures in the range 30-60 GWd/tU. Inventories were reported for 56 radionuclides considered to be important to accident analyses. These include 48 fission products and 8 actinides.

Total 3-GW core inventories were calculated as the sum of the inventories of three equal-volume 1-GW regions containing fuel of first-, second-, or third-cycle exposure. PWR calculations considered fuel with a power density of 38.303 W/gU, typical of the current North Anna-2 plant. Boiling water reactor (BWR) calculations considered fuel with an average 40%-moderator void and a power density of 24.34 W/gU, typical of Grand Gulf-1,2. Additional calculations of a three-region, three-level BWR core with 0, 40, and 70% void levels showed nuclide inventory variations as large as a factor of 2 with void level; however, total core nuclide inventories varied by no more than 3% from inventories calculated at 40%.

Region inventories of each fuel were evaluated in tandem EPRI-CELL[65] and CINDER-2[66] calculations with ENDF/B-V-based data libraries.[67] EPRI-CELL computes the space-, energy-, and burnup-dependent neutron spectrum within a cylindrical cell of a LWR fuel rod, and it generates an interface file of burnup-dependent collapsed four-group flux values and actinide cross sections. CINDER-2 calculations repeat the history of the EPRI-CELL calculation, generating the inventory and aggregate summation properties of its extensive nuclide library. Inventories so generated are edited to extract the desired 56-nuclide inventory.

Early reactor accident calculations employed fission-product inventories generated by assuming values in equilibrium with ^{235}U yield formation rates and ignoring neutron absorption effects.[68] Later inventory calculations treated neutron absorption and multiple contributions to fission yields but used a single extreme set of reactor conditions assumed to produce maximum core inventories. The high power density used in Ref. 69, for example, leads to high end-of-cycle densities of radionuclides but lower fuel mass, higher neutron

flux, and shorter cycle length for constant core power, fuel enrichment, and discharge exposure; the resulting core inventories of most actinides and long-lived fission products may be considerably lower than those encountered under normal operating conditions.

LWRs modified to accommodate fuel of higher initial enrichments and discharge exposures will likely retain existing core volumes and power densities. A survey of end-of-equilibrium-cycle (EOEC) PWR and BWR core inventories was conducted, retaining the power densities and fuel volume of currently licensed reactors. Cycle lengths were varied to accommodate the range of discharge exposures. Intermediate between-cycle shutdown periods and end-of-cycle decay periods were eliminated; time steps were chosen such that the EOEC three-region inventories for all discharge exposures were obtained from a single set of tandem calculations for each initial enrichment.

Additional PWR calculations were performed with intermediate 35-day shutdown periods for 3.8%, 30-GWd/tU and 4.8%, 60-GWd/tU fuels to demonstrate the effect of the between-cycle shutdown on EOEC inventories. Of the 56 nuclides examined, total-core EOEC inventories calculated with intermediate shutdowns differed by greater than 1% from constant-power inventories for 8 nuclides; the largest variation was a 7.1% increase in ^{242}Cm with the shutdowns because of the enhanced decay of ^{241}Pu and ^{242m}Am. An additional 3.8%, 30-GWd/tU calculation included intermediate shutdowns and linear boron letdown from 1250 ppmB to 0 ppmB during each cycle. All other calculations were made for a constant 450 ppmB. The effect of the linear boron treatment was a variation in total core EOEC inventory of greater than 1% for six nuclides because of the neutron spectrum modifications. The largest inventory change was a 2.1% increase in ^{244}Cm with the linear boron letdown.

No additional problems in examining between-cycle shutdowns on variations in reactivity-controlling poisons were studied for the BWR survey. The complexity of the spatial and temporal GdO_2 poison typical of BWR fuel rods is beyond the capabilities of EPRI-CELL methodology, but the effects of the burnable poison on total-core EOEC BWR inventories may be expected to be similar to those of the boron letdown on the PWR inventories.

Examination of the inventories at intermediate exposures reveals that half of the 48 fission products of interest do not reach maximum values with EOEC conditions. These nuclides are found to have maximum inventories in high-enrichment, low-exposure BWR fuel; this is principally due to their higher

cumulative fission yield fractions associated with ^{235}U, which contributes a greater fraction of the fission rate in this fuel. This effect is accentuated by the lower recoverable energy per fission associated both with ^{235}U fission and with low-exposure fuel in general. We have examined the inventories of these nuclides at 25 times during a 4.8% initial enrichment equilibrium cycle of 30-GWd/tU discharge BWR fuel.

Maximum inventory values generated in the PWR EOEC survey, the BWR EOEC survey, and the limited in-cycle BWR survey are compared in Table XIV. The

TABLE XIV

MAXIMUM 3-GW EQUILIBRIUM CORE RADIONUCLIDE INVENTORIES

	MAXIMUM TOTAL CORE CURIES			
	END-OF-EQUILIBRIUM CYCLE		IN-CYCLE	STD. REF.
NUCLIDE	PWR SURVEY	BWR SURVEY	BWR SURVEY	INVENTORY
KR 85	8.675E+05	1.330E+06		1.330E+06
KR 85M	2.483E+07	2.596E+07	2.863E+07	2.863E+07
KR 87	4.758E+07	4.978E+07	5.521E+07	5.521E+07
KR 88	6.629E+07	6.955E+07	7.736E+07	7.736E+07
KR 89	8.428E+07	8.874E+07	9.963E+07	9.963E+07
RB 86	1.590E+05	1.619E+05		1.619E+05
SR 89	9.182E+07	9.595E+07	9.832E+07	9.832E+07
SR 90	6.968E+06	1.115E+07		1.115E+07
SR 91	1.139E+08	1.188E+08	1.307E+08	1.307E+08
Y 90	7.206E+06	1.149E+07		1.149E+07
Y 91	1.151E+08	1.201E+08	1.216E+08	1.216E+08
ZR 95	1.397E+08	1.441E+08	1.442E+08	1.442E+08
ZR 97	1.365E+08	1.378E+08	1.418E+08	1.418E+08
NB 95	1.376E+08	1.441E+08		1.441E+08
MO 99	1.470E+08	1.474E+08	1.492E+08	1.492E+08
TC 99M	1.288E+08	1.291E+08	1.307E+08	1.307E+08
RU103	1.243E+08	1.225E+08		1.243E+08
RU105	8.858E+07	8.575E+07		8.858E+07
RU106	4.717E+07	5.226E+07		5.226E+07
RH105	8.132E+07	7.926E+07		8.132E+07
SB127	6.894E+06	6.746E+06		6.894E+06
SB129	2.480E+07	2.443E+07		2.480E+07
TE127	6.823E+06	6.706E+06		6.823E+06
TE127M	1.080E+06	1.086E+06		1.086E+06
TE129	2.372E+07	2.336E+07		2.372E+07
TE129M	4.402E+06	4.342E+06		4.402E+06
TE131M	1.560E+07	1.536E+07		1.560E+07
TE132	1.099E+08	1.093E+08		1.099E+08
I131	7.702E+07	7.647E+07		7.702E+07
I132	1.120E+08	1.112E+08		1.120E+08
I133	1.612E+08	1.616E+08	1.635E+08	1.635E+08
I134	1.806E+08	1.818E+08	1.866E+08	1.866E+08
I135	1.527E+08	1.529E+08	1.547E+08	1.547E+08
XE133	1.611E+08	1.616E+08	1.634E+08	1.634E+08
XE135	5.447E+07	6.397E+07	6.771E+07	6.771E+07
XE135M	3.417E+07	3.390E+07		3.417E+07
XE137	1.450E+08	1.455E+08	1.482E+08	1.482E+08
XE138	1.438E+08	1.458E+08	1.519E+08	1.519E+08
CS134	1.620E+07	2.088E+07		2.088E+07
CS136	4.336E+06	4.899E+06		4.899E+06
CS137	9.582E+06	1.476E+07		1.476E+07
BA140	1.445E+08	1.458E+08	1.485E+08	1.485E+08
LA140	1.463E+08	1.477E+08	1.496E+08	1.496E+08
CE141	1.337E+08	1.350E+08	1.362E+08	1.362E+08
CE143	1.291E+08	1.317E+08	1.376E+08	1.376E+08
CE144	9.820E+07	1.077E+08		1.077E+08
PR143	1.287E+08	1.314E+08	1.355E+08	1.355E+08
ND147	5.280E+07	5.323E+07	5.403E+07	5.403E+07
NP239	1.636E+09	1.517E+09		1.636E+09
PU238	2.737E+05	3.721E+05		3.721E+05
PU239	2.726E+04	3.048E+04		3.048E+04
PU240	3.487E+04	5.201E+04		5.201E+04
PU241	1.131E+07	1.205E+07		1.205E+07
AM241	1.310E+04	1.861E+04		1.861E+04
CM242	4.355E+06	5.999E+06		5.999E+06
CM244	6.362E+05	8.254E+05		8.254E+05

maximum inventory for each nuclide from these surveys is included in the standard reference inventory for use in reactor accident analyses. It should be clear that the standard reference inventory is not generated in a single fuel or under a single set of irradiation conditions. Also, we have probably not used the exact conditions within the range of parameter values examined under which each of the radionuclides reaches maximum inventory values. Our grid of enrichment and exposure values is sufficiently fine, however, to approach such maximum equilibrium-core inventories within a few per cent. Because of the prevalence of ^{235}U fission in a fresh 3-enrichment core, higher inventories for nuclides with high ^{235}U fission yield fractions will be generated there than in the standard reference inventory that is applicable to reload considerations.

E. Effects of Neutron Spectrum Changes from PWR Boron Letdown and BWR Void on $^{242,244}Cm$ Inventories (W. B. Wilson, R. J. LaBauve, and T. R. England)

We have recently completed a study of actinide production in PWR fuel, showing the exposure variation and cooling-time variation of the inherent neutron sources of spent PWR fuel.[70] The study used tandem EPRI-CELL/CINDER-2 calculations with ENDF/B-IV based data libraries to identify ^{242}Cm and ^{244}Cm as principal neutron sources in spent fuel. More recently, we have used similar calculations with ENDF/B-V based data libraries to demonstrate the effects on $^{242,244}Cm$ of reactor parameters affecting the neutron spectrum.

The effect of the boron letdown used for PWR reactivity control was examined in a pair of calculations of fuel with initial enrichment of 3.8% followed to a discharge exposure of 30 GWd/tU in three cycles. Boron was first considered constant at 450 ppmB; the second calculation considered boron to linearly decrease from 1250 ppmB at the beginning of each cycle to 0 ppmB at the end of each cycle. The $^{242,244}Cm$ inventories calculated for a 1-GW region were found to be not strongly affected by the boron treatment, as shown in Table XV.

TABLE XV

VARIATION OF CALCULATED $^{242,244}Cm$ FROM BORON TREATMENT IN PWR FUEL

Exposure (GWd/tU)	^{242}Cm Region Curies		^{244}Cm Region Curies	
	Constant B	B Letdown	Constant B	B Letdown
10	1.187+4	1.229+4	7.702+1	7.896+1
20	1.850+5	1.886+5	3.287+3	3.365+3
30	6.791+5	6.877+5	2.488+4	2.538+4

We have also examined the effects of the neutron spectrum variations from BWR voids on $^{242,244}Cm$ inventories. Calculations of 1/3-GW region inventories of 4.5% BWR fuel at 0%, 40%, and 70% void levels indicate large increases in ^{242}Cm and ^{244}Cm with void level. These calculations do not include the spectral effects of the burnable GdO_2. Inventories are compared in Table XVI.

TABLE XVI

VARIATION OF CALCULATED $^{242,244}Cm$ IN BWR FUEL FROM MODERATOR VOID FRACTION

Exposure (GWd/tU)	^{242}Cm Region Curies			^{244}Cm Region Curies		
	0% Void	40% Void	70% Void	0% Void	40% Void	70% Void
6	3.04+2	4.16+2	5.65+2	5.96-1	1.13+0	2.05+0
15	1.14+4	1.48+4	1.90+4	5.96+1	1.08+2	1.89+2
24	7.36+4	9.07+4	1.10+5	7.79+2	1.34+3	2.21+3
30	1.51+5	1.81+5	2.15+5	2.63+3	4.33+3	6.88+3
36	2.55+5	2.99+5	3.48+5	6.98+3	1.10+4	1.68+4
47	5.31+5	6.08+5	6.89+5	3.14+4	4.49+4	6.29+4
48	6.51+5	7.46+5	8.46+5	5.76+4	7.84+4	1.05+5

F. Examination of ASTM E-321, Standard Test Method for Atom Per Cent Fission in Uranium and Plutonium Fuel (Neodymium-148 Method) (W. B. Wilson, T. R. England, and R. J. LaBauve)

Fuel isotopics measurements generally rely on one or more techniques described by the American Society for Testing and Materials for the determination of fuel burnup. The most commonly used method has been ASTM Method E321-NY, where NY is a two-digit number designating the year of original adoption (67) or revision (69, 75, 79). All versions of E321 define sample burnup F_T in atom per cent fission, using measured nuclide density ratios in expressions that reduce to the following equations:

$$F_T = F' \times 100./(U' + Pu' + F'), \quad (17)$$

$$F' = \#\ \text{fissions}/\#^{238}U\ \text{atoms}, \quad (18)$$

$$U' = \#\ U\ \text{atoms}/\#^{238}U\ \text{atoms}, \quad (19)$$

and

$$Pu' = \#\ Pu\ \text{atoms}/\#^{238}U\ \text{atoms}. \quad (20)$$

The quantity F' is determined from

$$F' = \#^{148}\text{Nd atoms}/^{148}\text{Nd yield}/\#^{238}\text{U atoms}. \quad (21)$$

All versions of E321 relate exposure (MWd/tU) and burnup (atom % fission) with

$$F_T \text{ (MWd/tU)} = (9600 \pm 300) \times F_T \text{ (atom \% fission)}. \quad (22)$$

Revisions of E321 obviously have been made in pursuit of greater accuracy, although this may not be the result. We have not examined E321-67 or E321-69, although the latter is referred to in Ref. 71 where the ^{148}Nd cumulative yield is set at 1.68% in H. B. Robinson fuel measurements. E321-75 states that the ^{148}Nd yield should be "calculated from the fission yields of ^{148}Nd for each of the fissioning isotopes weighted according to their contribution to fission as measured in ASTM Method E244, Test for Atom Per cent Fission in Uranium Fuel (Mass Spectrometric Method)." However, the paragraph continues: "For ^{235}U fuels, [the ^{148}Nd yield] can be assumed to be the fractional yield for ^{148}Nd in ^{235}U thermal fission, which is 0.01618." No appropriate yield values are given for the other fissionable nuclides. The aim here toward a "better" ^{148}Nd yield value is cancelled by the "^{235}U fuels" proviso, which is open to interpretation. Indeed, no spent fuel isotopics measurement reviewed by us to date has included a determination of fission contributions or a weighted yield fraction. All measurements have assumed the ^{235}U fission yield.

Method E321-79 lists ^{148}Nd yield fractions for all four fissionable nuclides and includes a "K" factor to adjust ^{148}Nd for nonfission production from ^{147}Nd(n,γ). The yields here are from Ref. 72, which documented the third yield set iteration en route to the fifth and final yield set used in ENDF/B-V.

The ^{148}Nd cumulative fission yield fractions of ENDF/B-IV, -V, preliminary -VI, and E321-79 are listed in Table XVII. Reference to "^{235}U fuels" and the de facto acceptance of the use of the ^{235}U fission yield fraction for all fissions are absent in E321-79.

The ^{147}Nd(n,γ) cross section used in calculating K is from Ref. 73, where the reported 440-b thermal cross section depends linearly on the assumed 50% intensity of the 301.7-keV neutron capture gamma ray. The argument for this

50% assumption seems weak; a model code could be used to determine a more precise intensity and thus a more precise cross section. The ENDF/B-V evaluation for ^{147}Nd lists a 2200 m/s (n,γ) cross section of 49 b and resonance integral of 647.8 b. The E-321-79 treatment of the K factor and the ^{147}Nd(n,γ) cross section adjusts the 440 b cross section to a 300°C Maxwellian-averaged value of 247 b, assuming 1/v behavior. This 1/v extension of the Ref. 73 value is compared in Fig. 31 with the ENDF/B-V representation, which was based on a model code calculation adjusted to agree with a resonance integral measurement. Regardless, no spent fuel isotopics measurement reviewed by us to date has included a determination of K or any ^{148}Nd density adjustment to correct for neutron absorption effects.

TABLE XVII

^{148}Nd CUMULATIVE YIELD FRACTIONS

FISSIONING NUCLIDE	ENDF/B-IV	ENDF/B-V	PRELIMINARY ENDF/B-VI	ASTM E321-79
U-235(TH)	0.01690673	0.01670038	0.01674658	0.01671
U-238(FST)	0.02259347	0.02078896	0.02097547	0.02072
PU-239(TH)	0.01694488	0.01634225	0.01640564	0.01636
PU-241(TH)	0.01925721	0.01989327	0.01933803	0.02030

All versions of E321 assume that burnup and exposure are related by Eq. (22), which assumes that all fissions result in the realization of the same amount of heat, approximately 201.5 MeV. Our calculations of high-burnup Calvert Cliffs 1 fuel with EPRI-CELL show that the heat/fission realized, using the data of Ref. 74, increases from 201.5 MeV to 220.9 MeV at 46.8 GWd/t in 2.45% enriched fuel. This increase is due to the increase with A in recoverable energy/fission excluding capture effects and an increase with exposure of the average decay energy produced in neutron capture by the capture products and daughters. The cumulative effect of this increase is not so drastic, but the exposure-to-burnup ratio still exceeds 9600 by nearly 5% at 46.8 GWd/t.

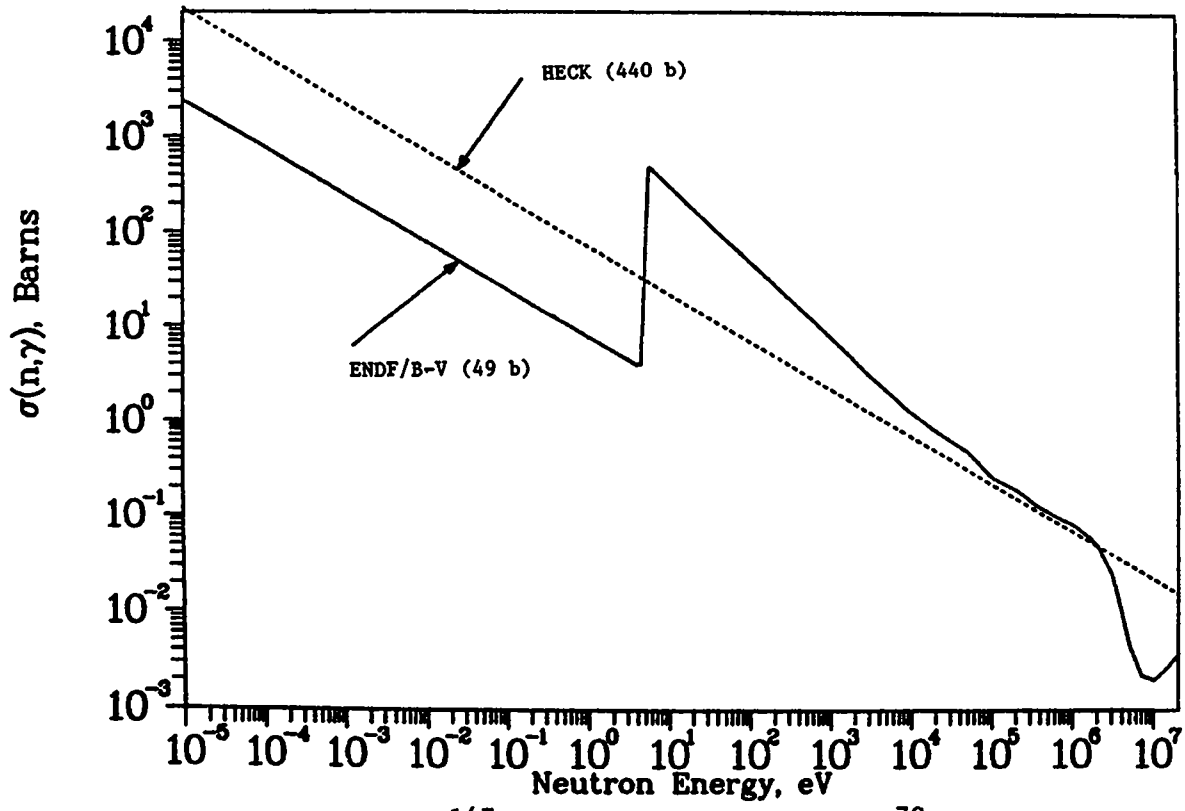

Fig. 31. Comparison of ^{147}Nd cross sections of Heck[73] and ENDF/B-V.

Unfortunately, complete compliance with ASTM Method E321-79 may produce different and less accurate results than those obtained with an earlier and less intricate version. We have constructed a reduced ENDF/B-V fission product library for CINDER-2, following and recording all ^{148}Nd modes of formation and loss. We have used the library in tandem EPRI-CELL/CINDER-2 calculations of Calvert Cliffs 1 fuel to 46.8 GWd/tU. The results of the exercise are given in Table XVIII. Note that exposure and burnup are listed at the left, as well as their ratio. The cumulative fission density and per cent contributions from each fissionable nuclide are then given--these would be determined experimentally with ASTM Method E244. The ^{148}Nd formed directly by yield is then given; this is always greater than 99.1% of all ^{148}Nd produced, corresponding to K $\geq$ .991. The direct yield tabulated is the ratio of ^{148}Nd formed directly to the cumulative fissions; this is the desired weighted yield of E321-79. The trace ^{148}Nd formed from ^{147}Nd(n,γ) is then tabulated, as well as the gross ^{148}Nd formed by both paths.

TABLE XVIII

CALCULATED PRODUCTION OF ^{148}Nd in 2.45% UO_2 CALVERT CLIFFS-1 PWR FUEL

CALC. MWD/T	CALC. A%F	MWD/T : A%F RATIO	*******CUMULATIVE FISSIONS****** #/CC	PERCENT CONTRIBUTION 235U	238U	239PU	241PU	148ND FROM MASS #/CC	%GROSS	148 YLD DIRECT YLD,%	148ND FROM 147ND(N,GAMMA) #/CC	%GROSS	GROSS 148ND #/CC	GROSS YLD,%	148ND LOST BY 148ND(N,GAMMA) #/CC	%GROSS	NET 148ND #/CC	NET YLD,%
356	0.037	9619	8.510+18	91.12	8.13	0.74	0.00	1.449+17	99.808	1.7029	2.784+14	0 192	1.452+17	1.7061	1.369+13	0.009	1.452+17	1.7060
826	0.086	9620	1.975+19	90.69	7.25	2.07	0.00	3.355+17	99.723	1.6988	9.329+14	0.277	3.365+17	1.7035	8.185+13	0.024	3.364+17	1.7031
1189	0.124	9631	2.839+19	89.91	7.09	3.00	0.00	4.819+17	99.687	1.6978	1.512+15	0.313	4.835+17	1.7031	1.724+14	0.036	4.833+17	1.7025
2941	0.305	9650	7.004+19	86.03	6.87	7.05	0.05	1.188+18	99.438	1.6957	6.712+15	0.562	1.194+18	1.7052	1.076+15	0.090	1.193+18	1.7037
4688	0.485	9675	1.113+20	82.43	6.89	10.52	0.16	1.887+18	99.329	1.6949	1.274+16	0.671	1.900+18	1.7063	2.766+15	0.146	1.897+18	1.7038
6432	0.663	9697	1.524+20	79.17	6.94	13.54	0.34	2.583+18	99.277	1.6946	1.880+16	0.723	2.602+18	1.7070	5.255+15	0.202	2.596+18	1.7035
8174	0.841	9719	1.933+20	76.22	7.01	16.18	0.59	3.276+18	99.245	1.6948	2.490+16	0.755	3.300+18	1.7076	8.564+15	0.259	3.292+18	1.7032
9915	1.018	9739	2.339+20	73.51	7.07	18.52	0.90	3.966+18	99.223	1.6952	3.105+16	0.777	3.997+18	1.7085	1.271+16	0.318	3.984+18	1.7030
11651	1.194	9758	2.744+20	70.99	7.14	20.61	1.26	4.653+18	99.206	1.6959	3.724+16	0.794	4.690+18	1.7094	1.771+16	0.378	4.673+18	1.7030
13396	1.371	9773	3.150+20	68.63	7.18	22.55	1.64	5.344+18	99.218	1.6966	4.211+16	0.782	5.386+18	1.7100	2.351+16	0.437	5.363+18	1.7025
15126	1.545	9791	3.550+20	66.47	7.25	24.23	2.05	6.027+18	99.203	1.6976	4.839+16	0.797	6.075+18	1.7112	3.031+16	0.499	6.045+18	1.7027
17206	1.754	9811	4.030+20	63.99	7.33	26.11	2.57	6.847+18	99.188	1.6990	5.602+16	0.812	6.903+18	1.7129	3.966+16	0.575	6.863+18	1.7030
19985	2.032	9837	4.669+20	60.93	7.43	28.35	3.29	7.940+18	99.198	1.7006	6.420+16	0.802	8.004+18	1.7144	5.313+16	0.664	7.951+18	1.7030
21983	2.231	9855	5.126+20	58.87	7.50	29.80	3.83	8.725+18	99.184	1.7022	7.175+16	0.816	8.797+18	1.7162	6.524+16	0.742	8.732+18	1.7034
23087	2.340	9865	5.378+20	57.77	7.54	30.56	4.13	9.159+18	99.176	1.7031	7.605+16	0.824	9.235+18	1.7172	7.248+16	0.785	9.162+18	1.7037
25614	2.591	9886	5.953+20	55.36	7.63	32.18	4.83	1.015+19	99.157	1.7051	8.627+16	0.843	1.024+19	1.7196	9.065+16	0.886	1.015+19	1.7044
26936	2.721	9897	6.254+20	54.15	7.67	32.98	5.20	1.067+19	99.164	1.7062	8.994+16	0.836	1.076+19	1.7205	1.009+17	0.938	1.066+19	1.7044
27817	2.809	9904	6.454+20	53.37	7.69	33.50	5.44	1.102+19	99.165	1.7069	9.280+16	0.835	1.111+19	1.7212	1.080+17	0.972	1.100+19	1.7045
29581	2.982	9919	6.853+20	51.87	7.75	34.46	5.92	1.171+19	99.153	1.7083	9.999+16	0.847	1.181+19	1.7229	1.235+17	1.046	1.168+19	1.7049
31356	3.157	9933	7.254+20	50.41	7.81	35.38	6.40	1.240+19	99.141	1.7098	1.074+17	0.859	1.251+19	1.7246	1.402+17	1.121	1.237+19	1.7053
33249	3.342	9948	7.680+20	48.91	7.87	36.30	6.92	1.314+19	99.130	1.7114	1.154+17	0.870	1.326+19	1.7264	1.592+17	1.201	1.310+19	1.7057
34702	3.484	9959	8.007+20	47 80	7.92	36.98	7.30	1.371+19	99.133	1.7125	1.199+17	0.867	1.383+19	1.7274	1.736+17	1.255	1.366+19	1.7058
36053	3.616	9970	8.310+20	46.80	7.96	37.58	7.66	1.424+19	99.125	1.7136	1.256+17	0.875	1.437+19	1.7287	1.888+17	1.314	1.418+19	1.7060
37568	3.764	9980	8.650+20	45.70	8.00	38.25	8.05	1.483+19	99.131	1.7148	1.301+17	0.869	1.496+19	1.7298	2.063+17	1.378	1.476+19	1.7059
39061	3.909	9991	8.984+20	44.67	8.05	38.86	8.42	1.542+19	99.124	1.7160	1.363+17	0.876	1.555+19	1.7311	2.248+17	1.445	1.533+19	1.7061
40019	4.002	9998	9.198+20	44.01	8.07	39.25	8.66	1.579+19	99.126	1.7167	1.392+17	0.874	1.593+19	1.7318	2.371+17	1.488	1.569+19	1.7061
40981	4.096	10005	9.412+20	43.37	8.10	39.62	8.90	1.616+19	99.132	1.7175	1.416+17	0.868	1.631+19	1.7325	2.496+17	1.531	1.606+19	1.7060
41058	4.103	10006	9.429+20	43.32	8.10	39.65	8.92	1.619+19	99.132	1.7174	1.418+17	0.868	1.634+19	1.7324	2.497+17	1.528	1.609+19	1.7060
42257	4.220	10014	9.696+20	42.54	8.14	40.11	9.21	1.666+19	99.133	1.7183	1.457+17	0.867	1.681+19	1.7333	2.659+17	1.582	1.654+19	1.7059
44256	4.413	10028	1.014+21	41.29	8.20	40.83	9.69	1.744+19	99.123	1.7199	1.543+17	0.877	1.760+19	1.7351	2.945+17	1.674	1.730+19	1.7060
46258	4.606	10042	1.059+21	40.08	8.25	41.51	10.15	1.822+19	99.111	1.7214	1.634+17	0.889	1.838+19	1.7368	3.247+17	1.766	1.806+19	1.7061
46835	4.662	10046	1.071+21	39.74	8.27	41.70	10.29	1.845+19	99.109	1.7218	1.658+17	0.891	1.861+19	1.7373	3.336+17	1.793	1.828+19	1.7061

The K factor of E321-79 is evaluated in the standard for a range of flux and fluence values, using the 274-b cross-section value for $^{147}Nd(n,\gamma)$ and assuming continuous reactor operation. These values are given in Table XIX. The Calvert Cliffs 1 fuel inventory calculations described above modeled a spent fuel sample discussed in the following sections, and the power history included intermediate shutdowns and partial power operation periods. Ignoring shutdowns, the fuel sample operated at an average integral flux of $\sim 2.5 \times 10^{14}$ $n/cm^2/s$ and an exposure of ~ 43 000 hours and was discharged at a fluence of ~ 3.9×10^{22} n/cm^2 and an exposure of ~ 46.8 GWd/tU. This far exceeds the maximum fluence (3×10^{21}) for which K has been evaluated, and the E321-79 method provides no guidance or data for the calculation of K.

TABLE XIX

K FACTORS FROM ASTM METHOD E321-79

TOTAL NEUTRON FLUX (N/CM**2/S)	NEUTRON FLUENCE (N/CM**2)				
	1E+20	3E+20	1E+21	2E+21	3E+21
3E+12	0.9985	0.9985	0.9985	0.9985	0.9985
1E+13	0.9956	0.9952	0.9950	0.9950	0.9950
3E+13	0.9906	0.9870	0.9856	0.9853	0.9852
1E+14	0.9858	0.9716	0.9598	0.9569	0.9559
3E+14	0.9835	0.9592	0.9187	0.9008	0.8941
1E+15	0.9826	0.9526	0.8816	0.8284	0.8006

At the above flux value, an interpolated value is obtained from Table XIX of K ≅ .910 at the maximum fluence. This corresponds to an exposure in the Calvert Cliffs 1 fuel of ~ 3.6 GWd/tU, where the value interpolated from the calculated (direct % gross) values of Table XVIII is K ≅ 0.994. The K factor of E321-79 indicates that, at an exposure of 3.6 GWd/tU, 9% of the ^{148}Nd formed has been produced from the $^{147}Nd(n,\gamma)^{148}Nd$ path. CINDER-2 calculations show that, at this low exposure, only 0.6% of the ^{148}Nd formed is from this path. These different contributions reflect the different cross-section values and/or flux interpretation used in their calculation.

No mention has been made of the ^{148}Nd loss by $^{148}Nd(n,\gamma)$, listed in Table XVIII. Note that the cumulative ^{148}Nd loss by the $^{148}Nd(n,\gamma)$ reaction exceeds the cumulative ^{148}Nd gain from $^{147}Nd(n,\gamma)$ at exposures exceeding ~ 24 GWd/tU. The net ^{148}Nd [gross - $^{148}Nd(n,\gamma)$ loss] and the net yield are the righthand entries of Table XVIII. Note that the calculated net yield varies only slightly during exposure, indicating that, for this fuel, increases in ^{148}Nd, due to

the increase with exposure in the weighted cumulative fission yield fraction (i.e., mass-148 yield from fission) and $^{147}Nd(n,\gamma)^{148}Nd$ production (both recognized in E321-79), are offset by the $^{148}Nd(n,\gamma)^{149}Nd$ loss that is not recognized in E321-79. Of course, these observations depend upon the accuracy of ENDF/B-V cumulative fission yield fractions and evaluated cross sections of both $^{147,148}Nd$.

G. Spent LWR Fuel Inventory Benchmarks (W. B. Wilson, R. J. LaBauve, and T. R. England)

We recently summarized our observations of the status of spent LWR fuel inventory benchmarks.[75]

A nuclide inventory measurement of benchmark quality might well include the following:

1. a full description of the fuel parameters (e.g., enrichment, pellet density, pellet diameter, clad thickness and material, pitch, etc.) and environment (e.g., core location, proximity to control rods, burnable poisons, etc.).
2. a value of sample burnup and/or exposure, as well as all measured nuclide ratios and the basic data and methodology used in the determination.
3. a detailed power history of the sample, plus dates of shutdown and measurements.
4. inventory values for a wide range of nuclides.
5. evaluated uncertainty values for all measured quantities.
6. complete documentation that can be referenced.

Unfortunately, inventory measurements are of inconsistent quality, completeness, and documentation. Measurements are characteristically funded by the utilities and the results are often proprietary. There exists no organized effort for the collection, examination, evaluation, normalization, documentation, and/or distribution of spent-fuel nuclide inventory benchmark data. We encourage the Electric Power Research Institute, because of its direct association with the utilities, to assume such a function.

A preliminary list of potential LWR spent-fuel nuclide inventory benchmarks is given in Table XX. Much of the information in this list is taken from Ref. 76; some of the measured data corresponding to the listed samples are presently proprietary.

TABLE XX

PRELIMINARY LIST OF POTENTIAL LWR
SPENT-FUEL NUCLIDE INVENTORY BENCHMARKS

REACTOR	TYPE	COUNTRY	CLAD	ENRICHMENT	#SAMPLES	EXPOSURE (GWD/T) MIN	MAX
DODEWAARD	BWR	NETHERLANDS	ZR	2.5% UO2	6	0.8	2.1
GARIGLIANO	BWR	ITALY	ZR	1.6% UO2	5	9.6	14.2
				2.1% UO2	13	8.7	12.4
JPDR-1	BWR	JAPAN	ZR	2.63% UO2	30	2.2	7.0
QUAD CITIES 1	BWR	USA	ZR	2.56% UO2 MO2		11.4	
VAK	BWR	W. GERMANY	ZR	2.33% UO2	10	7.7	14.9
CALVERT CLIFFS 1	PWR	USA	ZR	2.45% UO2	>21	16.1	52.2
H.B. ROBINSON 2	PWR	USA	ZR	2.56% UO2	4	24.6	30.9
SAN ONOFREE 1	PWR	USA	SS	3.82% MO2	6	6.4	21.1
SAXTON	PWR	USA		0.72% MO2	69	0.1	50.9
TRINO	PWR	ITALY	SS	2.71% UO2	13	7.8	16.1
				3.13% UO2	8	7.5	18.4
				3.90% UO2	2	12.3	12.3
YANKEE ROWE	PWR	USA	ZR	2.90% UO2	33		

Comparisons with integral measurements have demonstrated the accuracy of CINDER codes and libraries in calculating aggregate fission-product properties, including neutron absorption,[77] decay power,[78] and decay spectra.[79,80] It is desirable to compare the inventory of individual nuclides obtained from tandem EPRI-CELL/CINDER-2 calculations with those determined in documented benchmark inventory measurements of spent reactor fuel. In these calculations EPRI-CELL[81] computes the space-, energy-, and burnup-dependent neutron spectrum within a cylindrical cell of an LWR fuel rod. It generates a file of burnup-dependent collapsed four-group flux values and, for each selected actinide nuclide, four-group cross sections and densities at each space point. These and other data are read by a small utility program PHAZE, which prepares a CINDER-2 user input file for calculating the comprehensive nuclide inventory at any fuel space point or for the fuel average. Accuracy of the interfaced information depends upon the accuracy of the EPRI-CELL problem specification: power history; fuel description (pellet radius, density, pitch, isotopic composition, and temperature); clad description (material, inside radius, outside radius, and temperature); moderator description (percentage of void if BWR, parts-per-million boron, and temperature); and core structure description (extra region composition). Cooling intervals following shutdown must be input to PHAZE in order for the CINDER-2 input to include the decay-to-sample inventory measurements following irradiation.

The procedure of the tandem calculations must generally be repeated with power-history magnitude adjustments in order to have close agreement between a measured and calculated parameter, i.e., burnup (atom % fission), exposure (MWd/tU), or some selected atom ratio (e.g., $^{148}Nd:^{238}U$, $^{137}Cs:^{238}U$, etc.). In view of our observations in another section on quoted sample exposure and burnup values, we have generally attempted to normalize calculations to measurements by comparing atom ratios.

1. Three Mile Island-2 Air Sample. The Three Mile Island-2 (TMI-2) unit experienced an accident early on March 28, 1979, resulting in the release from the fuel of a portion of the fission-product inventory. The accident occurred after a short operating history described in monthly operating reports to NRC from the utility. The histogram representation of the TMI-2 power history and initial fuel conditions used in calculations is given in Table XXI, along with the power histories and initial fuel conditions used in calculations of all other fuels examined here.

Air samples taken from the TMI-2 containment building environment at 7:00 a.m. on March 31, 1979, were analyzed for I and Xe activities at 8:00 p.m. on that date at Bettis Atomic Power Laboratory (BAPL), as described in Ref. 82. Reported values included a simple decay correction to 7:00 a.m., which has been removed for our use. These reconstructed 8:00 p.m. measured values are given in Table XXII. We have used the TMI-2 power history and initial fuel content of Table XXI in tandem EPRI-CELL/CINDER-2 calculations, assuming a constant power distribution across the core. Calculated regional and core-average I and Xe activities are listed in Table XXII. Isotopic ratios were formed for all isotopes of the same element from measured and calculated activities for comparison in Table XXII.

Comparison of Table XXII measured and calculated activity ratios substantiates the large change in the ^{133}I to ^{133m}Xe decay branching fraction from 14% (ENDF/B-IV) to 2.88% (ENDF/B-V). However, these measured nuclide activities must be viewed critically, because they may not represent the activities of the same nuclides produced in the fuel. Some of the initial xenon resulting from direct fission yields and iodine decay was vented to the atmosphere. Most of the remaining xenon in the containment air sample resulted only from iodine decay in the water-soluble iodides. Once the air sample was extracted, there was no subsequent formation of xenon, but there was decay, for example, of $^{133m}Xe \rightarrow {}^{133}Xe \rightarrow {}^{133}Cs$. Therefore, the time of extraction, the subsequent

TABLE XXI

POWER HISTORIES USED FOR SPENT-FUEL CALCULATIONS

QUANTITY	TMI-2 AIR SAMPLE CY1; CORE TYP.		H. B. ROBINSON-2 CY1,2; ASSY.B05 ROD P8, 12"ABF		H. B. ROBINSON-2 CY1,2; ASSY.B05 ROD P8, 68"ABF		H. B. ROBINSON-2 CY1,2; ASSY.B05 ROD E14, 112"ABF		QUAD CITIES-1 CY2;ASSY.GEB-161 ROD BSG856,22"ABF		CALVERT CLIFFS-1 CY1-4;ASSY.BTO3 ROD AHS024,98"ABF	
INITIAL U234/CC	<4.39033+18>		4.44528+18		4.44528+18		4.44528+18		4.40031+18		4.20591+18	
INITIAL U235/CC	<5.82902+20>		5.66790+20		5.66790+20		5.66790+20		5.90354+20		5.70028+20	
INITIAL U236/CC	<3.67315+18>		3.52605+18		3.52605+18		3.52605+18		3.67408+18		3.70686+18	
INITIAL U238/CC	<2.17845+22>		2.12845+22		2.12845+22		2.12845+22		2.21785+22		2.24019+22	
POWER HISTORY:	TIME	AVG.	TIME	AVG.	TIME	AVG.	TIME	AVG.	TIME	AVG.	TIME	AVG.
TIME STEP	HRS.	W/CC	HRS.	W/CC	HRS.	W/CC	HRS.	W/CC	HRS.	W/CC	HRS.	W/CC
1	62.00	66.68	88.53	233.37	70.35	295.11	70.35	278.33	40.00	296.61	40.00	94.92
2	3531.50	0.00	354.11	237.80	281.39	300.53	281.39	283.47	152.00	302.40	200.00	127.97
3	315.50	57.19	663.95	237.86	527.60	300.49	527.60	283.44	360.00	226.25	475.00	101.46
4	110.00	120.91	663.95	237.80	527.60	300.43	527.60	283.41	384.00	306.00	92.00	0.0
5	178.00	0.00	892.53	237.79	703.46	300.44	703.46	283.42	288.00	233.62	807.00	127.04
6	365.00	162.33	892.53	237.69	703.46	300.34	703.46	283.33	480.00	272.53	692.00	114.18
7	105.0	0.00	744.00	280.89	741.78	300.22	741.78	283.23	360.00	128.13	1500.00	254.38
8	58.00	261.42	744.00	259.98	744.00	354.67	744.00	334.64	336.00	255.96	1500.00	253.59
9	26.50	0.00	696.00	283.91	744.00	328.31	744.00	309.75	408.00	210.49	1500.00	253.25
10	51.00	221.77	744.00	285.25	696.00	358.53	696.00	338.27	240.00	263.29	1500.00	252.95
11	636.50	0.00	853.30	289.73	744.00	360.15	744.00	339.83	360.00	206.91	1500.00	252.76
12	296.00	229.40	725.20	0.00	853.30	365.70	853.30	345.08	96.00	0.00	1497.00	252.60
13	149.00	0.00	455.99	219.33	725.20	0.00	725.20	0.00	528.00	243.61	738.00	0.00
14	233.00	269.00	893.51	218.20	455.99	278.17	455.99	262.28	1104.00	0.00	1500.00	253.41
15	320.00	248.77	744.00	270.15	893.51	275.00	893.51	259.49	384.00	122.23	1500.00	251.27
16	414.67	0.00	720.00	271.23	744.00	341.31	744.00	322.04	360.00	211.31	1798.00	251.93
17	9.33	3.64	744.00	279.46	720.00	342.56	720.00	323.21	360.00	190.26	270.00	182.91
18	672.00	268.43	720.00	244.14	744.00	352.89	744.00	332.98	504.00	211.22	392.00	147.50
19	135.75	299.11	744.00	192.19	720.00	308.36	720.00	290.94	96.00	0.00	192.00	0.00
20	16.50	0.00	744.00	156.45	744.00	241.80	744.00	228.09	624.00	127.22	484.00	127.83
21	15.75	185.08	634.22	160.61	744.00	197.84	744.00	186.60	384.00	215.00	1730.00	251.34
22	484.00	294.33	542.89	160.77	634.22	203.22	634.22	191.66	336.00	306.61	1730.00	251.55
23	92.00	COOLING	1455.30	0.00	542.89	203.19	542.89	191.64	552.00	245.04	923.00	260.51
24			967.60	147.18	1455.30	0.00	1455.30	0.00	96.00	0.00	2076.00	265.10
25			744.00	249.23	967.60	186.30	967.60	175.66	528.00	195.89	346.00	261.17
26			744.00	215.40	744.00	314.53	744.00	296.80	72.00	0.00	1800.00	0.00
27			720.00	224.45	744.00	272.04	744.00	256.66	240.00	183.08	815.00	242.50
28			744.00	214.17	720.00	283.57	720.00	267.53	480.00	259.69	122.00	0.00
29			720.00	162.81	744.00	270.58	744.00	255.25	480.00	272.17	753.00	254.84
30			744.00	197.93	720.00	205.83	720.00	194.14	504.00	272.14	1460.00	263.18
31			744.00	214.16	744.00	250.31	744.00	236.08	504.00	254.09	1460.00	264.73
32			672.00	220.58	744.00	270.60	744.00	255.27	480.00	254.18	1588.00	259.75
33			744.00	226.81	672.00	278.73	672.00	262.90	504.00	254.10	550.00	0.00
34			833.80	224.99	744.00	286.59	744.00	270.34			204.00	108.21
35			12162.00	COOLING	833.80	284.29	833.80	268.15			1120.00	262.81
36					12162.00	COOLING	42569.00	COOLING			1120.00	262.68
37											2064.00	0.00
38											1292.00	255.41
39											1292.00	251.68
40											1369.00	152.47
41											1369.00	152.93
42											219.00	76.77
43											1139.00	229.32
44											1642.00	265.07
45											1642.00	265.67
46											548.00	229.17
47											11232.00	COOLING
48											312.00	COOLING
49											264.00	COOLING

TABLE XXII

COMPARISON OF MEASURED AND CALCULATED TMI-2
CONTAINMENT BUILDING AIR SAMPLE ACTIVITY RATIOS

QUANTITY	MEASURED VALUE	CALCULATED VALUES 2.01% FUEL VALUE	%DIFF.	2.67% FUEL VALUE	%DIFF.	3.00% FUEL VALUE	%DIFF.	CORE AVERAGE VALUE	%DIFF.
BURNUP, ATOM%FISSION		0.337		0.338		0.339		0.338	
EXPOSURE, MWD/T		3265		3263		3261		3263	
SAMPLE ACTIVITIES: CURIES/LITER									
I131	6.0 -5								
I133	<1.9 -5								
XE133	6.29-1								
XE133M	1.35-2								
XE135	3.00-3								
FUEL INVENTORY: CURIES/CC									
I131		5.281+0		5.223+0		5.205+0		5.235+0	
I133		8.510-1		8.537-1		8.548-1		8.532-1	
XE133		1.155+1		1.159+1		1.161+1		1.158+1	
XE133M		2.284-1		2.279-1		2.278-1		2.280-1	
XE135		4.925-2		5.030-2		5.079-2		5.014-2	
ACTIVITY RATIOS:									
XE133M:XE133	0.0214	0.01977	-8	0.01966	-8	0.01962	-8	0.01968	-8
XE135:XE133	0.0048	0.00426	-11	0.00434	-9	0.00437	-8	0.00433	-9
XE135:XE133M	0.2230	0.21564	-3	0.22072	-1	0.22300	0	0.21988	-1
I133:I131	<0.3235	0.16116	-50	0.16345	-49	0.16423	-49	0.16298	-50

AIR SAMPLES TAKEN AT 7:00 AM MARCH 31,1979; MEASUREMENTS MADE AT BAPL AT 8:00 PM OF THE SAME DAY. REPORTED ACTIVITIES WERE DECAY CORRECTED TO THE TIME SAMPLES WERE TAKEN. VALUES QUOTED AS MEASURED ABOVE HAVE BEEN DECAY CORRECTED BACK TO THE TIME OF MEASUREMENT.

CALCULATED VALUES GIVEN FOR THE CORRESPONDING 88 HOURS COOLING.

time of measurements, and the fractional venting of the initial Xe content are critical to calculations of relative amounts of, for example, ^{133m}Xe and ^{133}Xe. Our calculations reflect only the extraction and measurement times. We are surprised at the good agreement with calculations in view of the complex transport process.

2. H. B. Robinson-2 Samples. Assembly B05 of H. B. Robinson-2 (HBR-2) cycles 1 and 2 was discharged on or about May 5, 1975. The fuel description and power history of this assembly are described in Ref. 83. Three samples of fuel were removed from rod P8 of this assembly and destructively analyzed at Battelle Columbus Laboratories (BCL) on September 24, 1975, as described in Ref. 71. Of the three samples analyzed, one has been described as atypical because of its close proximity to a space grid during operation. The two remaining samples of rod P8, designated here as P8A and P8B, were taken from 12 in. and 68 in. above the bottom of the fuel, respectively.

Results of HBR-2 P8A and P8B measurements are given as atom density ratios and as burnup and exposure values determined with ASTM method E321-69. We have made iterative tandem EPRI-CELL/CINDER-2 calculations to converge on close agreement between measured and calculated atom ratios of $^{148}Nd:^{238}U$. Each calculation used the same histogram power-history shape, constructed from the assembly-averaged power-history data of Ref. 83, adjusted in magnitude to produce the desired calculated atom ratio for the sample. The beginning-of-life nuclide densities and final histogram history used for these samples are given in Table XXI.

The measured atom ratios, reported without uncertainties, are compared with the calculated ratios for these two samples in Table XXIII. Here the calculated sample burnup values are lower than those reported for the samples because of the higher ^{148}Nd net yield value resulting from the calculation. The calculated exposure values are higher than the reported values because of the higher Q values determined in the CELL calculations.

Comparison of the measured and calculated U and Pu atom fractions of Table XXIII shows good agreement for major nuclides. The minor constituents, ^{234}U and ^{238}Pu, are not in good agreement; calculated values are less than measured values by as much as 17%. The amount of ^{234}U present in a spent fuel sample is due almost entirely to the undepleted portion of ^{234}U initially present in the clean fuel. Small contributions are made from $^{235}U(n,2n)$ and from the decay of ^{242}Cm and ^{238}Pu. Initial fuel concentrations are generally specified simply by weight per cent ^{235}U, and ^{234}U initial concentrations must be estimated.

TABLE XXIII

COMPARISON OF MEASURED AND CALCULATED H. B. ROBINSON-2 2.56% PWR SPENT-FUEL INVENTORY, CYCLES 1-2 ASSEMBLY B05 ROD P8, SAMPLES 12 in. and 68 in. ABOVE BOTTOM OF FUEL

	SAMPLE P8A, 12 IN. ABF			SAMPLE P8B, 68 IN. ABF		
QUANTITY	MEASURED VALUE	CALC. VALUE	%DIFF.	MEASURED VALUE	CALC. VALUE	%DIFF.
BURNUP, ATOM%FISSION	2.559	2.526	-1.30	3.221	3.173	-1.48
EXPOSURE, MWD/T	24570	24935	+1.48	30920	31494	+1.86
ATOM FRACTIONS:						
U234/U	0.00016	0.00014	-13.53	0.00014	0.00012	-12.03
U235/U	0.00816	0.00843	+3.27	0.00612	0.00604	-1.34
U236/U	0.00326	0.00320	-1.74	0.00352	0.00354	+0.58
U238/U	0.98842	0.98823	-0.02	0.99022	0.99030	+0.01
PU238/PU	0.01143	0.00952	-16.75	0.01676	0.01407	-16.07
PU239/PU	0.59557	0.59686	+0.22	0.54261	0.54319	+0.11
PU240/PU	0.23290	0.22679	-2.63	0.25101	0.23943	-4.61
PU241/PU	0.11842	0.12291	+3.79	0.12998	0.13697	+5.38
PU242/PU	0.04168	0.04393	+5.39	0.05964	0.06635	+11.24
ATOM RATIOS:						
PU239/U238	0.00494	0.00485	-1.79	0.00518	0.00496	-4.33
ND148/U238	0.000450	0.000450	-0.01	0.000570	0.000570	+0.03

MEASURED VALUES REPORTED IN BATTELLE COLUMBUS LABORATORIES REPORT BMI-1938,P16,(1975). CALCULATED VALUES FROM THE USE OF A DETAILED POWER HISTORY, A 506.75 DAY COOLING PERIOD, AND ENDF/B-V DATA IN ITERATIVE TANDEM EPRI-CELL/CINDER-2 CALCULATIONS TO CONVERGE UPON THE MEASURED ND148/U238 ATOM RATIO.

Plutonium-38 is not initially present and is produced by three main paths. For HBR-2 sample P8B, for example, the ranking of these paths evaluated for the measurement cooling time is as follows:

1. 58% $^{235}U(n,\gamma)^{236}U(n,\gamma)^{237}U\text{-}\beta^{-}\text{-}^{237}Np(n,\gamma)^{238}Np\text{-}\beta^{-}\text{-}^{238}Pu$
2. 21% $^{238}U(n,2n)^{237}U\text{-}\beta^{-}\text{-}^{237}Np(n,\gamma)^{238}Np\text{-}\beta^{-}\text{-}^{238}Pu$
3. 21% $^{242}Cm\text{-}\alpha\text{-}^{238}Pu$
4. 0.03% $^{238}U(n,\gamma)^{239}U\text{-}\beta^{-}\text{-}^{239}Np\text{-}\beta^{-}\text{-}^{239}Pu(n,2n)^{238}Pu.$

The formations of ^{234}U and ^{238}Pu are affected by (n,2n) reactions. The $^{238}U(n,2n)$ and $^{239}Pu(n,2n)$ cross sections are evaluated in the EPRI-CELL calculations for the temporal reactor flux, whereas the $^{235}U(n,2n)$ reaction is absent from the EPRI-CELL calculation and is evaluated from the TOAFEW-V[49] collapse of 154-group cross sections processed with a typical LWR flux.

An additional sample of HBR-2 assembly B05 fuel has recently been analyzed at Los Alamos. The sample, taken 112" above the bottom of the 144-in. rod E14, was not examined by standard techniques for determination of burnup. Inventories of 8 fission products and 14 actinides were measured in the determination of the rates at which actinides and fission products are leached from spent fuel under controlled oxidation-reduction conditions. Iterative tandem EPRI-CELL/CINDER-2 calculations were made, using scaled variations of the assembly B05 histogram power history, to converge upon the measured $^{137}Cs/^{238}U$ atom ratio. We converted atom volume densities (atoms/cm^3 oxide) to mass densities (atoms/gm oxide) by dividing by a density of 9.95 gms oxide/cm^3. Measured and calculated values are compared in Table XXIV. The -2.88% difference from the measured ^{137}Cs and -2.80% difference from the measured ^{238}U indicate a density normalization problem of that magnitude.

Of the eight fission products examined, the differences between the measured and calculated concentrations of ^{154}Eu and ^{155}Eu are exceptionally large. At high exposures, the inventories of these nuclides have been produced almost entirely from multiple neutron captures on lighter fission products.

Of the 14 actinides examined, the differences between the measured and calculated concentrations significantly exceed the measurement uncertainty for 4 of the nuclides. Two of these are ^{234}U and ^{238}Pu, which have low calculated values and were discussed above. Plutonium-240 and -242 also have calculated values significantly lower than measured values.

3. Quad Cities-1 Sample. Special test assemblies of UO_2 and mixed U-Pu oxide (MO_2) fuel were fabricated for loading in the Quad Cities-1 (QC-1) BRW core.[84,85] Fuel removed after one-cycle exposure in cycle 2 was cooled and analyzed at the G.E. Vallecitos facility.[86] Of the samples analyzed, we have selected a sample 21.5 in. above the bottom of the reactor fuel for EPRI-CELL/CINDER-2 modeling. Iterative tandem calculations were performed to converge upon the measured $^{148}Nd/^{238}U$ atom ratio. Calculations used a histogram power history, listed in Table XXI, constructed from a graphical total-core power history and semimonthly transverse irradiation probe (TIP) data indicating the

TABLE XXIV

COMPARISON OF MEASURED AND CALCULATED H. B. ROBINSON-2 2.56% PWR SPENT-FUEL INVENTORY, CYCLE 1-2, ASSEMBLY B05 ROD E14, SAMPLE 112 in. ABOVE BOTTOM OF FUEL

QUANTITY	MEASURED VALUE	CALCULATED VALUE	%DIFF.
BURNUP, ATOM%FISSION		2.998	
EXPOSURE, MWD/T		29711	
ATOM RATIO:			
CS137/U238	0.00174	0.00174	-0.08
NUCLIDE DENSITIES, ATOMS/GM OXIDE AT 4.86 YEARS COOLING			
SR 90	2.73+18	2.37+18	-13.17
RU106	>1.71+16	2.54+16	
SB125	7.45+15	8.39+15	+12.59
CS134	7.61+16	6.92+16	-9.01
CS137	3.75+18	3.64+18	-2.88
CE144	1.41+16	1.38+16	-1.89
EU154	3.92+16	6.59+16	+67.99
EU155	1.28+16	1.83+16	+43.16
U234	3.24+17	2.71+17	-16.24
U235	1.34+19	1.40+19	+4.38
U236	7.68+18	7.31+18	-4.82
U238	2.15+21	2.09+21	-2.80
NP237	8.19+17	7.64+17	-6.69
PU238	3.25+17	2.34+17	-28.00
PU239	1.08+19	1.03+19	-4.41
PU240	5.23+18	4.39+18	-16.01
PU241	2.18+18	2.11+18	-3.23
PU242	1.29+18	1.11+18	-13.57
AM241	6.55+17	6.23+17	-4.84
AM243	2.2 +17±20%	2.07+17	-6.11
CM242	1.8 +13	1.76+13	-2.23
CM244	5.1 +16±20%	4.21+16	-17.54

MEASUREMENTS BY LOS ALAMOS GROUP CNC-11; EXPERIMENTAL UNCERTAINTY ±5% UNLESS OTHERWISE INDICATED.

CALCULATED VALUES FROM THE USE OF A DETAILED POWER HISTORY, A 4.86-YEAR COOLING PERIOD, AND ENDF/B-V DATA IN ITERATIVE TANDEM EPRI-CELL/CINDER-2 CALCULATIONS TO CONVERGE UPON THE MEASURED CS137/U238 ATOM RATIO. CALCULATED ATOMS-PER-GRAM-OXIDE QUANTITIES FROM CALCULATED ATOMS-PER-CM^3-OXIDE VALUES /9.95G/CM^3.

relative power at a point close to the fuel sample. Because of the low elevation of the fuel sample, a 0% moderator void was used in the calculation. Measured and calculated quantities for this relatively low exposure fuel sample are compared in Table XXV. Measured values were decay corrected to shutdown before reporting, a practice to be discouraged because of inconsistencies in nuclear data and treatment. No record is generally made of the values of data and total correction.

TABLE XXV

COMPARISON OF MEASURED AND CALCULATED QUAD CITIES-1
2.56% BWR SPENT-FUEL INVENTORY, CYCLE 2, ASSEMBLY GEB-161
ROD BSG0856, SAMPLE 21.5 in. ABOVE BOTTOM OF FUEL

QUANTITY	MEASURED VALUE	CALCULATED VALUE	%DIFF.
BURNUP, ATOM%FISSION	1.193	1.215	+1.8
EXPOSURE, MWD/T	11450	11837	+3.4
ATOM FRACTIONS:			
U234/U	1.776-4± 1.0%	1.638-4	-7.8
U235/U	1.512-2± 0.6%	1.505-2	-0.5
U236/U	2.063-3± 0.5%	2.061-3	-0.1
U238/U	9.861-1± 0.5%	9.827-1	+0.01
PU239/PU	7.469-1± 0.1%	7.428-1	-0.5
PU240/PU	1.810-1± 0.3%	1.901-1	+5.0
PU241/PU	6.342-2± 0.5%	5.894-2	-7.1
PU242/PU	8.694-3± 1.3%	8.154-3	-6.2
AM241/AM	7.75 -1±68.0%	6.52 -1	-15.9
AM242/AM	6.42 -3±68.0%	6.88 -3	+7.5
AM243/AM	2.18 -1±68.0%	3.41 -1	+56.4
CM242/CM	8.08 -1± 0.9%	8.05 -1	-0.4
CM243+244/CM	1.92 -1± 6.0%	1.95 -1	+1.6
ATOM RATIOS:			
ND148/U238	2.123-4± 0.67%	2.129-4	+0.3
NP237/U238	8.33 -5±18.0%	8.89 -5	+6.7
PU239/U238	3.354-3± 0.10%	3.224-3	-3.9
AM241/U238	8.98 -6±890.%	3.785-6	-57.9
CM242/U238	8.86 -7±12.9%	5.810-7	-34.4

MEASUREMENTS BY G.E., RESULTS DECAY CORRECTED TO SHUTDOWN.

CALCULATED VALUES FROM THE USE OF A DETAILED POWER HISTORY AND ENDF/B-V DATA IN ITERATIVE TANDEM EPRI-CELL/CINDER-2 CALCULATIONS TO CONVERGE UPON THE MEASURED ND148/U238 ATOM RATIO.

Differences between measured and calculated U and Pu atom fractions appear to be quite good, although many exceed the small uncertainties given. Of these, the largest difference corresponds to the low calculated value of ^{234}U. ^{238}Pu is not reported. Differences between measured and calculated Am atom fractions do not exceed the associated large uncertainties, and the agreement with Cm atom fractions is very good.

Comparisons between measured and calculated atom ratios to ^{238}U must each be examined relative to the measurement uncertainty; of these, the most alarming is the low calculated value of ^{242}Cm.

The description of the complex spectrum effects of void, burnable poisons and control-rod spaces in BWR calculations may not be adequately treated with the EPRI-CELL methodology, and EPRI has cautioned against the reliance on EPRI-CELL-generated cross sections and fluxes without comparison with the results of a more complete treatment using a two-dimensional code such as EPRI-CPM.

4. Calvert Cliffs-1 Sample. Special high-exposure test assemblies have been installed in the core of the Calvert Cliffs-1 (CC-1) PWR in a program involving the utility, EPRI, Combustion Engineering (CE), and the Safeguards Program at Los Alamos. Some of the fuel was removed after four cycles of exposure and, after cooling, analyzed at BCL. The preliminary results of measurement, currently available without uncertainties, are considered proprietary by EPRI, and the measured and calculated atom fractions and atom ratios are not given in Table XXVI. However, EPRI has permitted our calculation and comparison of these quantities.

This fuel was irradiated to high exposure in a core composed of assemblies of lower exposure. This consideration and the large water-filled control rod locations in the CE core have led EPRI to caution against the reliance on the EPRI-CELL methodology in calculating accurate exposure-dependent cross sections and fluxes. We have, however, relied upon this methodology in our calculations.

The histogram power history generated for CC-1 fuel calculations, listed in Table XXVI, was generated from a simple full-core histogram power history presented graphically in Ref. 87. This full-core power history was scaled and used in iterative EPRI-CELL/CINDER-2 calculations converging upon the measured $^{148}Nd/^{238}U$ atom ratio.

TABLE XXVI

PRELIMINARY COMPARISON OF CALVERT CLIFFS-1
2.45% PWR SPENT-FUEL INVENTORY, CYCLES 1-4
ASSEMBLY BT-3 ROD AHS-024, SAMPLE 90 in. ABOVE BOTTOM OF FUEL

QUANTITY	MEASURED VALUE	CALCULATED VALUE	%DIFF.
BURNUP, ATOM%FISSION	4.776	4.662	-2.39
EXPOSURE, MWD/T	45854	46836	+2.14
ATOM FRACTIONS:			
U234/U *			-9.70
U235/U *			+23.00
U236/U *			-2.10
U238/U *			-0.04
PU238/PU **			-8.70
PU239/PU **			+7.10
PU240/PU **			-16.50
PU241/PU **			+19.60
PU242/PU **			-3.20
ATOM RATIOS:			
ND143/ND148			+17.10
ND144/ND148			-1.00
ND145/ND148			+6.80
ND146/ND148			+6.70
ND148/U238			-0.16
PU239/U238			+22.70
AM241/PU239 ***			+13.70
AM243/PU239 ***			+53.20
CM242/PU239 ***			-20.50
CM244/PU239 ***			+5.50

MEASUREMENTS PERFORMED AT BATTELLE COLUMBUS LABORATORIES ON 1/18/82(*), 1/29/82(**), AND 1/05/82(***).

CALCULATED VALUES FROM THE USE OF A DETAILED TOTAL-CORE POWER HISTORY, APPROPRIATE COOLING TIMES, AND ENDF/B-V DATA IN ITERATIVE TANDEM EPRI-CELL/CINDER-2 CALCULATIONS TO CONVERGE UPON THE MEASURED ND148/U238 ATOM RATIO.

Differences in measured and calculated U-atom fractions are not alarming. The 23% difference in the ^{235}U remaining corresponds to better than 2% agreement in the amount of ^{235}U depleted. The calculated value of ^{234}U, as before, is considerably lower than the measured value.

Differences in the remaining measured and calculated quantities are, in general, alarmingly large. In the absence of measurement uncertainties, however, it is not possible to make meaningful observations on the differences.

The high-exposure fuel of CC-1 is unique. The nuclear power industry is pursuing the use of higher fuel enrichments for higher discharge exposures. The NRC is currently investigating the effects of these parameters on hypothetical accident analyses. The validity of inventory calculations for high-exposure fuel has not been demonstrated beyond this work. The utilities and EPRI are encouraged to make the results of such measurements available for public benchmarking of inventory calculations.

We have examined six inventory samples of varying quality and completeness. The power histories used in the calculations have been listed for other users. We have compared calculated ratios of I and Xe isotopes with measurements of an early air sample taken from the containment building following the TMI-2 accident; these show excellent agreement. Five of the sample measurements and calculations included actinide inventories in spent fuel. The per cent difference of calculated values from measured values was determined for each sample and listed in Table XXVII, where fuel samples are ordered in increasing exposure. Examination of Table XXVII values shows that, as previously indicated, calculated inventories of ^{234}U and ^{238}Pu are routinely low. Trends are also seen in ^{240}Pu and ^{241}Pu differences, but of smaller magnitude.

TABLE XXVII

COMPARISON OF DIFFERENCES BETWEEN CALCULATED AND MEASURED ACTINIDE INVENTORIES

QUANTITY	QC-1 BSG856 22"ABF	HBR-2 P8 12"ABF	HBR-2 E14 112"ABF	HBR-2 P8 68"ABF	CC-1 AHS024 98"ABF
CALC. EXPOSURE, MWD/T	11837	24935	29711	31494	46836
% DIFFERENCES,	(CALC.-MEAS.)/MEAS.	*100			
U234/U	-7.8	-13.5	-13.9	-12.0	-9.7
U235/U	-0.5	+3.3	+7.4	-1.3	+23.0
U236/U	-0.1	-1.7	-2.1	+0.6	-2.1
U238/U	+0.01	-0.02	-0.03	+0.01	-0.04
PU238/PU	------	-16.8	-21.3	-16.1	-8.7
PU239/PU	------	+0.2	+4.2	+0.1	+7.1
PU240/PU	------	-2.6	-8.3	-4.6	-16.5
PU241/PU	------	+3.8	+5.8	+5.4	+19.6
PU242/PU	------	+5.4	-6.0	+11.2	-3.2
PU239/U238	-3.9	-0.01	-1.9	+0.03	+22.7

NOTE THAT QC-1 FUEL MEASUREMENTS DID NOT INCLUDE PU238.

H. Calculated Neutron Sources in Plutonium Oxalate [W. B. Wilson and R. T. Perry (Pennsylvania State University)]

We have previously calculated the (α,n) and spontaneous-fission neutron sources in plutonium process solutions.[88] The plutonium of the process appears downstream in the form of plutonium oxalate [$(Pu(C_2O_4)_2 \cdot 6H_2O]$. We have calculated the (α,n) neutron sources in this material because of (α,n) reactions of alpha particles of $^{238\text{-}242}Pu$ and ^{241}Am on ^{13}C and $^{17,18}O$. We have also calculated the SF neutron sources associated with these Pu and Am nuclides.

The (α,n) calculations used the methodology employed in previous calculations.[89,90] Alpha-particle spectra used in the calculation were taken from Ref. 89. Alpha-particle stopping cross sections used for H, C, and O were in the form of polynomial approximations to the data of Ziegler.[91] A polynomial fit for the Pu stopping cross section was made to values extended beyond U,

using ratios given by Northcliffe and Schilling,[92] as described in Ref. 89. These polynomials are of the form

$$\ell n\varepsilon = C_0 + \sum_{i=1}^{4} C_i \ell n^i E, \quad 0.5 \text{ MeV} \leqq E \leqq 10 \text{ MeV} \quad , \tag{23}$$

where ε is the stopping cross section (eV/10^{15} atoms/cm^2) and E is alpha particle energy (MeV). The coefficients of these polynomials are given in Table XXVIII.

Thresholds for (α,n) reactions for all constituents other than ^{13}C and $^{17,18}O$ exceed the 5.55-MeV maximum alpha-particle energy encountered here. The $^{13}C(\alpha,n)$ cross section was taken from Bair and Haas.[93] The $^{17,18}O(\alpha,n)$ cross sections were evaluated in an earlier work,[91] using data of Bair and Willard,[94] Bair and Haas,[93] Bair and del Campo,[95] and Hansen et al.[96]

Spontaneous fission data have been collected from a variety of sources and are summarized in Table XXIX. These are consistent with SF data used in Ref. 89, with the exception of modifications to the SF data of ^{240}Pu and ^{241}Pu. The ^{240}Pu SF branching of 5×10^{-8}, given in ENDF/B-V, has been replaced with a value calculated with the ^{240}Pu SF $\bar{\nu}$ given by Manero and Konshin[97] (as incremented in Ref. 89 to include the delayed contribution) and a SF half-life averaged from those given by Fieldhouse, Mather, and Culliford[98] and by Budtz-Jorgensen and Knitter.[99] There are no known measured values of the ^{241}Pu SF half-life or $\bar{\nu}$. Johnson[100] has estimated a ^{240}Pu SF $\bar{\nu}$ value using a linear extrapolation scheme and, using the systematics of Swiatecki,[101] a value of the ^{240}Pu SF half-life.

TABLE XXVIII

STOPPING CROSS-SECTION POLYNOMIAL COEFFICIENTS

Element	C_0	C_1	C_2	C_3	C_4
H	2.140643	-.3904633	-.2281173	.1005977	-.01706431
C	3.583970	-.2716777	-.2398218	.05884745	-.005158292
O	3.72130	-.168700	-.300138	.0700466	-.00377296
Pu	5.14860	-.171158	-.272723	.100975	-.0160365

TABLE XXIX

SPONTANEOUS FISSION DATA

Nuclide	Half-life[a] (Seconds)	SF Half-Life (Years)	SF Decay Branching	$\bar{\nu}$ (Neutrons /SF)	Neutrons Per Any Decay
^{238}Pu	2.7691+09	4.77+10	1.840-09[b]	2.22[b]	4.08-09
^{239}Pu	7.6084+11		4.400-12[a]	2.16[d]	9.50-12
^{240}Pu	2.0670+11	1.16+11	5.646-08	2.16[b]	1.22-07
^{241}Pu	4.6389+08	2.5 +15[c]	5.880-15	2.25[c]	1.32-14
^{242}Pu	1.1875+13		5.500-06[a]	2.15[b]	1.18-05
^{241}Am	1.3639+10		4.100-12[a]	2.27[d]	9.31-12

[a] ENDF/B-V.

[b] Ref. 97 (incremented in Ref. 89 to include delayed contribution).

[c] Ref. 100.

[d] Ref. 89 (linear extrapolation).

Using the data summarized above, we have calculated the (α,n) and SF neutron sources in $Pu(C_2O_4)_2 \cdot 6H_2O$. The steps in the calculation and the intermediate and final results are shown Table XXX.

TABLE XXX

NEUTRON SOURCES IN $Pu(C_2O_4)_2 + 6H_2O$ FROM $^{238-242}Pu$ AND ^{241}Am SPONTANEOUS FISSION AND FROM THE (ALPHA,N) REACTIONS OF THEIR DECAY ALPHAS WITH ^{13}C AND $^{17,18}O$

SOURCE	LAMBDA (/SECOND)	ALPHA MEV	ALPHA /DECAY	P(E) NEUTRON/ALPHA EMITTED C-13	O-17	O-18	TOTAL	NEUTS/SOURCE ATOM DK (A,N)	S.F.	TOTAL	NEUTS/S/GRAM SOURCE (A,N)	S.F.	TOTAL	NEUTS/S/CURIE SOURCE (A,N)	S.F.	TOTAL
PU-238	2.5031-10	5.359	0.0013	1.80-8	3.04-9	3.58-8	5.68-8	7.4-11								
		5.457	0.2872	1.98-8	3.26-9	3.83-8	6.13-8	1.76-8								
		5.499	0.7115	2.07-8	3.36-9	3.95-8	6.33-8	4.51-8								
								6.27-8	4.08-9	6.68-8	3.98+4	2.59+3	4.24+4	2.33+3	1.51+2	2.47+3
PU-239	9.1103-13	5.054	0.0002	1.27-8	2.38-9	2.87-8	4.38-8	8.7-12								
		5.075	0.0003	1.30-8	2.40-9	2.89-8	4.42-8	1.3-11								
		5.105	0.1150	1.34-8	2.45-9	2.96-8	4.54-8	5.22-9								
		5.143	0.1510	1.39-8	2.53-9	3.05-8	4.69-8	7.08-9								
		5.155	0.7331	1.41-8	2.56-9	3.08-8	4.74-8	3.47-8								
								4.71-8	9.5-12	4.71-8	1.08+2	2.18-2	1.08+2	1.74+3	3.52-1	1.74+3
PU-240	3.3534-12	5.014	0.0009	1.22-8	2.31-9	2.83-8	4.29-8	3.9-11								
		5.123	0.2650	1.36-8	2.49-9	3.00-8	4.61-8	1.21-8								
		5.168	0.7341	1.44-8	2.60-9	3.11-8	4.81-8	3.52-8								
								4.75-8	1.22-7	1.70-7	4.00+2	1.03+3	1.43+3	1.76+3	4.51+3	6.27+3
PU-241	1.4942-09	4.797	2.94-7	1.08-8	1.98-9	2.43-8	3.71-8	1.1-14								
		4.854	2.97-6	1.10-8	2.04-9	2.51-8	3.82-8	1.1-13								
		4.897	2.04-5	1.11-8	2.10-9	2.60-8	3.91-8	8.0-13								
		4.972	3.19-7	1.16-8	2.20-9	2.76-8	4.14-8	1.3-14								
		4.999	1.01-7	1.20-8	2.27-9	2.81-8	4.23-8	4.3-15								
		5.042	2.50-7	1.26-8	2.36-9	2.87-8	4.37-8	1.1-14								
								9.5-13	1.3-14	9.6-13	3.59+0	4.94-2	3.64+0	3.55-2	4.90-4	3.60-2
PU-242	5.8370-14	4.755	0.0010	1.06-8	1.92-9	2.37-8	3.61-8	3.6-11								
		4.856	0.2240	1.10-8	2.04-9	2.51-8	3.80-8	8.53-9								
		4.901	0.7750	1.12-8	2.11-9	2.61-8	3.93-8	3.05-8								
								3.90-8	1.18-5	1.18-5	5.68+0	1.72+3	1.72+3	1.45+3	4.38+5	4.39+5
AM-241	5.0821-11	5.322	0.0002	1.71-8	2.96-9	3.49-8	5.50-8	1.1-11								
		5.389	0.0133	1.85-8	3.11-9	3.66-8	5.82-8	7.7-10								
		5.417	0.0001	1.90-8	3.17-9	3.73-8	5.93-8	5.9-12								
		5.443	0.1281	1.95-8	3.23-9	3.80-8	6.06-8	7.77-9								
		5.486	0.8527	2.04-8	3.33-9	3.91-8	6.28-8	5.35-8								
		5.513	0.0020	2.09-8	3.39-9	3.98-8	6.40-8	1.3-10								
		5.544	0.0035	2.16-8	3.47-9	4.07-8	6.57-8	2.3-10								
								6.24-8	9.3-12	6.24-8	7.94+3	1.18+0	7.94+3	2.31+3	3.44-1	2.31+3

I. Calculating Fission-Product Decay-Energies and Spectra Using Adjusted Data (D. C. George, R. J. LaBauve, and T. R. England)

Reference 102 describes a method of obtaining sets of parameters to be used to calculate fission-product beta-ray and gamma-ray decay-energies and spectra for mixtures of ^{235}U and ^{239}Pu fuels. This method combines the results of experiments with summation calculations that used ENDF/B-V[103] data as input to the CINDER-10[104] code.

Sets of parameters are now available for the fuels and incident neutron energies that are listed in Table XXXI. In creating the additional parameter sets, experimental results were used to augment the summation results wherever possible. Specifically, data from the Oak Ridge National Laboratory (ORNL) spectral experiment[105] and the Los Alamos experiment[80] were used. In the Oak Ridge experiment, ^{241}Pu was irradiated with thermal neutrons for several times and aggregate fission-product decay-energy spectra for both gamma-ray and beta-ray decay were measured for a range of cooling times. The Los Alamos spectral experiment measured the gamma-ray decay-energy spectra from ^{233}U that had been irradiated with thermal neutrons. Parameter sets for fuels for which no experimental measurements were available were derived from summation calculations that used ENDF/B-V data as input to the CINDER-10 code. These summation results were processed as described in Refs. 106 and 107.

A derivative, ADENAMF, of the code ADENA[102] was written to calculate fission-product beta- and gamma-decay energies and spectra in 19 or fewer energy groups from any mixture of 2 fuels listed in Table XXXI. Figure 32 compares the ADENAMF calculation of gamma-ray decay energy for ^{241}Pu with the ORNL experimental data.

TABLE XXXI

PARAMETER SETS

Uranium	Plutonium
^{233}U	^{239}Pu
^{235}U Thermal*	Thermal**
Thermal**	Fast
Fast	14-MeV
^{238}U 14-MeV	^{240}Pu Fast
Fast	^{241}Pu Thermal**
	^{232}Th
	Fast

*Parameter sets based on experimental results plus calculation for gamma only.
**Parameters sets based on experimental results plus calculation for both beta and gamma.

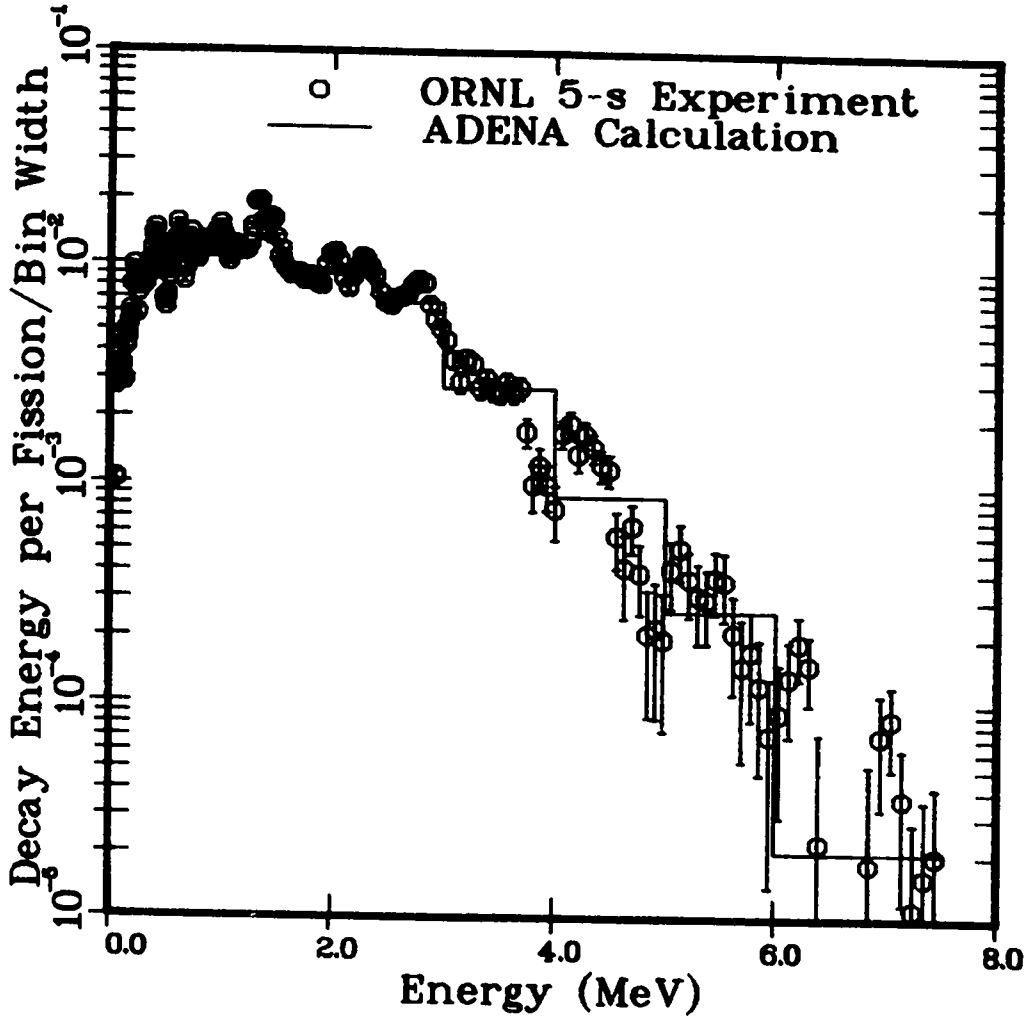

Fig. 32. Gamma energy for cooling time = 98 s.

IV. NEUTRONIC CALCULATIONS FOR THE COMPACT REVERSED-FIELD PINCH REACTOR

[R. J. LaBauve and M. E. Battat (T-Division Consultant)]

The starting point for these calculations was a scaled layout of a 1000-MWe (net) DT/CRFPR design with the corresponding key physics and engineering parameters, reported by Hagenson and Krakowski.[108] The initial parameter studies were made using this model. Specifically, we examined the effects of varying the thickness and material composition in the blanket and the third wall. Following this parameter survey, a "canonical" model was devised. Pending a more careful examination of the engineering aspects of the design, the canonical model is satisfactory for further exploratory studies.

Neutronics calculations were performed using the ONEDANT discrete-ordinates transport code[109] in the S_8P_3 approximation. A multigroup coupled cross-section set (30 neutron + 12 gamma ray), XSLIBA, was used for the calculations. XSLIBA is a 35-element (a few isotopes are included) library compiled by G. L. Woodruff of the University of Washington. Data for kerma factors, displacements per atom (dpa), and H and He production were retrieved from the KERMA8 file compiled by D. J. Dudziak (T-1). Activation cross sections were prepared from data contained in the GAMMON activation library.[110]

Because the major radius of the plasma is 4.30 m (27-m circumference), an infinite-cylinder geometry was specified for our problems. For an infinite cylinder, input and output quantities are normalized to a height of 1 cm. For example, a wall loading (I_W) of 19.5 MW/m^2 at a minor plasma radius of 0.75 m corresponds to 91.89 MW (19.5 x 2π x 0.75) per meter of height at the first wall, or 918.9 kW per cm of height. Converting kW to MeV/s, we obtain an energy current of 5.74 x 10^{18} MeV/s. Based on a value of 14.06 MeV/neutron, the source current at the first wall is 4.08 x 10^{17} neutrons/s, and this is the normalization factor we input to ONEDANT. Of course, the ONEDANT output, in terms of per cm of height, can be converted to more convenient units if desired.

Before discussing the calculational results, we list below the definitions of some of the quantities referred to in this study. The quantity P_{XX} is a linear heating rate and can be expressed in units of, for example, MW/m or kW/cm.

P_{FW}, P_{SW}, P_{TW} = linear heating rate in first, second, and third walls

P_B = linear heating rate in blanket

P_{TFC}, P_{PFC} = linear heating rate in toroidal and poloidal field coils

M_N = blanket energy multiplication

= $(P_{FW}+P_{SW}+P_B+P_{TW})/P_W$

P_W = MW/m incident on the first wall

= 91.89 for I_W of 19.5 MW/m^2 (see text)

e_B = blanket efficiency

= $M_N P_W$ / $(M_N P_W+P_{TFC}+P_{PFC}+P_{LOSS})$. P_{LOSS} assumed to be zero.

B_R = tritium breeding ratio.

The material compositions and reference geometry used for the parametric studies are shown in Table XXXII and Fig. 33, respectively. All calclulations were normalized to a wall loading of 19.5 MW/m^2. The material list in Table XXXII is self-explanatory with one exception. The Pb-Li eutectic in the blanket is a liquid consisting of $Pb_{83}Li_{17}$.[111] For this study, the ^6Li enrichment was fixed at 60 %.

TABLE XXXII

MATERIAL COMPOSITIONS--CRFPR NEUTRONICS SURVEY CALCULATIONS

(A) PRIMARY MATERIALS

COPPER - 8.96 G/CM3			
WATER - 1.0			
$PB_{83}LI_{17}$ - 9.40	60% LI6 ENRICHED		
PCASS ST STL - 7.86	66.7 W/O FE	13.7 W/O CR	
	2.0 W/O MO	15.6 W/O NI	
	2.0 W/O MN		

(B) MIXTURES

FIRST WALL -	60 V/O COPPER	29 V/O WATER (40 V/O AT 0.726 G/CM3)
SECOND WALL -	60 V/O PCASS	29 V/O WATER (40 V/O AT 0.726 G/CM3)
BLANKET -	PB-LI + PCASS IN VARIED PROPORTIONS	
THIRD WALL -	90 V/O PCASS	7.26 V/O WATER (10 V/O AT 0.726 G/CM3)
TF AND PF COILS -	10 V/O PCASS 10 V/O WATER	80 V/O COPPER

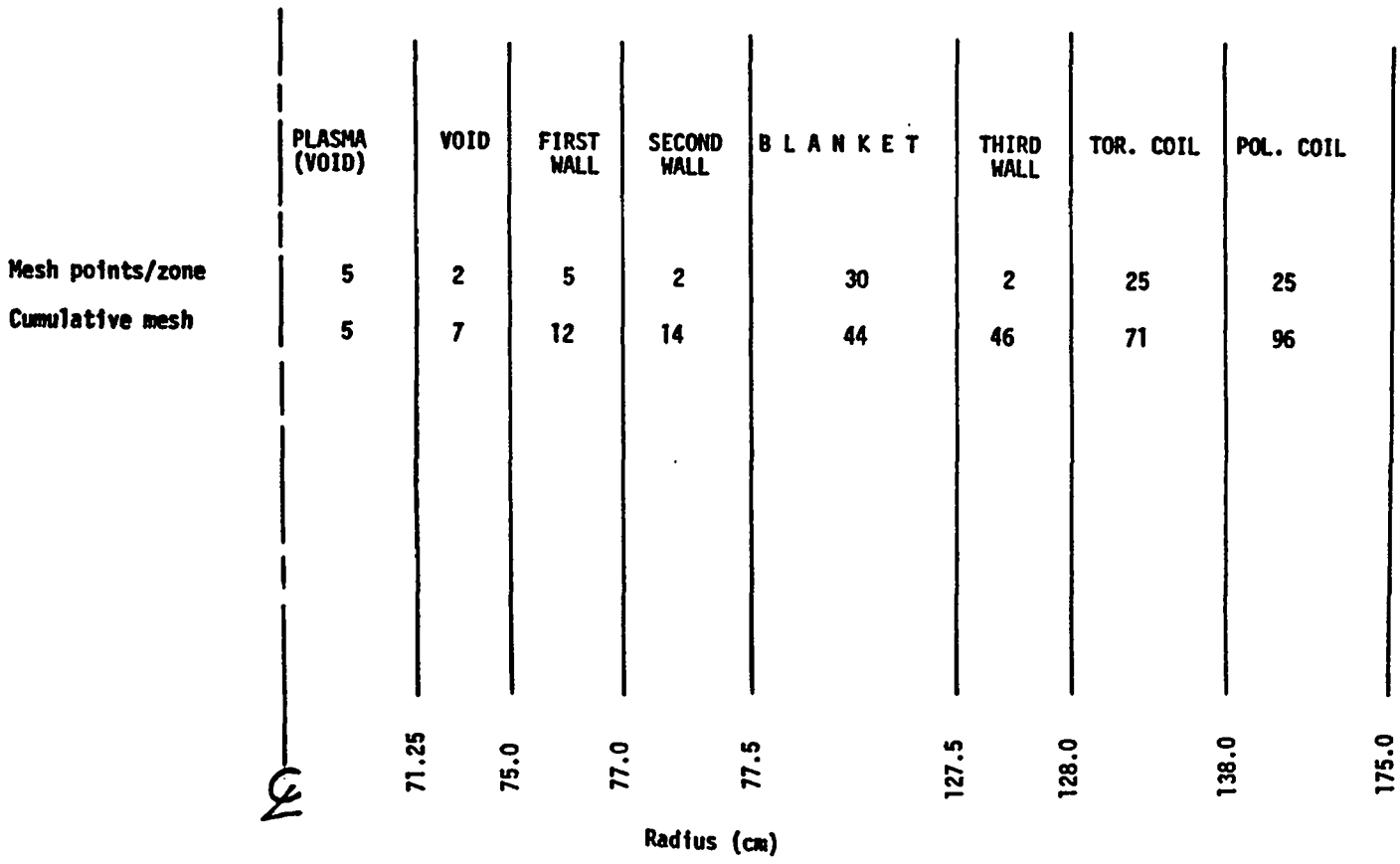

Fig. 33. CRFPR survey calculational model. Infinite-cylinder geometry. Blanket and third-wall thicknesses variable. Pb-Li/PCASS ratio in the blanket was also varied.

The first problem examined was the effect of varying blanket thickness on selected neutronics parameters. The third-wall thickness was fixed at 0.5 cm and a blanket composed of 90 volume per cent (v/0) Pb-Li and 10 v/0 stainless steel alloy (PCASS) was assumed. Results are tabulated in Table XXXIII, and selected results are plotted in Fig. 34. It is seen that M_N, e_B, and BR increase as blanket thickness is increased. As expected, P_{TFC} and P_{PFC} decrease as the blanket is thickened. Note that the maximum blanket efficiency is about 0.94.

TABLE XXXIII

EFFECT OF VARYING BLANKET THICKNESS ON CRFPR NEUTRONICS PARAMETERS. BLANKET IS 90 v/0 Pb-Li + 10 v/0 PCASS. THIRD WALL -- 0.5-cm THICK.

Blanket thickness - m ⟶	0.3	0.4	0.5	0.6
MW/m incident on first wall	91.89	91.89	91.89	91.89
MW/m total	130.07	127.48	125.50	124.06
MW/m in coils	24.37	16.19	10.68	6.97
Blanket energy multiplication (M_N)	1.15	1.21	1.25	1.27
Blanket efficiency (e_B)	0.813	0.873	0.915	0.944
Breeding ratio (BR)	0.920	1.036	1.120	1.180
First-wall heating - MW/m				
Total	20.74	20.90	20.96	20.98
Neutron	7.60	7.64	7.66	7.66
Gamma-ray	13.14	13.26	13.30	13.32
Toroidal coil heating - MW/m				
Total	14.95	10.09	6.77	4.48
Neutron	1.61	1.00	0.62	0.38
Gamma-ray	13.34	9.09	6.15	4.10
Poloidal coil heating - MW/m				
Total	9.42	6.10	3.91	2.48
Neutron	0.51	0.30	0.17	0.10
Gamma-ray	8.91	5.80	3.74	2.38
Max dpa/y - Cu in TFC	26.0	15.1	8.75	5.07
Max dpa/y - Cu in PFC	4.96	2.73	1.51	0.841
Max appm He/y - Cu in TFC	21.1	6.83	2.24	0.734
Max appm He/y Cu in PFC	3.44	1.13	0.373	0.123
Max appm H /y - Cu in TFC	99.9	36.7	13.7	5.16
Max appm H /y - Cu in PFC	15.5	5.57	2.02	0.747

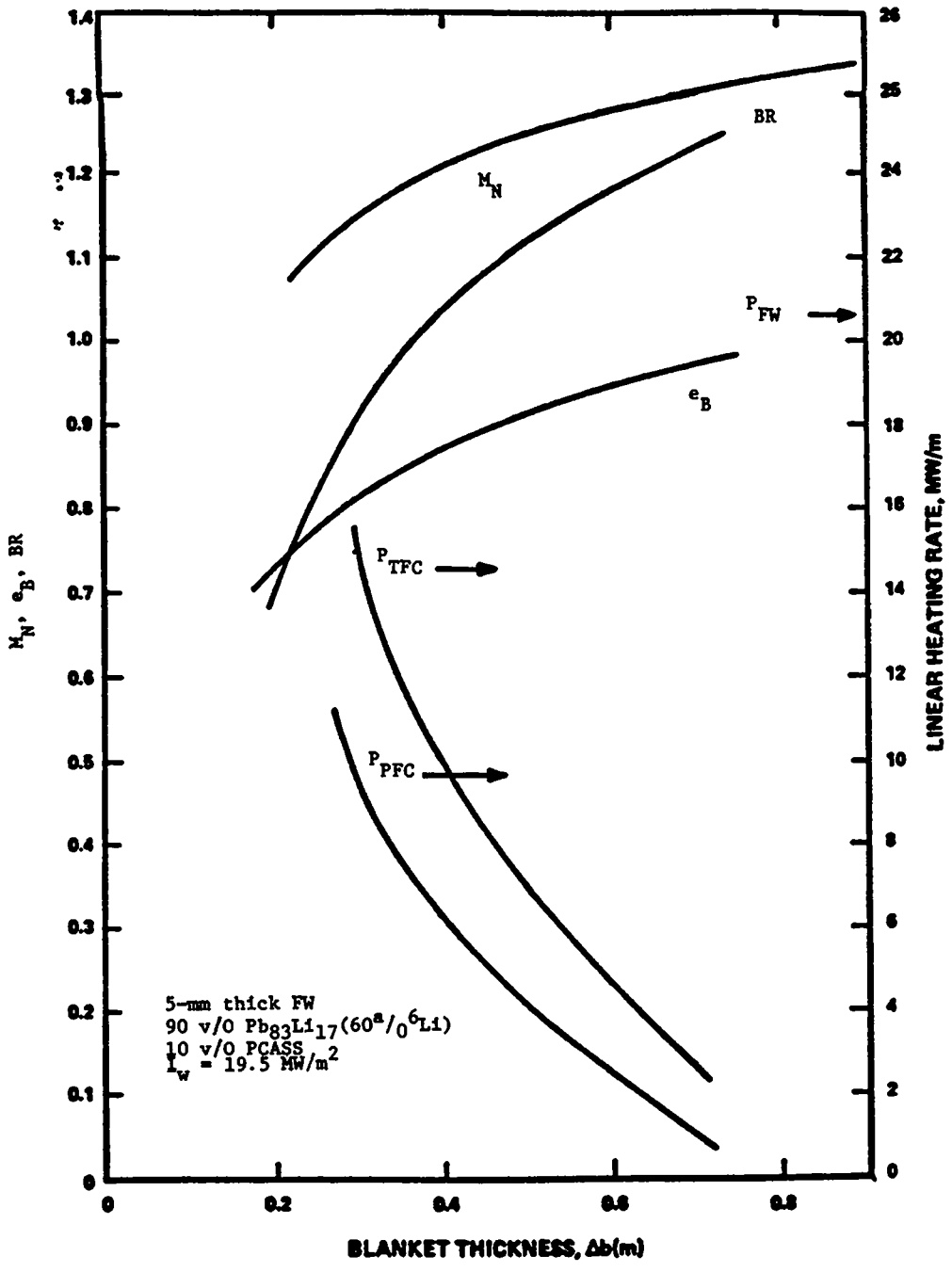

Fig. 34. Effect of varying blanket thickness on CRFPR parameters. Blanket is 90 v/0 Pb-Li and 10 v/0 PCASS. Third wall: 0.5 cm thick.

Next, ONEDANT calculations were made for a 0.5-m-thick blanket with third-wall thicknesses ranging from 0.5 to 12.5 cm. A 90/10 Pb-Li/PCASS mixture was specified for the blanket. Results are summarized in Table XXXIV and plotted in Fig. 35. Also indicated in Table XXXIV are the results for an 80/20 Pb-Li/PCASS blanket with 2.5- and 7.5-cm-thick third walls. The variations of M_N, e_B, and BR are not very dramatic, but P_{TFC} and P_{PFC} vary within a factor of 2 and 4, respectively. Comparing results for the 90/10 and 80/20 blanket, we observe that M_N and e_B are higher for the 80/20 case, but the breeding ratio is lower by about 10 %.

TABLE XXXIV

EFFECT OF VARYING THIRD-WALL THICKNESS ON CRFPR NEUTRONICS PARAMETERS. 0.5-m BLANKET WITH 90/10 Pb-Li/PCASS. RESULTS FOR 80/20 BLANKET ARE SHOWN IN PARENTHESES. P_{XX} VALUES ARE IN UNITS OF MW/m. I_W = 19.5 MW/m^2.

Third-Wall (cm) →	0.5	2.5	5.0	7.5	12.5
P_{FW}	20.96	20.96 (21.17)	20.96	20.96 (21.16)	20.96
P_{SW}	4.08	4.08 (4.12)	4.08	4.08 (4.12)	4.08
P_B	89.56	89.51 (95.77)	89.58	89.65 (95.92)	89.73
P_{TW}	0.23	1.22 (1.08)	2.57	3.97 (3.50)	6.62
M_N	1.25	1.26 (1.33)	1.28	1.29 (1.36)	1.32
e_B	0.915	0.922 (0.936)	0.934	0.945 (0.955)	0.966
BR	1.120	1.122 (1.029)	1.125	1.128 (1.034)	1.130
P_{TFC}	6.77	6.50 (5.63)	5.82	4.98 (4.24)	3.22
P_{PFC}	3.92	3.25 (2.68)	2.53	1.93 (1.57)	1.04

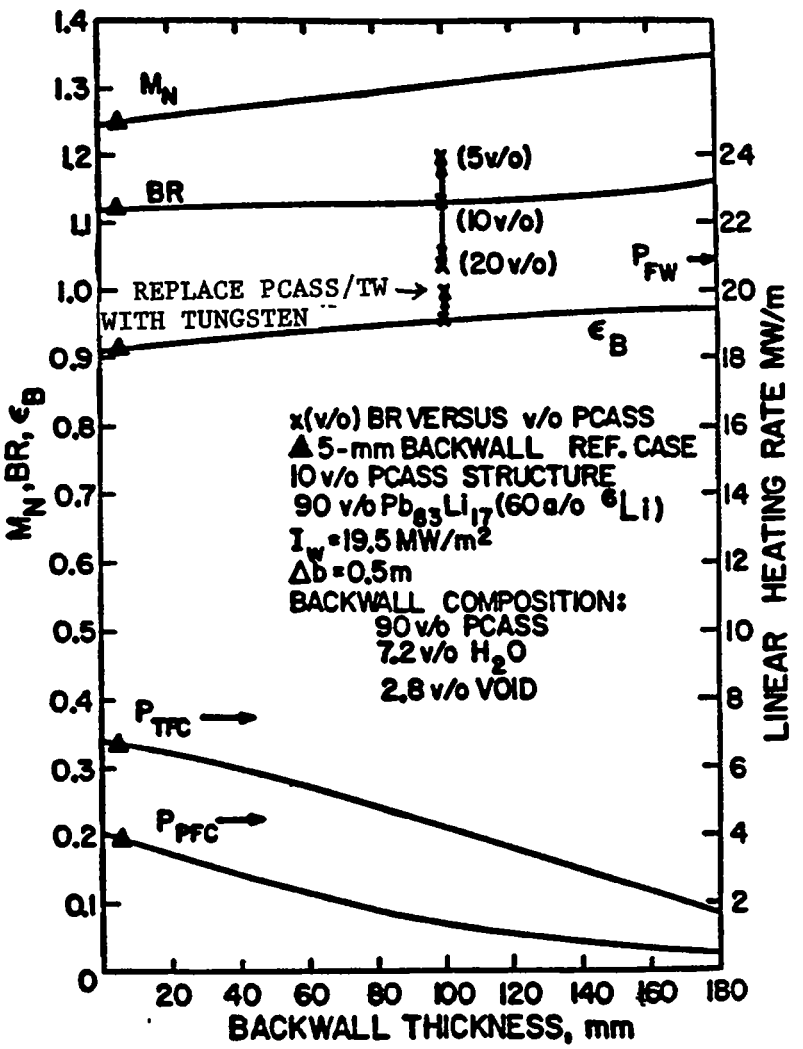

Fig. 35. Effect of varying third-wall thickness in CRFPR parameters. 0.5-m blanket with 90/10 Pb-Li/PCASS.

In all of the parametric studies thus far, the third-wall material was 90 v/0 PCASS and 7.26 v/0 water (10 v/0 at 0.726 g/cm^3). If the third wall could be made to absorb more neutrons, the blanket efficiency would increase and the coil heating would decrease. To this end, we considered a 0.1-m-thick third wall consisting of varying proportions of tungsten, boron carbide, and PCASS, with coolant water provided. Also, the 90/10 Pb-Li/PCASS blanket used previously was replaced by a more realistic 95/5 mixture. Calculational results, assuming a homogeneous distribution of these materials, are shown in Table XXXV. The results indicate a blanket efficiency of 0.98 for the W/B_4C and W cases. The breeding ratio, however, is lower than that for the 90 v/0 PCASS configuration.

TABLE XXXV

EFFECT OF VARYING THIRD-WALL MATERIALS. 0.1-m-THICK THIRD WALL. 0.5-m BLANKET WITH 95 v/O Pb-Li AND 5 v/O PCASS. P_{XX} IN UNITS OF MW/m. IN ALL CASES, THIRD-WALL COOLANT IS 10 v/O WATER AT DENSITY OF 0.726 G/cm^3.

	0.4 W + 0.4 B_4C + 0.1 PCASS	0.8 W + 0.1 B_4C	0.9 W	0.9 PCASS
P_{FW}	20.81	20.82	20.82	20.82
P_{SW}	4.07	4.07	4.08	4.08
P_B	86.72	87.32	87.60	89.34
P_{TW}	6.21	8.25	9.31	5.78
P_{TFC}	1.16	1.63	1.93	4.38
P_{PFC}	0.59	0.75	0.85	1.64
P_{TOT}	119.56	122.84	124.59	126.04
M_N	1.282	1.311	1.326	1.306
e_B	0.985	0.981	0.978	0.952
BR	1.11	1.13	1.13	1.18
Max dpa/y				
Cu - TFC	1.18	1.45	1.62	2.89
Cu - PFC	0.204	0.226	0.245	0.492
Max appm He/y				
Cu - TFC	0.532	0.386	0.355	0.599
Cu - PFC	0.091	0.069	0.064	0.103
Max appm H/y				
Cu - TFC	2.61	1.90	1.76	3.54
Cu - PFC	0.429	0.324	0.302	0.551

After consideration of the parametric studies discussed above, a "canonical" or "reference" design was adopted for a starting point for further calculations on this concept, as desired. The material and geometric specifications for this design are shown in Table XXXVI and Fig. 36. The important features of this design are (1) a 0.5-m-thick blanket with 95/5 Pb-Li/PCASS, and (2) a 0.1-m-thick third wall with 2.5-cm-thick alternating layers of B_4C and tungsten (Pb-Li coolant provided). Also, the 80 v/O copper in the coils was replaced by 70 v/O copper plus 10 v/O MgO. Thicknesses and material compositions of the other regions are the same as those used in the parametric studies. Parameters of interest for this design are tabulated in Table XXXVII. Calculational results for heating rates, dpa, neutron fluence, and neutron spectra are presented below.

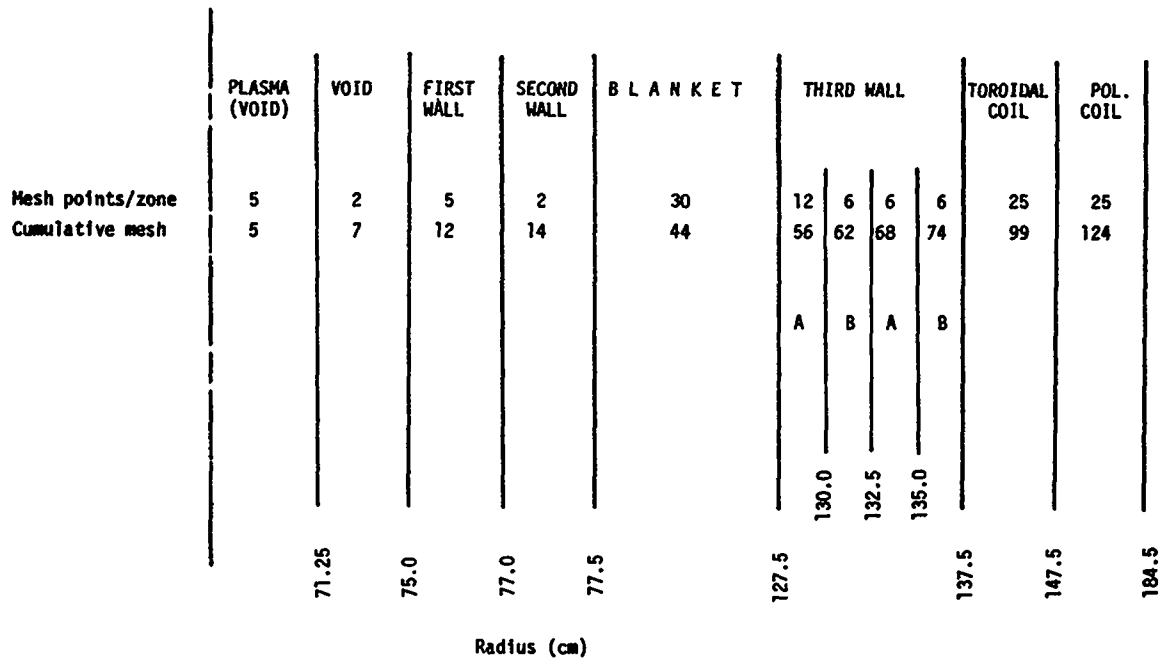

Fig. 36. CRFPR canonical model. Infinite-cylinder geometry. Third-wall materials: A - B_4C/SS/Pb-Li, B - W/SS/Pb-Li. Blanket is 95 v/o $Pb_{83}LI_{17}$ (60% ^6Li enrichment) and 5 v/o SS (PCASS).

TABLE XXXVI

MATERIAL COMPOSITIONS-- CRFPR CANONICAL MODEL

(A) PRIMARY MATERIALS

COPPER - 8.96 G/CM3		
WATER - 1.0		
PB 83 LI 17 - 9.40	60% LI6 ENRICHED	
PCASS ST STL - 7.86	66.7 W/O FE 2.0 W/O MO 2.0 W/O MN	13.7 W/O CR 15.6 W/O NI
B4C - 2.5		
TUNGSTEN - 19.3		
MG-O - 3.65		

(B) MIXTURES

FIRST WALL -	60 V/O COPPER	29 V/O WATER (40 V/O AT 0.726 G/CM3)
SECOND WALL -	60 V/O PCASS	29 V/O WATER (40 V/O AT 0.726 G/CM3)
BLANKET -	95 V/O PB-LI	5 V/O PCASS
THIRD WALL (A) -	80 V/O B4C 10 V/O PCASS	10 V/O PB-LI
THIRD WALL (B) -	80 V/O TUNG 10 V/O PCASS	10 V/O PB-LI
TF AND PF COILS -	10 V/O PCASS 10 V/O WATER	70 V/O COPPER 10 V/O MG-O

TABLE XXXVII

CFRPR CANONICAL MODEL. 0.5-m BLANKET WITH 95/5 Pb-Li/PCASS. 0.1-m THIRD WALL WITH ALTERNATING LAYERS OF B_4C AND TUNGSTEN. I_W = 19.5 MW/m^2. P_{XX} IN UNITS OF MW/m.

P_{FW}	20.81
P_{SW}	4.07
P_B	86.62
P_{TW}	7.40
P_{TFC}	1.56
P_{PFC}	0.84
P_{TOT}	121.20
M_N	1.294
e_B	0.980
BR	1.12

	Zone	Material	Maximum	Minimum	Average
dpa/y	Blanket	PCASS	170	7.0	45.6
	TFC	Cu	1.72	0.30	0.81
	PFC	Cu	0.26	3.1E-04	0.041
appm H/y	Blanket	PCASS	3604	14.1	520
	TFC	Cu	2.64	0.52	1.31
	PFC	Cu	0.45	1.2E-03	0.077
appm He/y	Blanket	PCASS	1085	3.7	151
	TFC	Cu	0.51	0.11	0.26
	PFC	Cu	0.093	3.1E-04	0.016

The Cu dpa/y in the first wall and the magnet coils are plotted as a function of radius in Figs. 37 and 38. A similar curve for stainless steel (PCASS) is shown in Fig. 39. Maximum, minimum, and average values of dpa/y, appm H/y, and appm He/y for steel (blanket) and Cu (coils) are tabulated in Table XXXVII.

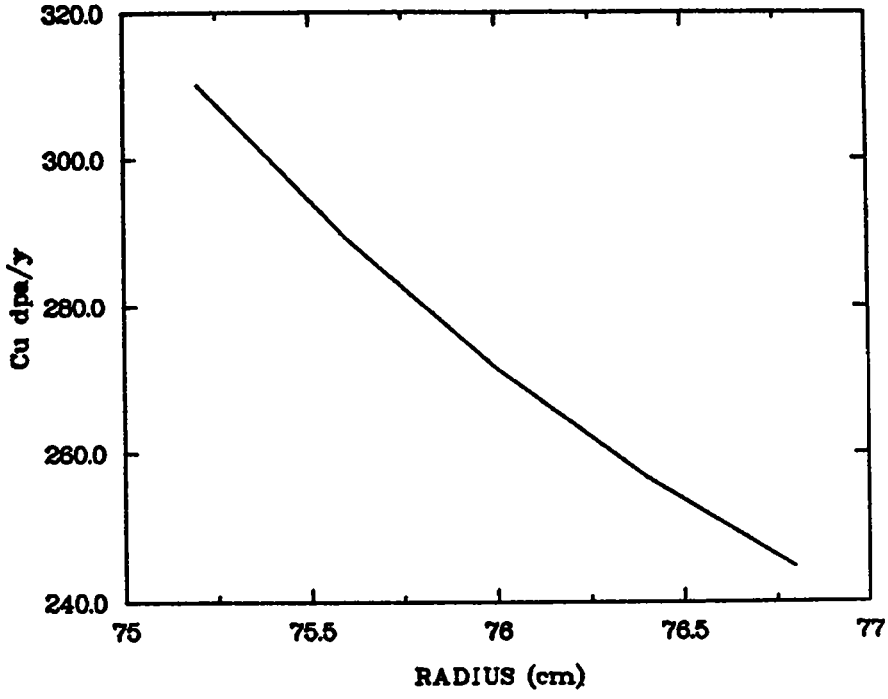

Fig. 37. CRFPR canonical model--19.5-MW/m^2 wall loading. Cu dpa/y in first wall.

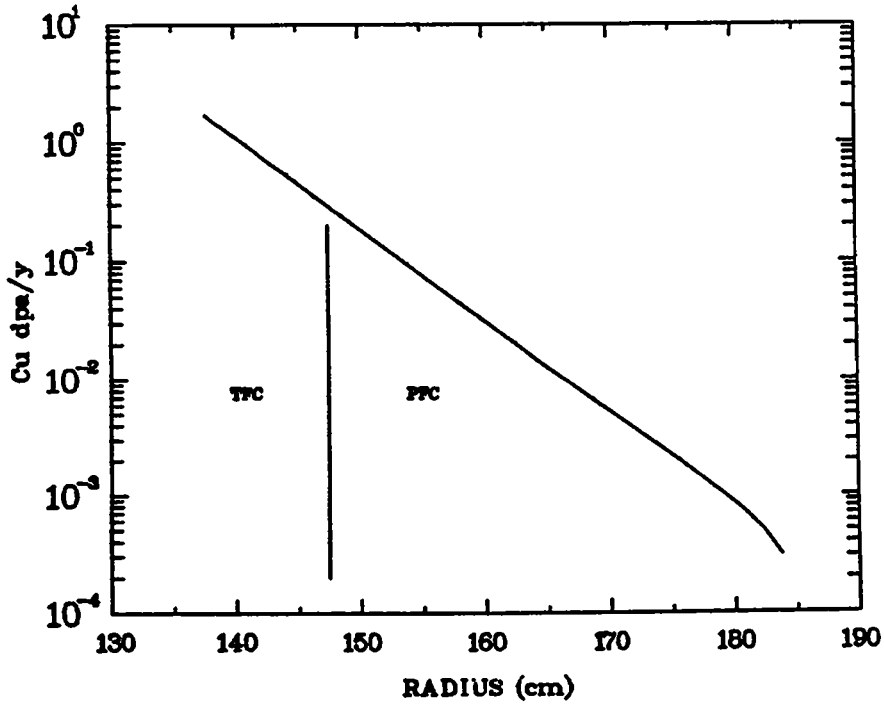

Fig. 38. CRFPR canonical model--19.5-MW/m^2 wall loading. Cu dpa/y in TFC and PFC coils.

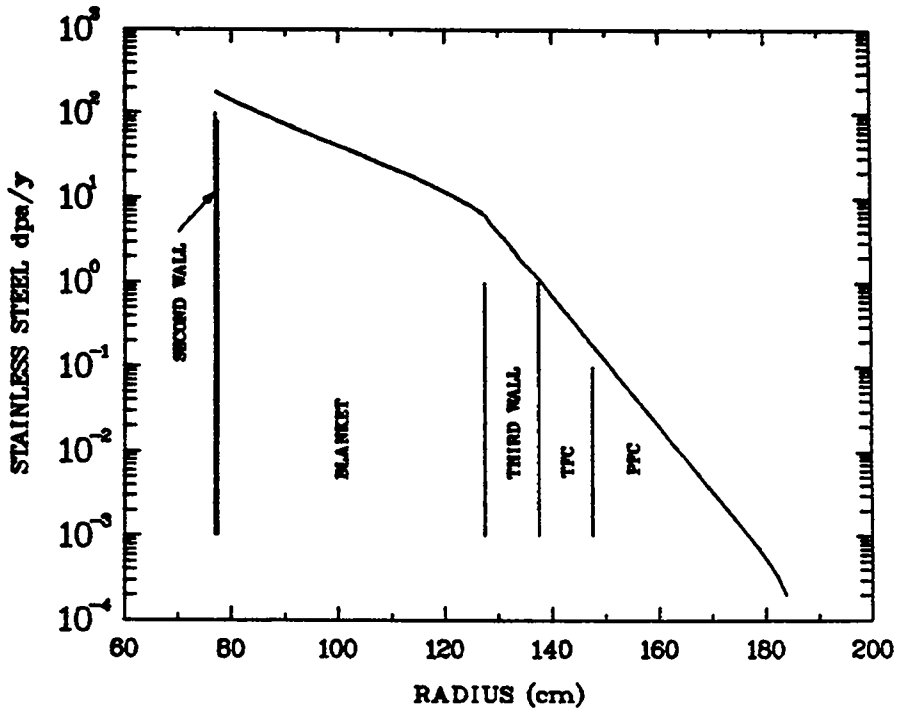

Fig. 39. CRFPR canonical model--19.5-MW/m^2 wall loading. Stainless steel (PCASS) dpa/y.

Heating rates (W/cm^3) in the system are plotted in Fig. 40. The thermal spikes are of interest. Across the blanket/third-wall interface, the heating rate jumps from 3.5 to 17.5 W/cm^3. At the third-wall interface, a decrease from 8.3 to 2.1 W/cm^3 is observed. The heating rate figures can be translated to rad/s if they are divided by the material density (g/cm^3) and multiplied by 10^5 (1 J = 10^7 ergs and 100 ergs/g = 1 rad). For example, the material density in the first wall is 5.67 g/cm^3 and the maximum heating rate is 239 W/cm^3; this yields 4.2 x 10^6 rad/s, with 1.6 x 10^6 and 2.6 x 10^6 rad/s attributable to neutrons and gamma rays, respectively. For the TFC, the corresponding figures are 8.05 g/cm^3, 2.13 W/cm^3, and 2.6 x 10^4 rad/s; the neutron and gamma-ray components are 3.4 x 10^5 and 2.2 x 10^6 rad/s, respectively.

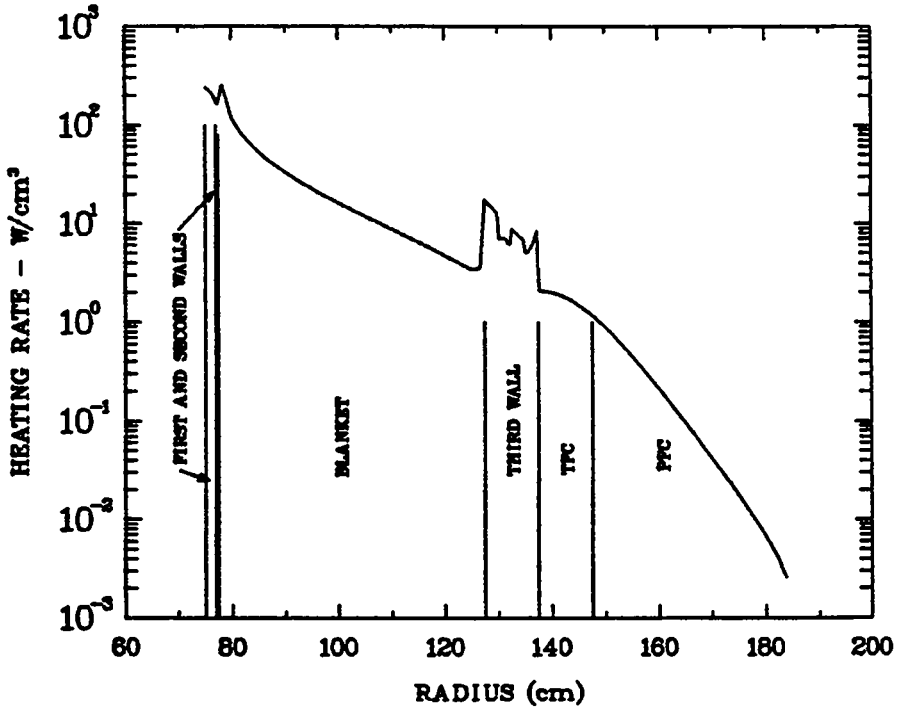

Fig. 40. CRFPR canonical model--19.5-MW/m^2 wall loading. Heating rates vs radius.

Volumetric heating rates and neutron fluences for one-year steady state operation are tabulated in Table XXXVIII. Neutron fluences, for neutron energies greater than 0.1 MeV and 1-year operation, are plotted in Fig. 41. To give some indication of the neutron spectrum, we show in Figs. 42 to 45 the neutron flux per unit lethargy at selected radii. These are as follows:

Fig. 42--first mesh point in first wall,
Fig. 43--middle of blanket,
Fig. 44--first mesh point in TFC, and
Fig. 45--first mesh point in TFC.

It is noted that the attenuation of the 14-MeV neutrons between the first wall and the TFC is only a factor of 10^4. The presence of a significant epithermal component in the first-wall spectra is due to the moderating effect of the coolant water in that region.

TABLE XXXVIII

CRFPR CANONICAL MODEL. VOLUMETRIC HEATING RATES AND NEUTRON FLUENCES (n/cm^2) FOR ONE-YEAR STEADY-STATE OPERATION. I_W = 19.5 MW/m^2.

Region	Max MW/m^3	Min MW/m^3	Avg. MW/m^3	Max Neutron Fluence
First wall	239	193	218	2.1E+23
Second wall	173	163	168	2.0E+23
Blanket	256	3.51	26.9	2.0E+23
Third wall	17.5	8.33	8.89	1.9E+22
TF coil	2.13	1.20	1.74	3.6E+21
PF coil	1.08	0.0003	0.218	5.2E+20

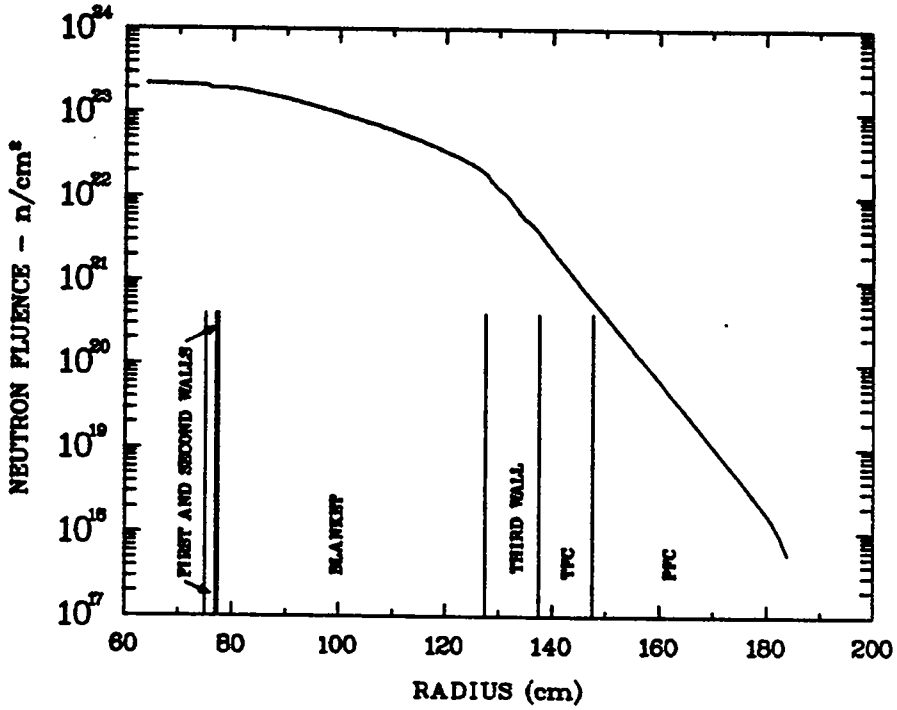

Fig. 41. CRFPR canonical model--19.5-MW/m^2 wall loading. Neutron fluences for energies greater than 0.1 MeV and 1-year operation.

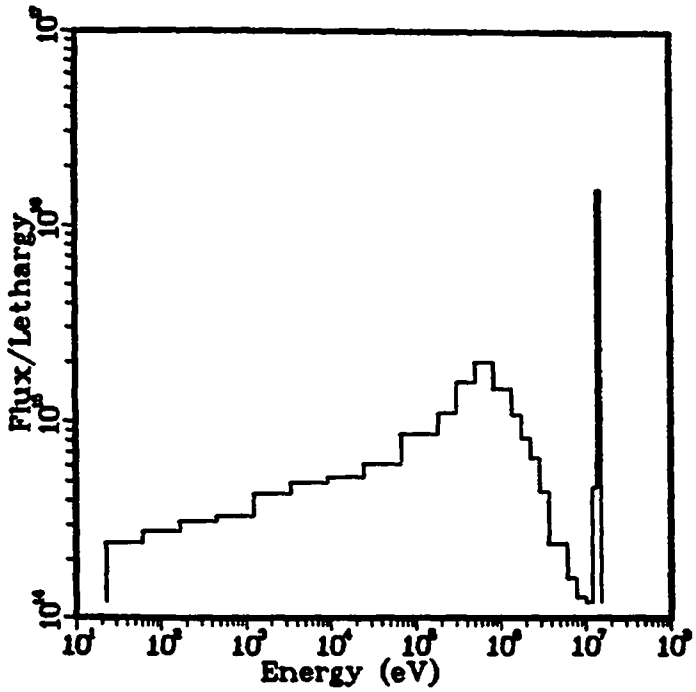

Fig. 42. CRFPR canonical model--19.5-MW/m^2 wall loading. Neutron spectrum just inside first wall.

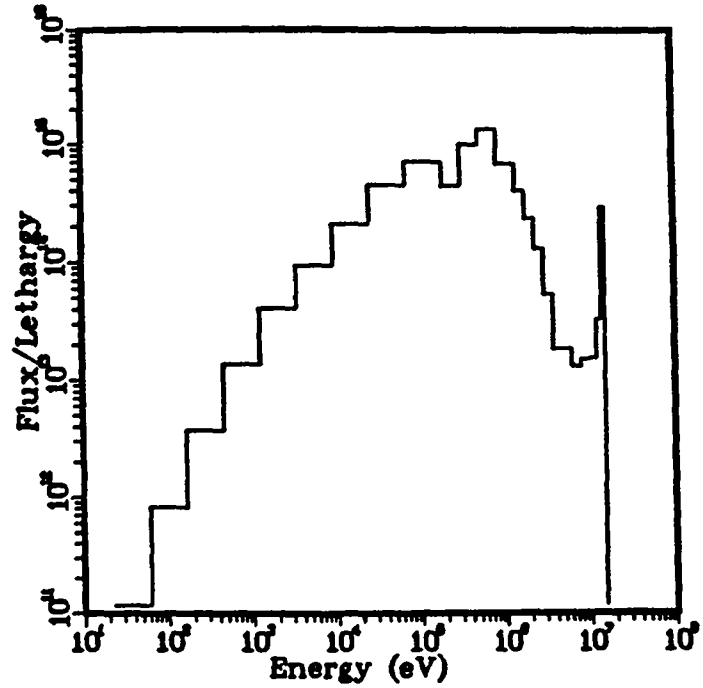

Fig. 43. CRFPR canonical model--19.5-MW/m^2 wall loading. Neutron spectrum in midblanket.

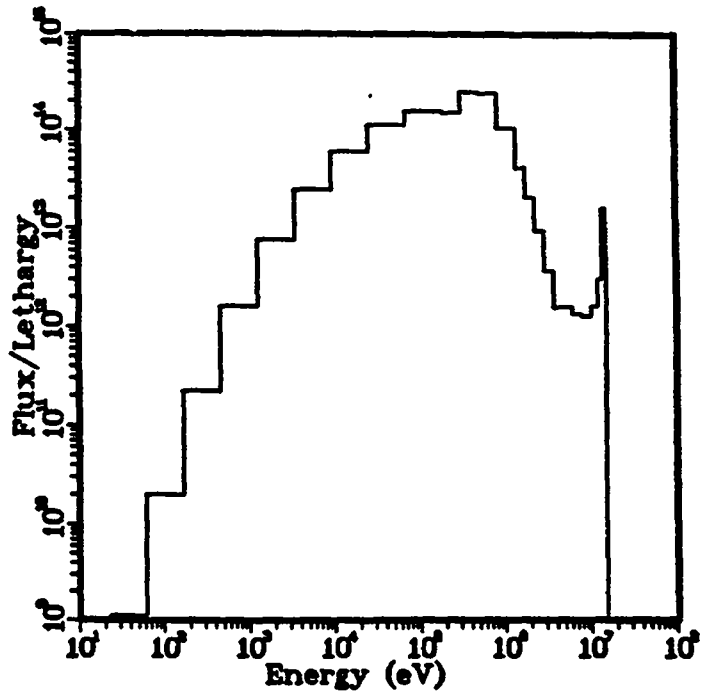

Fig. 44. CRFPR canonical model--19.5-MW/m^2 wall loading. Neutron spectrum just inside TFC.

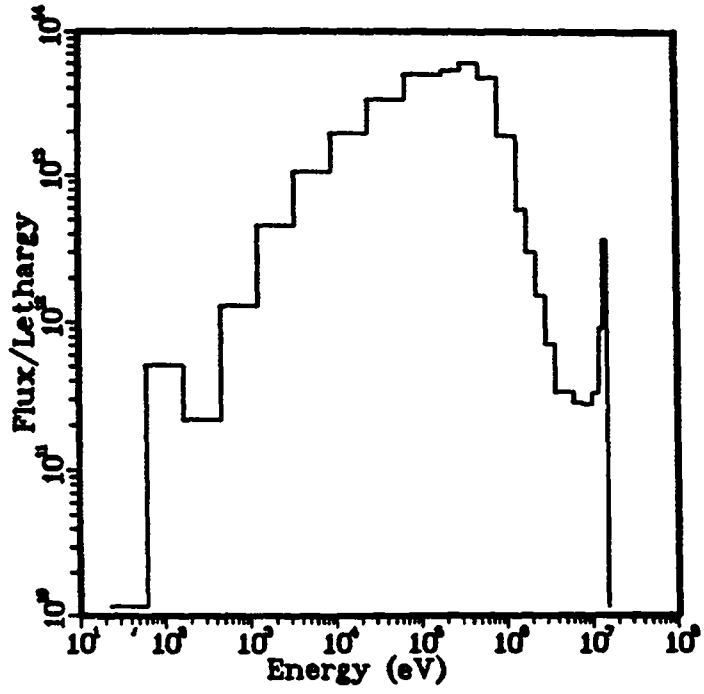

Fig. 45. CRFPR canonical model--19.5-MW/m^2 wall loading. Neutron spectrum just inside PFC.

Quantitative estimates have been obtained for the transmutation of copper, in the first wall and field coils, to nickel and zinc. The reactions of interest and the half-lives of the radioactive products are

$^{63}Cu(n,p)^{63}Ni$. . . .	100 yr
$^{63}Cu(n,\gamma)^{64}Cu$. . . .	12.7 h
$^{65}Cu(n,p)^{65}Ni$. . . .	2.52 h
$^{65}Cu(n,\gamma)^{66}Cu$	5.10 min

In turn, these radioactive products decay (beta and orbital electron capture) to the following stable isotopes:

$$^{63}Ni \rightarrow {}^{63}Cu$$
$$^{64}Cu \rightarrow {}^{64}Zn \ (40\%)$$
$$^{64}Cu \rightarrow {}^{64}Ni \ (60\%)$$
$$^{65}Ni \rightarrow {}^{65}Cu$$
$$^{66}Cu \rightarrow {}^{66}Zn$$

The production rate for a nuclear reaction is defined as

$$P = \sigma N \phi \quad , \tag{24}$$

where P = production rate (atoms/cm^3-s),
σ = activiation cross section,
N = atom density of target material, and
ϕ = neutron flux.

In a multigroup calculation, Eq. (24) is summed over all neutron groups. The decay rate can be written as

$$dN_A/dt = P_A - \lambda_A N_A \ , \tag{25}$$

with λ_A being the decay constant. For an irradiation time T, the number of activated atoms/cm^3 (N_A) is

$$N_A = (P_A/\lambda_A)\ (1 - e^{-\lambda_A T}) \ . \tag{26}$$

Finally, if the activated atoms of species A decay to stable isotopes B, the governing equation is

$$dN_B/dt = \lambda_A N_A \quad . \tag{27}$$

If we substitute Eq. (26) into Eq. (27) and solve for N_B, we obtain

$$N_B = (P_A/\lambda_A)\ (\lambda_A T + e^{-\lambda_A T} - 1). \tag{28}$$

Assuming an irradiation time of 1 year and using the appropriate production rates and decay constants, we can compute the concentrations of nickel and zinc. It is convenient to express the transmutant densities as fractions of the copper atom densities in the target material. Results of these calculations are summarized in Table XXXIX.

TABLE XXXIX

NICKEL AND ZINC PRODUCTION FROM NEUTRON ACTIVATION OF COPPER

	First Wall	Toroidal Field Coil	Poloidal Field Coil
Average Ni/Cu	2.55E-02	2.63E-04	2.86E-05
Maximum Ni/Cu	2.78E-02	3.14E-04	1.56E-04
Average Zn/Cu	2.15E-02	2.68E-04	2.79E-04
Maximum Zn/Cu	2.30E-02	3.24E-04	1.55E-04

REFERENCES

1. R. M. Kulsrud, H. P. Furth, E. J. Valeo, and M. Goldhaber, "Fusion Reactor Plasmas with Polarized Nuclei," PPL-1912 (1982); see also, "Polarized Plasmas May Prove Useful for Fusion Reactors," Phys. Today, 17 (August 1982).

2. H. Zankel and G. M. Hale, "Approximate Coulomb Correction to Elastic N-d Scattering," Phys. Rev. C 24, 1384 (1981).

3. H. Zankel and G. M. Hale, "Difference of Neutron and Proton Analyzing Power in Elastic N-d Scattering Between 5 and 14 MeV," Phys. Rev. C (to be published), Los Alamos document LA-UR-82-2264.

4. C. Fayard, G. H. Lamot, and E. Elbaz, Proc. Troisieme Session d'Etudes de Physique Nucléaire, La Troussuire, 1975, Report No. LYCEN 7502; G. H. Lamot, Thesis, Lyon, 1975.

5. W. Tornow, C. R. Howell, R. C. Byrd, R. S. Pedroni, and R. L. Walter, "Analyzing Power Measurements for $^{2}H(\vec{n},n)^{2}H$ Scattering at 10 MeV Compared to Few-Nucleon Calculations and Data for $^{2}H(\vec{p},p)^{2}H$ Scattering," Phys. Rev. Lett. 49, 312 (1982).

6. W. Grüebler, V. König, P. Schmelzbach, B. Jenny, H. Bürgi, P. Doleschall, G. Heidenreich, H. Roser, F. Seiler, and W. Reichart, "Proton-Deuteron Elastic Scattering," Phys. Lett. B 74, 173 (1978).

7. G. M. Hale, D. C. Dodder, and J. C. DeVeaux, "Charged-Particle Elastic Cross Sections," in P. G. Young, Comp., "Applied Nuclear Data Research and Development," Los Alamos National Laboratory report LA-9468-PR (August 1982). p. 2.

8. G. M. Hale, D. C. Dodder, and J. C. DeVeaux, "Charged-Particle Elastic Cross Sections," Proc. Int. Conf. Nucl. Data Sci. Technol., Antwerp, Antwerp, Belgium, September 6-10, 1982 (to be published).

9. P. G. Young, E. D. Arthur, C. Philis, P. Nagel, and M. Collin, "Analysis of $n+^{165}Ho$ and ^{169}Tm Reactions," Proc. Conf. Nucl. Data Sci. Technol., Antwerp, Belgium, September 6-10, 1982 (to be published).

10. D. I. Gerber, L. G. Strömberg, M. D. Goldberg, D. E. Cullen, and V. M. May, "Angular Distributions in Neutron-Induced Reactions, Vol. II, Z = 21 to 94," Brookhaven National Laboratory report BNL 400, 3rd Ed., Vol. II (June 1970).

11. J. Raynal, "Optical Model and Coupled-Channel Calculations in Nuclear Physics," International Atomic Energy Agency report IAEA-SMR-9/8 (1970).

12. Ch. Lagrange, O. Bersillon, and D. G. Madland, Nucl. Sci. Eng. (to be published).

13. C. L. Dunford, "A Unified Model for Analysis of Compound Nucleus Reaction," Atomics International report AI-AEC-12931 (1980).

14. P. G. Young and E. D. Arthur, "GNASH: A Preequilibrium, Statistical Nuclear-Model Code for Calculation of Cross Sections and Emission Spectra," Los Alamos Scientific Laboratory report LA-6947 (November 1977).

15. E. D. Arthur,"Calculation of Neutron Cross Sections on Isotopes of Yttrium and Zirconium," Los Alamos Scientific Laboratory report LA-7789-MS (April 1979).

16. J. Raynal, "Optical Model and Coupled-Channel Calculations in Nuclear Physics," Int. Atomic Energy Agency report IAEA-SMR-9/8 (1970).

17. E. D. Arthur, "Improvements of the Fission Channel in COMNUC," in P. G. Young, Comp., "Applied Nuclear Data Research and Development," Los Alamos National Laboratory report LA-9262-PR (March 1982), p. 9.

18. H. C. Britt and J. B. Wilhelmy, "Simulated (n,f) Cross Sections for Exotic Actinide Nuclei," Nucl. Sci. Eng. 72, 222 (1979).

19. J. D. Cramer and H. C. Britt, "Neutron Fission Cross Sections for ^{231}Th, ^{233}Th, ^{235}U, ^{237}U, ^{239}U, ^{241}Pu, and ^{243}Pu from 0.5 to 2.25 MeV Using (t,pf) Reactions," Nucl. Sci. Eng. 41, 177 (1970).

20. B. B. Back, O. Hansen, H. C. Britt, and J. D. Garrett, "Fission of Doubly Even Actinide Nuclei Induced by Direct Reactions," Phys. Rev. C 9, 1924 (1974).

21. B. B. Back, H. C. Britt, O. Hansen, B. Leroux, and J. D. Garrett, "Fission of Odd-A and Doubly Odd Actinide Nuclei Induced by Direct Reactions," Phys. Rev. C 10, 1948 (1974).

22. E. D. Arthur, "Determination of Deformed Optical Model Parameters for Neutron Reactions on ^{235}U and ^{239}Pu," in C. I. Baxman and P. G. Young, Comps., "Applied Nuclear Data Research and Development," Los Alamos National Laboratory report LA-8874-PR (July 1981). p. 15.

23. P. A. Dickey and P. Axel, "^{238}U and ^{232}Th Photofission and Photoneutron Emission Near Threshold," Phys. Rev. Lett. 35, 501 (1975).

24. A. Gavron, H. C. Britt, P. D. Goldstone, J. B. Wilhelmy, and S. E. Larsson, "Complexity of the Potential-Energy Surface for Fission of ^{238}U," Phys. Rev. Lett. 38, 1457 (1977).

25. J. H. McNally, J. W. Barnes, B. J. Dropesky, P. A. Seeger, and K. Wolfsberg, "Neutron-Induced Fission Cross Section of ^{237}U," Phys. Rev. 9, 717 (1974).

26. D. G. Gardner, "Neutron Reactions on ^{237}U," Lawrence Livermore Laboratory report UCID-16885, Rev. 1 (1975).

27. Ch. Lagrange, O. Bersillon, and D. G. Madland, "Coupled-Channel Optical-Model Calculations for Evaluating Neutron Cross Sections of Odd-Mass Actinides," Nucl. Sci. Eng. (to be published).

28. D. G. Madland and J. R. Nix, "New Calculation of Prompt Fission Neutron Spectra and Average Prompt Neutron Multiplicities, Nucl. Sci. Eng. 81, 213 (1982).

29. J. Terrell, "Fission Neutron Spectra and Nuclear Temperatures," Phys. Rev. 113, 527 (1959).

30. A. H. Wapstra and K. Bos, "The 1977 Atomic Mass Evaluation," At. Data Nucl. Data Tables 19, 175 (1977).

31. W. D. Myers, Droplet Model of Atomic Nuclei (IFI/Plenum Data Co., New York, 1977).

32. A. H. Wapstra and K. Bos, on tape available from National Nuclear Data Center, Brookhaven National Laboratory (March 1982), At. Data Nucl. Data Tables (to be published).

33. P. Möller and J. R. Nix, "Atomic Masses and Nuclear Ground-State Deformations Calculated with a New Macroscopic-Microscopic Model," At. Data Nucl. Data Tables 26, 165 (1981).

34. D. G. Madland, "Calculation of the Prompt Neutron Spectrum and $\bar{\nu}_p$ for the Spontaneous Fission of ^{252}Cf," Trans. Am. Nucl. Soc. 38, 649 (1981).

35. J. P. Unik, J. E. Gindler, L. E. Glendenin, K. F. Flynn, A. Gorski, and R. K. Sjoblom, "Fragment Mass and Kinetic Energy Distributions for Fissioning Systems Ranging from Mass 230 to 256," Phys. Chem. Fission, Proc. IAEA Symp., 3rd, Rochester, N.Y., August 13-17, 1973 (International Atomic Energy Agency, Vienna, 1974), Vol. II, p. 19.

36. F. D. Becchetti, Jr., and G. W. Greenlees, "Nucleon-Nucleus Optical-Model Parameters, A>40, E<50 MeV," Phys. Rev. 182, 1190 (1969).

37. J. W. Boldeman, D. Culley, and R. J. Cawley, "The Fission Neutron Spectrum from the Spontaneous Fission of ^{252}Cf," Trans. Am. Nucl. Soc. 32, 733 (1979).

38. J. Weber, H. C. Britt, and J. B. Wilhelmy, "Comparison of ^{252}Cf Spontaneous Fission with ^{252}Cf(t,pf)," Phys. Rev. C 23, 2100 (1981).

39. A. C. Wahl, "Systematics of Nuclear Charge Distribution in Fission: The Zp Model," J. Radioanal. Chem. 55, 111 (1980).

40. D. C. Hoffman and M. M. Hoffman, "Post-Fission Phenomena," Ann. Rev. Nucl. Sci. 24, 151 (1974).

41. S. Amiel, "Delayed Neutrons in Fission," Phys. Chem. Fission, Proc. IAEA Symp., 2nd, Vienna, Austria, July 28-August 1, 1969 (International Atomic Energy Agency, Vienna, 1969), p. 569.

42. J. R. Smith, "Status of ^{252}Cf $\bar{\nu}$ and Its Impact on Thermal Reactor Parameters," Proc. Symp. Nucl. Data Probl. Therm. React. Appl., Brookhaven National Laboratory, 1978; Electric Power Research Institute report EPRI-NP-1093 (1979), p. 5-1.

43. R. R. Spencer, R. Gwin, and R. Ingle, "A Measurement of the Average Number of Prompt Neutrons from Spontaneous Fission of Californium-252," Nucl. Sci. Eng. 80, 603 (1982).

44. R. L. Walsh and J. W. Boldeman, "Fine Structure in the Neutron Emission $\bar{\nu}(A)$ from ^{252}Cf Spontaneous Fission Fragments," Nucl. Phys. A 276, 189 (1977).

45. D. G. Madland and J. R. Nix, "Calculation of the Prompt Neutron Spectrum and Average Prompt Neutron Multiplicity for the Spontaneous Fission of ^{252}Cf," Proc. Int. Conf. Nucl. Data Sci. Technol., Antwerp, Belgium, September 6-10, 1982 (to be published).

46. D. G. Madland, "New Fission Neutron Spectrum Representation for ENDF," Los Alamos National Laboratory report LA-9285-MS (ENDF-321) (April 1982).

47. D. W. Muir, R. M. Boicourt, and R. E. MacFarlane, "NJOY Covariance Modules, ERRORR and COVR," in P. G. Young, Comp., "Applied Nuclear Data Research and Development," Los Alamos National Laboratory report LA-9468-PR (August 1982). pp. 39-46.

48. R. E. MacFarlane, D. W. Muir, and R. M. Boicourt, "The NJOY Nuclear Data Processing System, Volume I: User's Manual," Los Alamos National Laboratory report LA-9303-M (ENDF-324) (May 1982), pp. 12-14.

49. W. B. Wilson, T. R. England, R. J. LaBauve, and R. M. Boicourt, "TOAFEW-V Multigroup Cross-Section Collapsing Code and Library of 154-Group-Processed ENDF/B-V Fission-Product and Actinide Cross Sections," Electric Power Research Institute report NP-2345, Research Project 975-2, Interim Report (April 1982).

50. J. Grundl and C. Eisenhauer, "Fission Rate Measurements for Materials Neutron Dosimetry in Reactor Environments," Proc. ASTM-EURATOM Symp. React. Dosim., 1st, Petten, The Netherlands, 1975, Commission of the European Communities report EUR-5667 (1977).

51. W. P. Poenitz and T. Tamura, "Investigation of the Prompt-Neutron Spectrum for Spontaneously Fissioning ^{252}Cf," Proc. Int. Conf. Nucl. Data Sci. Technol., Antwerp, Belgium, September 6-10, 1982 (to be published).

52. J. W. Boldeman, D. Culley, and R. J. Cawley, "The Fission Neutron Spectrum from the Spontaneous Fission of ^{252}Cf," Trans. Am. Nucl. Soc. 32, 733 (1977).

53. J. A. Grundl, C. M. Eisenhauer, and E. D. McGarry, "Compendium of Benchmark Neutron Fields for Reactor Dosimetry," LWR Pressure Vessel Dosimetry progress report NUREG/CR-0551 (1978).

54. D. M. Gilliam, "Integral Measurement Results in Standard Fields," Proceedings Int. Symp. Neutron Stand. and Appl., NBS Special Publication 493, U.S. Dept. of Commerce, Washington, DC (March 1977).

55. B. A. Magurno, "Status of the Dosimetry File for ENDF/B-V," Proc. Advis. Group Meet. Nucl. Data React. Dosim., INDC(nds)-103M, (Nuclear Data Section, International Atomic Energy Agency, Vienna 1979), p. 1.

56. R. E. MacFarlane, R. J. Barrett, D. W. Muir, and R. M. Boicourt, "The NJOY Nuclear Data Processing System: User's Manual, " Los Alamos Scientific Laboratory report LA-7584-M (ENDF-272) (December 1978).

57. W. Mannhart, "Measurement and Evaluation of Integral Data in the Cf-252 Neutron Field," Proc. Int. Conf. Nucl. Data Sci. Technol., Antwerp, Belgium, September 6-10, 1982 (to be published).

58. W. Mannhart and F. G. Perey, "Covariance Matrices of Cf-252 Spectrum Averaged Cross Sections,"Proc. ASTM-EURATOM Symp. React. Dosim., 3rd, Ispra, Italy, 1979, Commission of the European Communities report EUR6813EN-FR, Vol. II (1980), p. 1016.

59. D. R. Harris, W. A. Reupke, and W. B. Wilson, "Consistency Among Differential Nuclear Data and Integral Observations: The ALVIN Code for Data Adjustment, for Sensitivity Calculations, and for Identification of Inconsistent Data," Los Alamos Scientific Laboratory report LA-5987 (December 1975).

60. F. M. Mann, C. Dunn, and R. E. Schenter, "Beta Decay Properties from a Statistical Model," Phys. Rev. C 25, No. 1, 524 (January 1982).

61. T. R. England, W. B. Wilson, R. E. Schenter, and F. M. Mann, "Aggregate Delayed Neutrons and Spectral Calculations using Preliminary Precursor Data Evaluated for ENDF/B-VI," Los Alamos National Laboratory document LA-UR-82-84 (April 1982). See also T. R. England, W. B. Wilson, R. E. Schenter, F. M. Mann, "Delayed Neutron Spectral Calculation Using Augmented ENDF/B-V Data," Trans. Am. Nucl. Soc. 41, 567 (1982)

62. F. M. Mann, M. Schreiber, R. E. Schenter, and T. R. England, "Compilation of Neutron Precursor Data," Proc. Int. Conf. Nucl. Data Sci. Technol., Antwerp, Belgium, September 16-10, 1982 (to be published).

63. T. R. England and W. B. Wilson, "TMI-2 Decay Power: LASL Fission-Product and Actinide Decay Power Calculations for the President's Commission on the Accident at Three Mile Island," Los Alamos Scientific Laboratory report LA-8041-MS (October 1979, Rev. March 1980).

64. W. B. Wilson, T. R. England, and R. J. LaBauve, "Extended Burnup Calculations for Operating Reactor Reload Reviews," Los Alamos National Laboratory report LA-9563-MS (to be published by the Nuclear Regulatory Commission as a NUREG report).

65. W. R. Cobb and W. J. Eich, "A New Cell Depletion Code," Trans. Am. Nucl. Soc. 24, 442 (1976).

66. W. B. Wilson, T. R. England, R. J. LaBauve, M. E. Battat, D. E. Wessol, and R. T. Perry, "Status of CINDER and ENDF/B-V Based Libraries for Transmutation Calculations," Proc. Int. Conf. Nucl. Waste Transmutation, Austin, Texas, July 22-24, 1980 (University of Texas at Austin, March 1981), p. 673.

67. W. B. Wilson, T. R. England, and R. J. LaBauve, "Formation and Testing of ENDF/B-V Based Fission-Product and Actinide Data Libraries for CINDER-2," in P. G. Young, Comp., "Applied Nuclear Data Research and Development," Los Alamos National Laboratory report LA-9262-PR (March 1982). p. 51.

68. J. J. DiNunno, F. D. Anderson, R. E. Baker, and R. L. Waterfield, "Calculation of Distance Factors for Power and Test Reactor Sites," U.S. Atomic Energy Commission report TID-14844 (March 23, 1962).

69. U.S. Nuclear Regulatory Commission, "Reactor Safety Study, An Assessment of Accident Risks in U. S. Commercial Nuclear Power Plants; Appendix VI: Calculation of Reactor Accident Consequences," WASH-1400 (NUREG-75/014) (October 1975).

70. G. E. Bosler, J. R. Phillips, W. B. Wilson, R. J. LaBauve, and T. R. England, "Production of Actinide Isotopes in Simulated PWR Fuel and Their Influence on Inherent Neutron Emission," Los Alamos National Laboratory report LA-9343 (July 1982).

71. A. A. Bauer, L. M. Lowry, and J. S. Perrin, "Progress on Evaluating Strength and Ductility of Irradiated Zircolay During July Through September, 1975," Battelle Columbus Laboratories report BMI-1938 (September 1975).

72. B. F. Rider and M. E. Meek, "Compilation of Fission Product Yields, Vallecitos Nuclear Center, 1977," General Electric Co. document NEDO-12154-2, July 1977.

73. V. D. Heck, H. Borner, J. A. Pinston, and R. Roussille, "Neutron Capture Cross Section of ^{147}Nd," Atomkernenergie 24, 141 (1974).

74. R. Sure and C. Beck, "Fission Energy Release for 16 Fissioning Nuclides," Electric Power Research Institute report EPRI-NP-1771 (March 1981).

75. W. B. Wilson, R. J. LaBauve, and T. R. England, "Calculations of Spent Thermal Reactor Fuel Nuclide Inventories and Comparisons with Measurements," Proc. Semin./Workshop Therm. Reac. Benchmark Calc., Tech., Results, and Appl.," Brookhaven National Laboratory, Upton, N.Y., May 17-18, 1982 (to be published), Los Alamos National Laboratory document LA-UR-82-2341 (May 1982).

76. C. L. Timmerman, "Isotopic Safeguards Data Bank (ISTLIB) and Control Program (MISTY)," Battelle Pacific Northwest Laboratory report PNL-2726 (ISPO-34) (September 1978).

77. W. B. Wilson and T. R. England, "Status of Fission-Product Data for Absorption Calculations," in Electric Power Research Institute report EPRI-NP-1098 (June 1979).

78. T. R. England, R. E. Schenter, and F. Schmittroth, "Integral Decay-Heat Measurements and Comparisons to ENDF/B-IV and V," Los Alamos Scientific Laboratory report NUREG/CR-0305, LA-7422-MS (August 1978). (See also Ref. 79, Sec. 10-1 for primary data in this report.)

79. J. K. Dickens, T. R. England, T. A. Love, J. W. McConnell, J. F. Emergy, K. J. Northcutt, and R. W. Peelle, "Delayed Beta- and Gamma-Ray Production Due to Thermal-Neutron Fission of ^{239}Pu: Tabular and Graphical Spectral Distributions for Times After Fission Between 2 and 14 000 Sec.," Oak Ridge National Laboratory report ORNL/NUREG-66 (NUREG/CR-1172) (January 1980).

80. E. T. Jurney, P. J. Bendt, and T. R. England, "Fission Product Gamma Spectra," Los Alamos Scientific Laboratory report LA-7620-MS (January 1979).

81. "EPRI-CELL Code Description," in "ARMP: Advanced Recycle Methodology Program," Electric Power Research Institute report CCM-3 (September 1977), Chap. 5, Pt. II.

82. R. E. English, "Technical Staff Analysis Report on Chemistry to President's Commission on the Accident at Three Mile Island," October 1979, p. 12.

83. S. J. Dagbjartsson, B. A. Murdock, D. E. Owen, and P. E. MacDonald, "Axial Gas Flow in Irradiated PWR Fuel Rods," Idaho National Engineering Laboratory report TREE-NUREG-1158 (September 1977).

84. W. E. Bailey, T. J. Black, R. L. Crowther, S. Y. Ogawa, R. A. Probstle, M. L. Thompson, and R. A. Walters, "Use of Plutonium Fuel in Boiling Water Reactors; Phase II Extension, Research Project 72-2; Interim Report Covering Period July 1972 to December 1974," Electric Power Research Institute report EPRI-72-2 (June 1975).

85. N. H. Larsen, G. R. Parkas, and O. Raza, "Core Design and Operating Data for Cycles 1 and 2 of Quad Cities 1," Electric Power Research Institute report EPRI-NP-240 (1976).

86. R. A. Walters, "Irradiation and Measurement Data to Support the LASL Gamma and Neutron Measurements at Vallecitos," General Electric N.E.B.G., San Jose, Calif., letter RAW78-081 to W. B. Wilson, Los Alamos National Laboratory, October 4, 1978.

87. E. J. Ruzauskas, S. R. Pati, and N. Fuhrman, "EPRI/C-E Joint Fuel Performance Program, Task A, Test Fuel Rod Irradiation in 14 x 14 Assemblies in Calvert Cliffs 1 (CC-1)," Combustion Engineering Power Systems report RP586-1 (April 8, 1981).

88. W. B. Wilson, R. T. Perry, D. G. Madland, N. Ensslin, and J. E. Stewart, "Calculated Neutron Sources in Pu Process Solutions," in P. G. Young, Comp., "Applied Nuclear Data Research and Development," Los Alamos National Laboratory report LA-9468-PR (August 1982). p. 75.

89. R. T. Perry and W. B. Wilson, "Neutron Production from (α,n) Reactions and Spontaneous Fission in ThO_2, UO_2, and $(U,Pu)O_2$ Fuels," Los Alamos National Laboratory report LA-8869-MS (June 1981).

90. R. T. Perry and W. B. Wilson, "The (α,n) Neutron Production by Alpha Particles in PuO_2, UO_2, and Th_2 Fuels," in C. I. Baxman and P. G. Young, Comps., "Applied Nuclear Data Research and Development Quarterly Progress Report," Los Alamos Scientific Laboratory report LA-8524-PR (September 1980), p. 20.

91. J. F. Ziegler, Helium Stopping Powers and Ranges in All Elemental Matter, Vol. 4 of The Stopping and Ranges of Ions in Matter series (Pergamon Press, New York, 1977).

92. L. C. Northcliffe and R. F. Schilling, "Range and Stopping Power Tables for Heavy Ions," Nucl. Data A 7, 233 (1970).

93. J. K. Bair and F. X. Haas, "Total Neutron Yield from the Reactions $^{13}C(\alpha,n)^{16}O$ and $^{17,18}O(\alpha,n)^{20,21}Ne$," Phys. Rev. C 7, 1356 (1973).

94. J. K. Bair and H. B. Willard, "Level Structure in Ne^{22} and Si^{30} from the Reactions $O^{18}(\alpha,n)Ne^{21}$ and $Mg^{26}(\alpha,n)Si^{29}$," Phys. Rev. 128, 299 (1962).

95. J. K. Bair and J. Gomez del Campo, "Neutron Yields from Alpha-Particle Bombardment," Nucl. Sci. Eng. 71, 18 (1979).

96. L. F. Hansen, J. D. Anderson, J. W. McClure, B. A. Pohl, M. L. Stelts, J. J. Wesolowski, and C. Wong, "The (α,n) Cross Sections on ^{17}O and ^{18}O Between 5 and 12.5 MeV," Nucl. Phys. A 98, 25 (1967).

97. F. Manero and V. A. Konshin, "Status of the Energy-Dependent $\bar{\nu}$-Values for the Heavy Isotopes (Z>90) From Thermal to 15 MeV and of $\bar{\nu}$-Values for Spontaneous Fission," At. Energy Rev. 10, 637 (1972).

98. P. Fieldhouse, D. S. Mather, and E. R. Culliford, "The Spontaneous Fission Half-Life of ^{240}Pu," J. Nucl. Energy 21, 749 (1967).

99. C. Budtz-Jorgensen and H. H. Knitter, "Measurement of the Neutron Induced Fission Cross Section and of the Spontaneous Fission Half-Life of ^{240}Pu," Proc. Specialists' Meet. Nucl. Data Plutonium Americium Isot. React. Appl.," Brookhaven National Laboratory report BNL-50991 (May 1979), p. 239.

100. D. L. Johnson, "Evaluation of Neutron Yields from Spontaneous Fission of Transuranic Isotopes," Trans. Am. Nucl. Soc. 22, 637 (1975).

101. W. J. Swiatecki, "Systematics of Spontaneous Fission Half-Lives," Phys. Rev. 100, 937 (1955).

102. D. C. George, R. J. LaBauve, T. R. England, "Application of Adjusted Data in Calculating Fission-Product Decay Energies and Spectra," Los Alamos National Laboratory report LA-9362-MS, June 1982.

103. Fission-Product Decay Library of the Evaluated Nuclear Data File, Version V (ENDF/B-V). [Available from and maintained by the National Nuclear Data Center (NNDC) at Brookhaven National Laboratory.]

104. T. R. England, R. Wilczynski, and N. L. Whittemore, "CINDER-7: An Interim Report for Users," Los Alamos Scientific Laboratory report LA-5885-MS (April 1975). [CINDER-10, the version used in this report is unpublished. It is described in Los Alamos Scientific Laboratory report LA-6472-PR (August 1976), p. 60, and in Los Alamos Scientific Laboratory report LA-6266-PR (March 1976), p. 13.]

105. J. K. Dickens, T. A. Love, J. W. McConnell, and R. W. Peelle, "Fission-Product Energy Release for Times Following Thermal-Neutron Fission of Plutonium-239 and Plutonium-241 Between 2 and 14 000 s," Nucl. Sci. Eng. 78, 126-46 (1981).

106. R. J. LaBauve, T. R. England, D. C. George, and M. S. Stamatelatos, "The Application of a Library of Processed ENDF/B-IV Fission-Product Aggregate Decay Data in the Calculation of Decay-Energy Spectra," Los Alamos Scientific Laboratory report LA-7483-MS (September 1978).

107. R. J. LaBauve, D. C. George, and T. R. England, "FITPULS, A Code for Obtaining Analytic Fits to Aggregate Fission-Product Decay-Energy Spectra," Los Alamos Scientific Laboratory report LA-8277-MS (March 1980).

108. R. L. Hagenson and R. A. Krakowski, "Compact Reversed-Field Pinch Reactors (CRFPR): Sensitivity Study and Design-Point Determination," Los Alamos National Laboratory report LA-9389-MS (July 1982).

109. R. D. O'Dell, F. W. Brinkley, Jr., and D. R. Marr, "User's Manual for ONEDANT: A Code Package for One-Dimensional, Diffusion-Accelerated, Neutral-Particle Transport," Los Alamos National Laboratory report LA-9184-M (February 1982).

110. M. E. Battat, R. J. LaBauve, and D. W. Muir, "The GAMMON Activation Library," Los Alamos Scientific Laboratory report LA-8040-MS (September 1979).

111. D. K. Sze, R. Clemmer, and E. T. Cheng, "LiPb, A Novel Material for Fusion Applications," Proc. Top. Meet. Technol. Controlled Nucl. Fusion, 4th, King of Prussia, Pennsylvania, October 14-17, 1980.

Printed in the United States of America
Available from
National Technical Information Service
US Department of Commerce
5285 Port Royal Road
Springfield, VA 22161

Microfiche (A01)

Page Range	NTIS Price Code	Page Range	NTIS Price Code	Page Range	NTIS Price Code	Page Range	NTIS Price Code
001-025	A02	151-175	A08	301-325	A14	451-475	A20
026-050	A03	176-200	A09	326-350	A15	476-500	A21
051-075	A04	201-225	A10	351-375	A16	501-525	A22
076-100	A05	226-250	A11	376-400	A17	526-550	A23
101-125	A06	251-275	A12	401-425	A18	551-575	A24
126-150	A07	276-300	A13	426-450	A19	576-600	A25
						601-up*	A99

*Contact NTIS for a price quote.

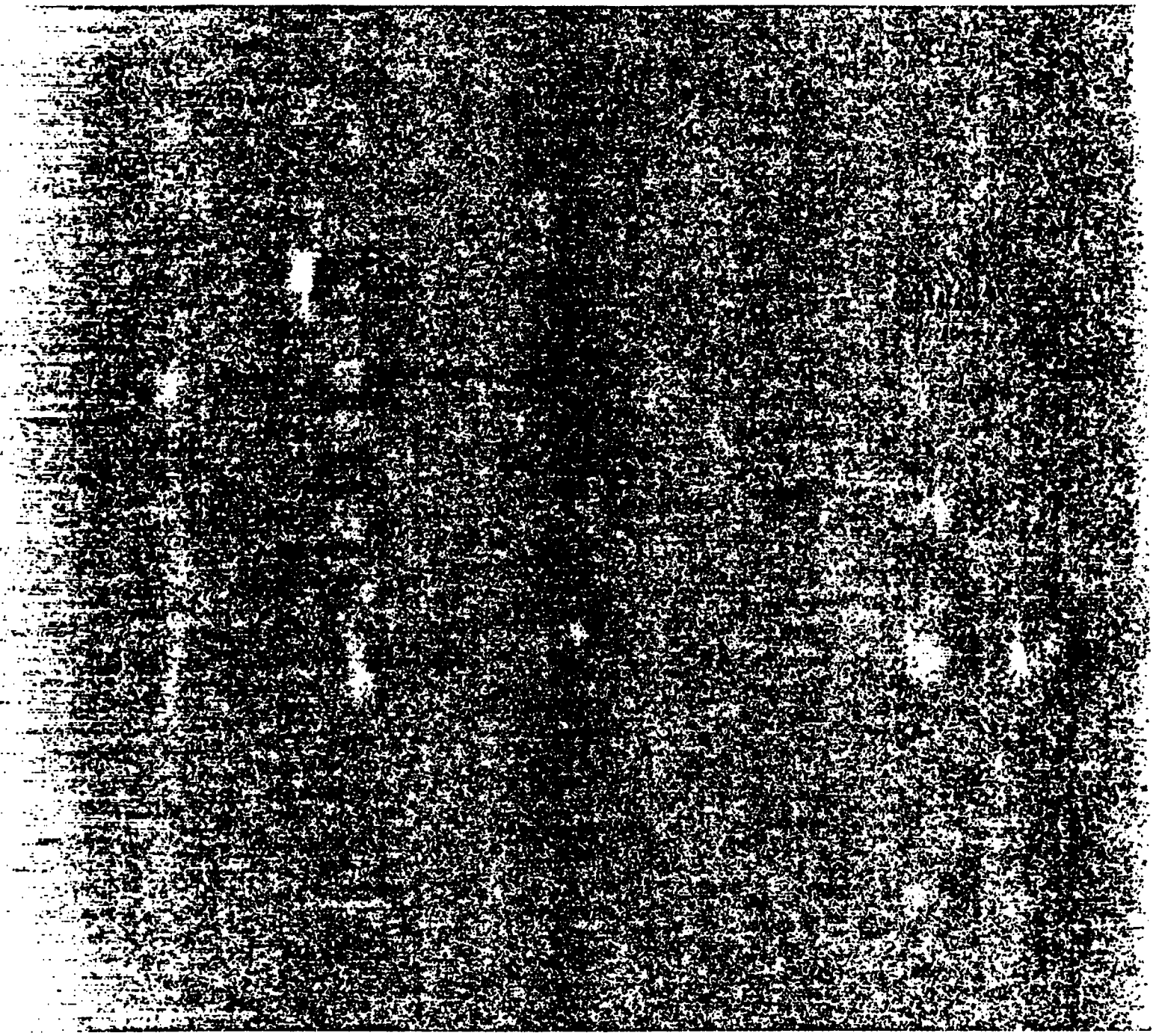

Los Alamos